

Nano-protoplasm: the Ultimate Unit of Life

Gilbert Ling

Damadian Foundation for Basic and Cancer Research
Tim and Kim Ling Foundation for Basic and Cancer Research
110 Marcus Drive, Melville, NY 11747
Email: gilbertling@dobar.org

Abstract: Among the most promising scientific achievements of the 19th century was the recognition that the laws governing the dead world also govern the world of the living and that life has a physical basis called protoplasm. Regrettably, the definition of protoplasm provided then was (inseparably) incorrect, offering a (legitimate) reason for rejecting the concept of protoplasm by an overwhelming majority of later investigators, teachers and other opinion-makers. Without a recognized physical basis, *Life* itself also faded into the limbo of the unexplainable. However, eventually the needed relevant parts of physics and chemistry to give a more cogent definition of protoplasm became available. That then made possible the construction in the early 1960's of a unifying theory of the living cell, named the association-induction (AI) hypothesis.

Historically speaking, the AI Hypothesis is the heir to the general concept of protoplasm as the physical basis of life—incorrect as the initial definition of protoplasm was notwithstanding. In the AI Hypothesis (AIH) the true or ultimate physical basis of life is not what the advocates of the protoplasm once considered as the physical basis of life. What they saw and construed as the physical basis of life is a particular kind of *macroscopic* protoplasm. In the AI Hypothesis, the basic unit (or physical basis) of life is *microscopic* protoplasm or *nano-protoplasm*, of which all macroscopic protoplasm is made. The AI Hypothesis also had no difficulty offering a new definition to what *life* is in terms of fundamental physical-chemical laws.

Nano-protoplasm is defined by what it is and what it does. In greater detail, it is defined (i) by its chemical composition given in Equation 1 on p. 124; (ii) by the mutual spatial and energetic relationships among the components as illustrated diagrammatically in Figure 5 on p. 125; and (iii) by the ability of these components to exist as coherent assemblies in either one of two alternative states, the *resting* and *active living* (or *dead*) state as according to Equation 5 on p. 142. The review then describes the AIH-based electronic and molecular mechanisms for the coherent assemblage of the components, for the maintenance of the living states and for the auto-cooperative transitions between the resting and active (or dead) living state.

Having completed the theoretical section, the review goes on to describe the experimental testing of the theory carried out in the past forty-some years (and even in time before that by authors who knew nothing of the theory.) These experimental studies fall into two broad categories. In the first category, are the experiments performed on ultra-simple models of nano-protoplasm made up

from pure chemicals as prescribed in Equation 1 on p. 124. The results show that they indeed behave qualitatively like that illustrated in Figure 5 and quantitatively follow the dictates of Equation 5. In the second category of experimental testing, parallel studies were carried out on nano-protoplasm as part of living cells — in carrying out each one of the four classical functions of cell physiology: (1) solute and water distribution; (2) solute and water permeability; (3) cellular resting and action potentials; (4) cellular swelling and shrinkage. The results show that the nano-protoplasm *in situ* too qualitatively behave like that shown in Figure 5 and quantitatively follow the dictates of Equation 5.

The review ends on a discussion section, examining how cogent do the experimental data accumulated thus far support to the AI version of the concept of nano-protoplasm as the most basic unit of life.

IN 1839, German zoologist, Theodor Schwann (and German botanist, Mathias Schleiden) introduced the Cell Theory in a monograph, entitled *Mikroskopische Untersuchungen über die Übereinstimmung in der Struktur und dem Wachstum der Tiere und Pflanzen* (*Microscopic Researches into the Accordance in the Structure and Growth of Animals and Plants*) {Schwann 1839; Schleiden 1838; Smith 1847 (English translation).} According to this theory, animals and plants alike are made of basic units called *cells*.

In the same monograph, Schwann also suggested the essence of what would become known later as the **membrane theory**, namely, that both plant and animal cells are membrane-enclosed cavities filled with clear liquid water (Schwann 1839, p. 197, see also Endnote 1.) A third concept Schwann introduced in his monograph was that the cell membrane possesses “*metabolische Kraft*” (“metabolic power”) which controls the chemical composition of fluids inside and outside the cell (*ibid.*, p. 194, p. 197.) This idea became known later as the **membrane pump hypothesis** (see Ling 2007.)

Schwann’s introduction of the cell theory was a landmark event in the history of cell physiology. For that, he deserved the honor he received. Nonetheless, recognition must also be given to four other investigators who had advanced a similar idea at the same time or even before Schwann. They are Oken (1805); Dutrochet (1837); Purkinje (1834) and Valentin (1836.)

Careful study of Schwann and Schleiden’s original writing revealed that Schwann’s ideas on the anatomy and physiology of the living cell were based on a sequence of mistakes that he (and Schleiden) had made (see Ling 2007, pp. 7–9.) These mistakes were made due at least in part to the limited resolving power of the microscope then available. But Schwann could have corrected these mistakes if he had responded to observations that contradicted his several postulations (see below.) However, that was not what he did. Spending just five years in Berlin on this entire Cell Theory enterprise (1834 to 1839), he did not modify his theory and its ancillary ideas after leaving Berlin in 1839 (see Rothschuh 1973, p. 345.)

Despite all these shortcomings, Schwann’s book was met with “an almost unanimous chorus of praise.” (Harris 1999, p. 106.) Moreover, its thesis was adopted by the German textbooks with little or no criticism nor question asked (Harris *ibid.*, p. 106.) The conditions for the creation of a sacred cow were in the making.

1. Protoplasm began with a different name

Four years *before* Schwann announced his Cell Theory, the French zoologist, Felix Dujardin had already described a water-insoluble, and gelatinous material that oozed out from within a crushed protozoon (then called *infusoria*) (Dujardin 1835.) This material was definitely not the clear watery liquid that Schwann described and gave the impression that he (Schwann) had seen in many animal and plant cells.

In addition, Dujardin pointed out that he was not the first to discover this living jelly but only gave it a (specific) name, *sarcode* (from the Greek word *sarkodes* for fleshy.) He then cited the still earlier observers of the living jelly, including Abraham Trembley, C. F. Wolff, O.F. Miller, Lorentz Oken and others. {For sources of these referred work, see Baker (1949, Part II, pp. 88–89) and Hall (1969, vol. 2, pp. 172–175.)}

Eleven years after Dujardin gave the name, sarcode to the “living jelly” from animal cells, the German botanist, Hugo von Mohl gave the name, protoplasm to a substance that lies just under the cell wall of plants cells (von Mohl 1846.) Ferdinand Cohn, professor of botany in Breslau University, concluded that Dujardin’s sarcode and von Mohl’s protoplasm are essentially the same thing (Cohn 1847.) In 1852, Robert Remak suggested to call both sarcode and protoplasm protoplasm (Remak 1852.) And this suggestion was widely adopted and stayed.

von Mohl was apparently unaware that six years earlier, the Czech micro-anatomist, Jan E. Purkinje had already used the word *protoplasma* to describe the living substance of both plant and animal cells (Purkinje 1840.) In fairness, one should also not forget that the word protoplasm may be more appealing, perhaps even more accurate than sarcode but the replacement of sarcode by protoplasm should not obscure Dujardin’s historical role in its introduction.

Climaxing this period of rapid advances made in understanding the living cell and its material makeup were two more episodes that followed within the next two decades. In 1861 Max Schultze (1825–1874), professor of Botany in Bonn, pronounced his protoplasmic doctrine, according to which a living *cell is a membrane-less lump of protoplasm containing a nucleus* (Schultze 1861, 1861a; see also Hall 1951, p. 449.) In 1868, Thomas Huxley (1825–1895,) the one-time opponent to the concept of protoplasm (Huxley 1853), gave his famous Sunday evening lay sermon in an Edinburgh church. Convinced by the rapidly-gathering new evidence against his earlier view, Huxley lost no time in accepting the concept of protoplasm and adding with eloquence matching his zeal, that protoplasm is *the Physical Basis of Life* (Huxley 1869.)



Max Schultze
(1825–1874)

For that and his life-long dedication to the search for truth, Thomas Huxley was lauded as the greatest English scientist of the 19th Century — by another straight-shooting, fearless soul, the American journalist, Thomas Mencken (1880–1956) (Mencken 1925.)

1.1 Locy's vision

A string of spectacular *firsts* occurred in America in the year 1908. They included Wilbur Wright's 1000-feet flight at Kitty Hawk in North Carolina and Henry Ford's mass-production of the Model T Ford. It was in that heady atmosphere of supreme confidence in the future that the first edition of *Biology and Its Makers* was published by William A. Locy, Professor of Biology at the Northwestern University of Illinois, USA (Locy 1908.) The following quote is from the third edition of the book (Locy 1923, p. 274.)

"It is easy, looking backward, to observe that the period between 1840 and 1860 was a very important one for modern biology. Many new ideas were coming into existence, but throughout this period we can trace distinctly, step by step, the gradual approach to the idea that protoplasm, the living substance of organism, is practically the same in plants and in animal. Let us picture to ourselves the consequence of the acceptance of this idea. Now for the first time physiologists began to have their attention directed to the actually living substance; now for the first time, they saw clearly that all future progress was to be made by studying this living substance — the seat of vital activity. This was the beginning of modern biology."

1.2 One hundred years later

One full century has passed since Locy's visionary forecast. And, it was an extraordinary century — the bloodiest in the entire human history. Among the wreckage was the once exciting enthusiasm for, and heart-felt trust in science.

Some believe that we are on the way to another Dark Age. Others, including myself, believe that we are just very slow in shedding our violence-prone tribal past and in replacing it with a more inclusive and gentler set of ethical guidelines for the coming generations. That important advances have been achieved, notwithstanding, in what once were beyond the wildest dreams gave us hope.

Thus, protected from the devastation of wars by two immense bodies of water, some Americans have recaptured enough optimism, resources and energy to continue the spectacular scientific achievements of the past. They did that in landing Men on the Moon, in deciphering the human genome and in inventing the computer science and industry.

Unfortunately, or on the surface at least, it was an altogether different story in the direction of progress that matters most to our kind. Namely, the understanding of life at its most basic level as symbolized by the concept of protoplasm.

1.2.1 Many lost sight of the subject

The majority of those willing and able to give an answer would say that no progress has been made on the study of protoplasm — because the concept of protoplasm was wrong.



Thomas Huxley
(1825–1895)

The Encyclopedia Britannica Online offers what it sees as the reason. “As the cell has become fractionated into its component parts, protoplasm, as a term no longer has meaning.” (Encyclopedia Britannica Online.)

As it stands today, none of the standardized biology textbooks even mention the word, protoplasm. On the contrary, all the high school and college biology textbooks teach as established truth the *membrane (pump) theory* — completely oblivious of the fact that this theory had been ***thoroughly and unequivocally disproved more than forty years ago*** (Ling 1962, Chapter 8; Ling 1997a; Ling 2006a; Ling 2007.)

Meanwhile, fundamental science in general and biological science in particular have been undergoing a progressive fragmentation. In the words of Will Durant in his *History of Philosophy*: “*We suffocated with uncoordinated facts, our minds are overwhelmed with science breeding and multiplying into speculative chaos for want of synthesis and a unifying philosophy*” (Durant 1926-1961, p. 91.) (At this point, I would like you to take note of this quote. I will come back to it shortly.)

With continued fragmentation, scientists have been engaged in learning *more and more on less and less*. As an illustration, we now know the value of π to 1.24 trillion places (Kanada 2002.) At the same time, **the brightest and the most knowledgeable among us seem unable to tell what life is.**

True, physicist Irwin Schrödinger once wrote a highly popular booklet on *What Is Life?* (Schrödinger 1944.) It has been reprinted at least eighteen times. Nonetheless, Schrödinger did not answer the question he posed in the title. (See Ling 1994, p 194, line 20.) Francis Crick of the DNA fame, admitted in his book, *Life Itself, Its Origin and Nature*: “***It is not easy to give a compact definition of either ‘life’ or ‘living.’***” (Crick 1981, p. 49.) In my opinion, Crick’s difficulty might be linked to the near-universal adoption as established truth of the membrane (pump) theory of the living cell. Being an unusually conscientious person, perhaps he could not bring himself to say that the physical basis of life is a continuous phospholipid bilayer with big pores for big ions, small pores for small ions in addition to countless non-energy-consuming, magic pumps (see Ling 1997a, p. 130.)

If you accept my interpretation of why Crick could not or would not tell us what life and living are, you would be in a stronger position to grapple with another even more startling revelation. Namely, why historian Thomas Hall chose to conclude his highly valuable monumental treatise on: *Ideas on Life and Matter* with the remark, “***maybe there is in fact ‘no such thing’ as life***” (Hall, 1969 Vol. 2, p. 376.)

Thus on the surface at least, fragmentation might have played a role in blurring the line between what is important and what is not. There is a fear that in blurring what is important and what is not, fragmentation might have taken away the long-range purpose of, and hence justification for continuing public support for scientific research. Unfortunately, this is more than the product of my personal habit of worrying too much about the future.

Forty leading scientists and science philosophers lent themselves to be interviewed on their views of the current status of science by John Horgan, a reporter of the magazine, *Scientific American*. This forty include physicists (Freeman Dyson, Murray Gell-Mann, Hans Bethe, Stephen Hawkins, Richard Feynman,) chemists (Francis Crick, Ilya Prigogine, J. D. Bernal,) biologists (Stephen Jay Gould, John Eccles,) and science philosophers (Thomas Kuhn, Paul Feyerabend and Karl Popper.) It seems reasonable to assume that each of the forty scientists agrees in principle with the essence of what Horgan wrote

in his book summarized in the book's title, *The End of Science* with the subtitle, *Facing the Limits of Knowledge in the Twilight of the Scientific Age* (Horgan 1996.)

1.2.2 A few see a hidden path to a great future

Then, I took issue publicly with the central theme of Horgan's book. (Ling 2001, p. iii.) I pointed out that as far as life science is concerned, what was actually ending was not life science itself but a universally-taught but erroneous theory — the membrane (pump) theory. This theory began as an honest mistake. It immediately got into the (German) textbooks. In time, it became a sacred cow, immune to the dictate of logic and contradicting scientific evidence — up to this moment at least.

That said, we are at last ready to unveil an alternative answer to the question posed earlier: What progress has been made in the study of the living substance since Locy made his visionary remark?

According to a minority view, fragmentation of an immature science is a highly wasteful mishap that should be avoided whenever feasible. However, in the development of a science as complex and deep as cell physiology, fragmentation might have been inevitable as a transient stage toward a final happy ending.

Thus to learn walking, a child must try one step at a time and take lightly the stumbling and falls that come with the early efforts. Every child seems reassured by a belief that one-day he (or she) will be able to walk like his (or her) parents. By analogy, the reassurance needed to see in the fragmented study of cell physiology a purpose other than merely the beginning of the end, is a similar belief that *one day we will be able to put Humpty Dumpty together again.*

The belief that we will be able to put Humpty Dumpty together again is shared among a few cell physiologists. They are onto something that is still unknown to the vast majority of biomedical scientists and teachers worldwide. Indeed, that something is nothing other than what Durant referred to as (missing) a unifying philosophy — aka **a unifying theory** — which could reverse the trend toward ending to that of a new beginning. That unifying theory bears the name, the **association-induction hypothesis**.

As the only surviving unifying theory, the association-induction hypothesis has gone a long way in establishing the validity of the concept of protoplasm — but under a definition quite different from those offered earlier (see below.) Nonetheless, that new definition could be seen as growing out of the seeds that Dujardin, von Mohl, Max Schultze, Thomas Huxley and their likes had planted. You will discover below how those seeds become alive again on the addition of water.

With a happy ending assured, one could then look at the past fragmentation for what it really was, at once bad and good. Bad because it is highly wasteful. The good side of fragmentation includes the physical fragmentation of living cells into smaller and smaller pieces and subjecting them to all kinds of harsh treatments so that in the end, we could isolate its components in *pure* forms. Among them, the most important are the proteins and their component parts, the α -amino acids.

Table 1, compiled by Professor Ross Gortner (1885–1942), provides a brief summary of the discovery of the twenty α -amino acids (Gortner 1938.) From leucine by Proust in 1818 to nor-valine by Abderhalden and Bahn in 1930, it took 112 years of hard work, intelligence and skill to discover, to isolate and to determine their chemical structures. Together, the 20 essential α -amino acids make up most proteins — in a way not unlike how

TABLE 1. The history of the discoveries of the amino acids.
(from R.A. Gortner 1938)

THE NATURALLY OCCURRING AMINO ACIDS (The existence of a few of these amino acids is doubtful, as noted by "?")		
Year	Common Name and Scientific Name (When Known)	Discoverer
1818	Leucine, β -iso-propyl- α -amino-propionic acid	Proust
1820	Glycine or glycocoll, α -amino-acetic acid	Braconnot
1846	Tyrosine, β -(<i>p</i> -hydroxyphenyl) α -amino-propionic acid	Liebig
1865	Serine, β -hydroxy- α -amino-propionic acid	Cramer
1868	Aspartic acid, α -amino-succinic acid	Ritthausen
1868	Glutamic acid, α -amino-glutaric acid	Ritthausen
1875	Alanine, α -amino-propionic acid	Schützenberger and Bourgeois
1877	Ornithine, α - δ -diamino-valeric acid	Jaffe
1883	Phenylalanine, β -phenyl- α -amino-propionic acid)	Schulze
1889	Lysine, α - ϵ -di-amino-caproic acid	Drechsel
1895	Arginine, α -amino- δ -guanidino valeric acid	Hedin
1896	Histidine, β -imidazole- α -amino-propionic acid	Kossel
1896	Iodo-gorgonic acid, 3,5-di-iodo tyrosine	Drechsel
1899	Cystine, β - β' -di-thio-di-(α -amino propionic acid)	Mörner
1901	Tryptophane, β -indol- α -amino-propionic acid	Hopkins and Cole
1901	Proline, pyrrolidine- α -carboxylic acid	Fischer
1901	Cysteine, α -amino- β -thio-lactic acid	Emden
1902	Hydroxy-proline, hydroxy-pyrrolidine- α -carboxylic acid	Fischer
1904	Caseanic acid, $C_{12}H_{24}N_2O_8$ (?)	Skraup
1904	Diamino-tri-hydroxy-dodecanoic acid, $C_{12}H_{26}N_2O_8$ (?)	Fischer and Abderhalden
*	Dodecan-diamino-di-carboxylic acid, $C_{12}H_{24}N_2O_4 \cdot H_2O$ (?)	Fränkel and Friedmann
1905	Iso-leucine, β -methyl- β -ethyl- α -amino-propionic acid	Winterstein
1906	Valine, α -amino-iso-valeric acid	Fischer
1907	Hydroxy-tryptophane [position of ($-\text{OH}$) uncertain (?)]	Ahderhalden and Kempe
*	β -Bz.-hydroxy-Pr.-dihydro-indolyl-alanine (?)	Abderhalden and Sickel
1924	β -alanine, 8-amino-propionic acid	Engeland
1908	Nor-leucine, α -amino- <i>n</i> -caproic acid	Abderhalden and Weil
1913	α -aminon. butyric acid	Foreman
1913	Dopa, 3,4-di-hydroxy-phenylalanine	Guggenheim
1913	3,5-dibrom-tyrosine	Mörner
1914	Citrulline, α -amino- δ -carbamido-valeric acid	Koga and Odake (Wada, 1930)
1918	β -hydroxy-glutamic acid	Dinkin
1919	Thyroxine, β -(3,5,3'5'-tetra-iodio-4'-hydroxy-di-phenyl-ether)- α -amino-propionic acid	Kendall
*	Methionine, γ -methylthiol- α -amino-butyric acid	Mueller
1922	Hydroxy-lysine	Schryver
1925	$C_4H_11O_3N$ (?)	Gortner and Hoffman
*	$C_4H_9O_3N$, hydroxy-amino-butyric acid	Schryver and Biston
1926	Treonine, β -hydroxy- α -amino-butyric acid	Rose
1935	Hydroxy-valine	Schryver and Biston
1926	Canavanine, α -amino- γ -hydroxy-guanidino-butyric acid	Kitagawa and Torniyama
1929	Norvaline, α -amino- <i>n</i> -valeric acid	Abderhalden and Bahn
1930	Cannline, α -amino- γ -(<i>o</i>)hydroxylamino-butyric acid	Kitagawa and Yamada
1932	Djenkolic acid, <i>l</i> -cysteine-thiolformacetal	vnn Veen and Hijman

* The compounds within the bracket are probably identical.

the 26 letters of the alphabets make up the English language. This monumental collective work — like countless others, now-nearly forgotten but invaluable past achievements in science — set the stage for a momentous forward leap.

That forward leap was achieved almost single-handedly by the great German chemist, Emil Fischer. It was Fischer who worked out the structure of proteins — and their “backbone”, the polypeptide chain, which he named in the same memorable year, 1908 mentioned earlier (Fischer 1906, 1908.)

A hundred years hence, it is time for us to put the isolated proteins back to where they came from, the living cells. However, to initiate that task, we need the help of yet another scientific giant, the Austrian mathematician and physicist, Ludwig Boltzmann (1844–1906.)

Boltzmann invented the new branch of physics called *Statistical Mechanics*, which links the properties and behaviors of microscopic atoms and molecules {in dimensions measured in Angstrom units (10^{-8} cm) or nanometers (10^{-7} cm)} to the macroscopic properties and behaviors of matter, living and dead {visible to the naked eye with or without a light microscope, in microns (10^{-4} cm.) or still larger.} How unspeakably tragic it was that hurt and depressed by the unrelenting rejection of his peers, Boltzmann took his own life at the age of sixty two. Ironically, among those who opposed Boltzmann was physical chemist, Wilhelm Ostwald (1853–1932) who had played a key role in the development of the ill-fated membrane theory (see Ling 2007.)

Thus, through the genius, the dedication and unspeakable personal sacrifices of the brightest of our kind, basic physics and chemistry have at last reached the necessary maturity — by the time my generation of cell physiologists arrived on the scene. As a result, the study of protoplasm as an integral and coherent entity could start to move forward once more. And with it, came a new definition of life that is in full harmony with the laws that govern the dead world as well. (Ling 1962, p. xxii; Ling 1969; Ling 1984, p. 147; Ling 1992, p. 31; Ling 2001, pp. 148–156.)

2. The association-induction (AI) hypothesis

The unifying theory called the association-induction hypothesis began in an embryonic form over 50 years ago under a name given later: “Ling’s Fixed Charge Hypothesis” (Ling 1952.) It completed itself with the addition of the Polarized-Oriented Multilayer (POM or PM) theory of cell water thirteen years later in 1965 (Ling 1965.) The main theme of the theory, however, was presented in 1962 in a book entitled *A Physical Theory of the Living State: the Association-Induction Hypothesis* (Ling 1962.)

Statistical Mechanics is not required for a Ph.D. degree in the physiological sciences or for a M.D. degree but (elementary) Statistical Mechanics is an integral part of the AI hypothesis. For this reason, the first chapter of my 1962 book is on basic Statistical Mechanics (in



Emil Fischer
(1852–1919)



Ludwig Boltzmann
(1844–1906)

association and dissociation phenomena.) At the end of this chapter, I also recommended three textbooks on Statistical Mechanics: one by Gurney (1949), one by Rushbrooke (1949) and another one by Fowler & Guggenheim (1939.) For those biologists with no prior training in this branch of physics, Ronald Gurney's *Introduction to Statistical Mechanics* was, and still is most highly recommended

2.1 Nano-protoplasm (NP), the basic unit of all living matter

Dujardin described his sarcode as “glutinous, diaphanous substance, insoluble in water that contracts into globular lumps, sticks to the dissecting needles and can be drawn out like mucus and above all are found in all lower animals between other structural element.” (Je propose de nommer ainsi ce que d'autres observateurs ont appelé une gelée vivante, cette substance glutineuse diaphane, insoluble dans l'eau, se contractant en masse globuleuses s'attachant aux arguilles de dissection et se lasissant étirer comme du mucus, enfin se trouvant dans tous les animaux inférieurs interposée aux autres éléments de structure” (Dujardin 1835.)

All these descriptions are on the *macroscopic* properties of the substance that makes up the bulk of a protozoon. Neither he, nor von Mohl, nor Max Schultze, nor Thomas Huxley could go much farther than these descriptions. Yet, to claim that the material thus characterized is the physical basis of life presents problems. For example, the cell nucleus does not look like what was described as sarcode or protoplasm. If the cell nucleus is not protoplasm, is it also not part of the physical basis of life? What then is it? This and other seemingly non-resolvable problems are readily resolved in the association-induction hypothesis.

2.1.1 Two kinds of protoplasm, one macroscopic and the other microscopic

According to the AI Hypothesis, there are two kinds of protoplasm: one macroscopic and one microscopic. Macroscopic protoplasm includes what Max Schultze and Thomas Huxley called protoplasm. In addition, it also includes what makes up the nucleus, the cell membrane and sundry other cytological structures that Schultze and Huxley did not (know or) consider as protoplasm.

In the AI Hypothesis, macroscopic protoplasm remains the physical basis of life at a higher level, just as the cells are also the physical basis of life at an even higher level. Neither all macroscopic protoplasm nor all living cells look alike, for the same reason that men and women don't look alike but are both humans. This is so, because outer appearance is only a part of their human characteristics. The characteristics that men and women do share are deeper. All macroscopic protoplasm, like all living cells also share something at a deeper, more basic level.

In the AI Hypothesis, that something deeper and at a more basic level is embodied in the *microscopic protoplasm*. In the past, I have referred to microscopic protoplasm as a *biological fixed charge system* (Ling 1962, p. 53.) or an *elementary living machine* (Ling 2001, p. 152.) I now give it a new name. This new name is ***nano-protoplasm*** or **NP** for short.

2.1.2 Describing a typical nano-protoplasm unit

To introduce a typical example of what I call ***nano-protoplasm***, I start out with a mature mammalian red blood cell like the two shown in Figure 1. First, a mature mammalian red blood cell (or rbc hereafter) has no nucleus. That absence has simplified my introductory

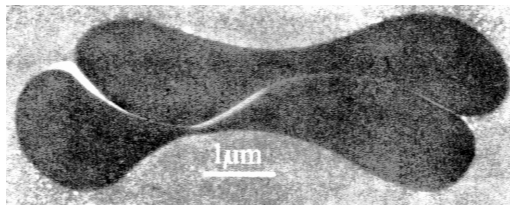


FIGURE 1. Electron micrographs of the cross-sections of two mature human red blood cells (in blood plasma.) Cryofixed, freeze-dried and embedded in Lowicryl. (Gift of L. Edelmann, 2007)

presentation. Thus, using the language of Max Schultze, each rbc is no longer a lump of protoplasm with a nucleus, but a lump of protoplasm, period. But a mature rbc's appealing simplicity goes beyond the lack of a nucleus.

Fully 65% of the weight of each rbc is water. Of the remaining 35% dry matter, 97% comprises just *one* single protein, hemoglobin. That too is an unusual simplicity in another dimension.

To be counted amongst the remaining 1% of a rbc's makeup is about 100 millimoles of the potassium ion (K^+) per kilogram of fresh cells and even lesser amount of organic products of energy metabolism, including adenosine triphosphate (ATP) and 2,3-disphosphoglycerate (2,3-DPG) (Ponder 1948, pp. 119–121.)

A third simplicity is the lack of visible structure inside a mature red blood cell. Even under an electron microscope, the entire inside of the cell appears homogeneous as demonstrated in Figure 1.

Then, there is a fourth kind of simplicity: its stability. A mature mammalian red blood cell can be mechanically divided into the finest pieces without liberating its hemoglobin (Best and Taylor, 1945, p. 7.)

Taking advantage of all these engaging attributes of a rbc, one can use an imaginary knife and cut a rbc into smaller and smaller pieces until finally each piece is left with just one hemoglobin molecule. In addition, each piece also contains some seven thousand water molecules, twenty K^+ , a single molecule of ATP or 2,3-DPG, all directly or indirectly attached to the single hemoglobin molecule. Together, they make up a ***nano-protoplasm*** unit of rbc cytoplasm. Like a flock of flying geese, or a military regiment in war, it is a *dynamic structure*. Whereas the individual elements come and go, a formula, $(Hb)_1 (H_2O)_{7000} (K^+)_20 (ATP)_1$ describing their overall composition stays more or less constant. In a following section, a more general formula for all nano-protoplasms will be given.

Now, 34% of the weight of each mature mammalian rbc is hemoglobin. Thus, in each liter of rbc, there are 340 grams of this protein. Dividing 340 by its molecular weight, 68,000 daltons, one obtains the concentration of hemoglobin in one liter of rbc: 5 mM. Since each unit of nano-protoplasm (or NP unit) contains one hemoglobin molecule, the concentration of NP units in one liter of rbc is also 5 mM. If one assumes that each nano-protoplasm unit is spherical, its diameter would be 8.6 nano-meters (nm.) This affirms calling the smallest unit of life, nano-protoplasm.

Figure 2, taken from my first book mentioned above (Ling 1962), shows that other normal living cells are similar to the rbc in the broad categories of their chemical makeup. Water is invariably the most abundant, proteins the next and ions and smaller molecules (lumped under ash) make up by far the least abundant. (Note that in the bar graphs of Figure 2, the column of ash has been multiplied by a factor of 10.)

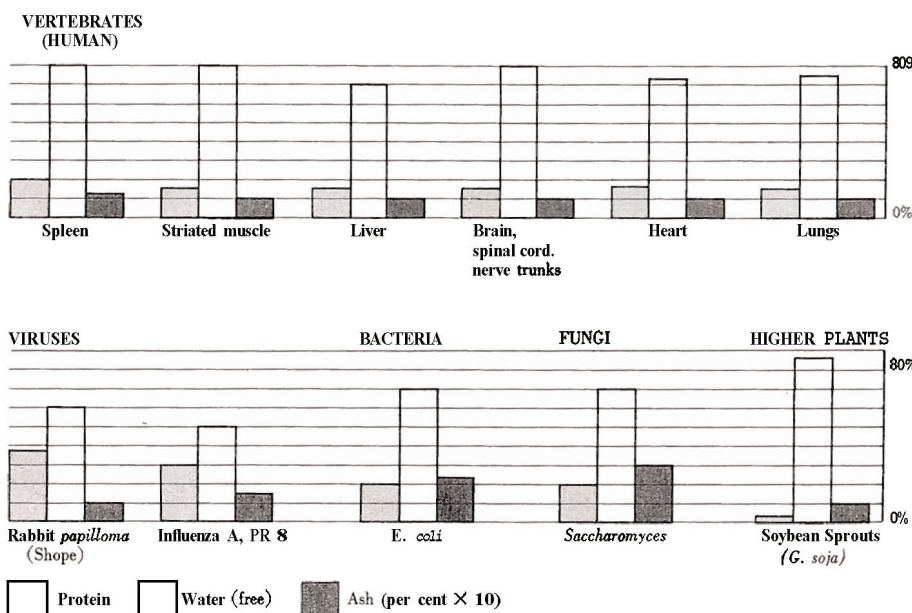
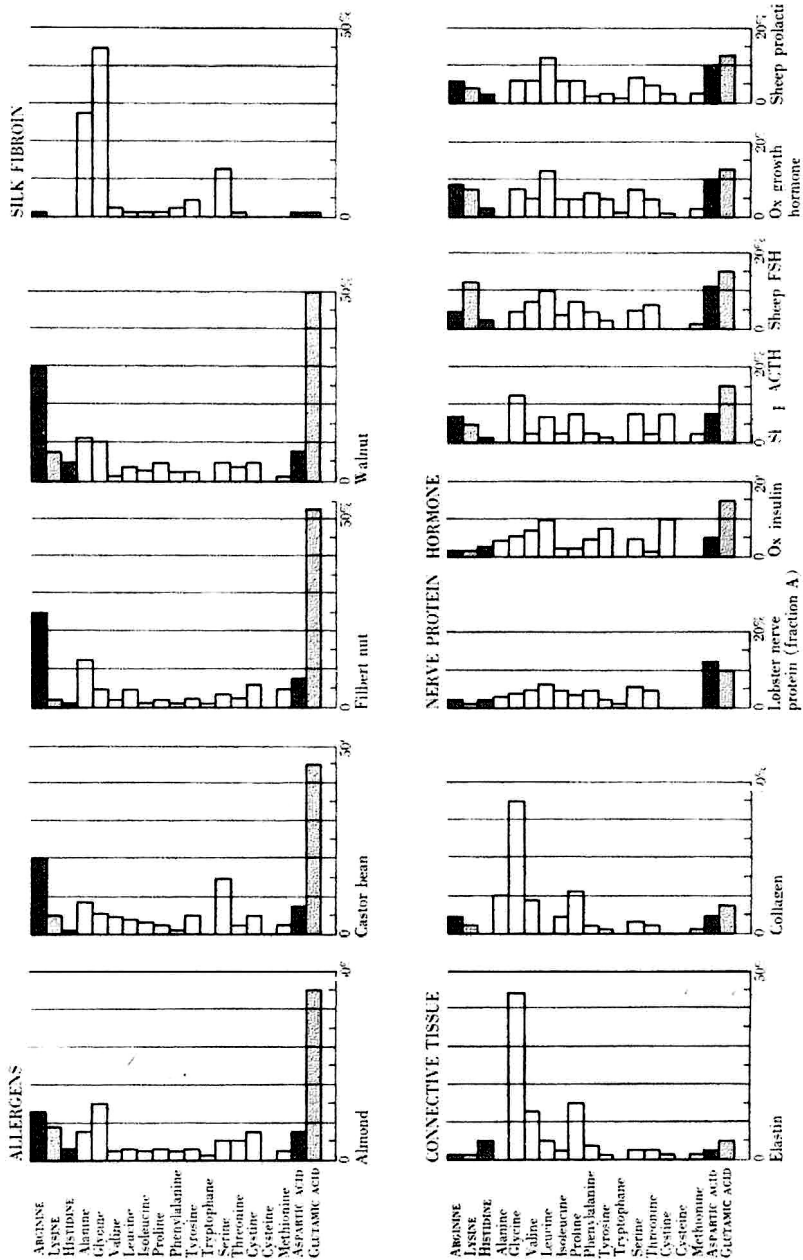


FIGURE 2. The weight percentage of proteins, water and salts in representative species of different phyla of living beings. (Data on virus, bacteria, fungi and higher plants from Spector 1956. Data on humans from Mitchell *et al.*, 1945.) (from Ling 1962)

Figure 3, also from my 1962 book, shows the similarity among the proteins forming the living matter. That is, *physiologically active* proteins (in contrast to supportive proteins like silk fibroin, elastin) contain high percentages of two categories of tri-functional amino-acid residues: (i) aspartic acid and glutamic acid residues, which when incorporated into a protein molecule, endow the protein with (fixed) negative electric charges or *fixed anion* in the form of β -, and γ -carboxyl groups respectively; (ii) lysine and arginine (and histidine), which when incorporated into a protein could endow the protein (fixed) positive electric charges or *fixed cations* in the form of ϵ -amino and guanidyl groups respectively.

On the contents of fixed anions and fixed cations, physiologically active hemoglobin is no exception. 11% of its amino acid residues bear fixed anions and an approximately equal percentage (10 %) of the amino acid residues bear fixed cations (Dayhoff 1972, vol. 5, p. D-61, D-72.)

As mentioned earlier, each NP unit may contain just a single protein molecule characteristic of that particular protoplasm like the rbc cytoplasmic protoplasm described above. In more complex protoplasm, each NP unit may contain two or more protein molecules of different kinds and number. In that case, the protein moiety of the NP unit shown as $(Hb)_1$ in the formula given earlier would be replaced by the formula, $(A_1 B_m C_n \dots Z_1)$, where each of the symbols, A, B, C...Z represents a different component protein and the subscripts, l, m, n etc. are positive integers except the last protein component Z in which the subscript is always 1 (one). Appropriate changes in the subscripts of the other moieties like water, K^+ etc. from that given in the formula are of course included. We then have a general formula for all nano-protoplasm as follows:



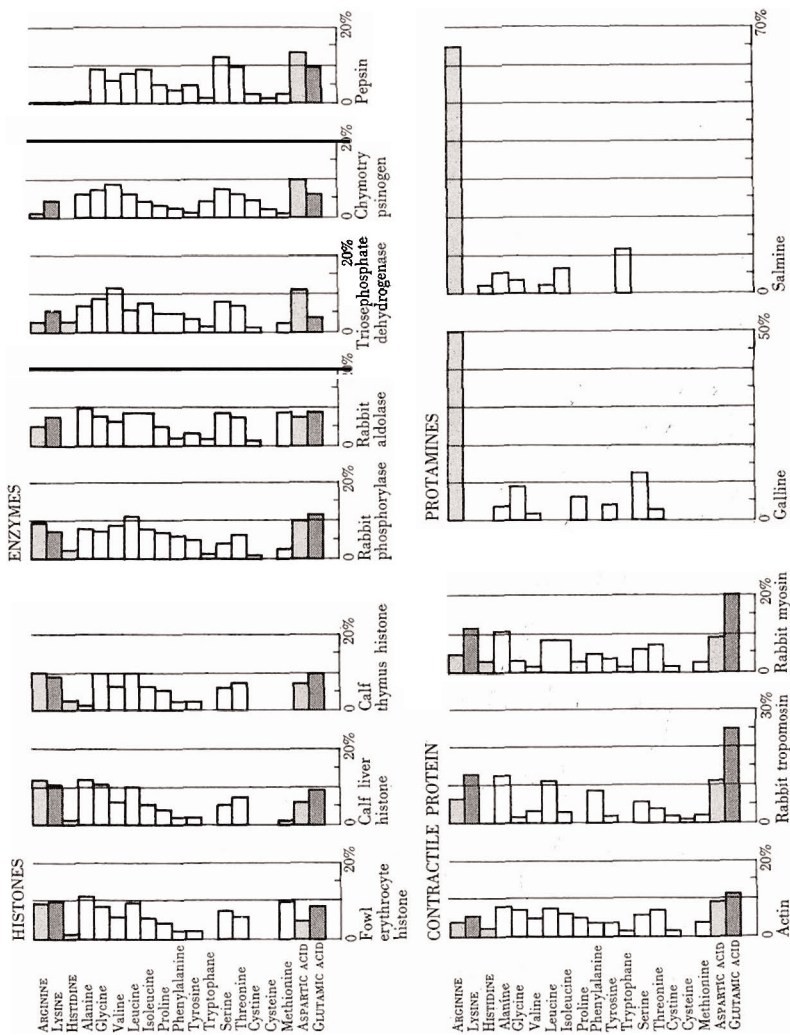


FIGURE 3. The amino acid composition of some representative proteins. Data given as percentages of total number of amino-acid residues. (from Ling 1962)

$$\text{nanoprotoplasm} = (A_1 B_m C_n \cdots Z_1) (H_2 O)_{ax1000} (K^+)_{bx10} (ATP)_c , \quad (1)$$

where a, b, c and l, m, n are all positive numbers.

2.1.3 What all nano-protoplasm share; what make some nano-protoplasm distinct

All proteins contain a long polypeptide chain, which is one of the unique products of the living machine. When fully-extended it can cover a long distance. As mentioned above, protoplasmic proteins as a rule contain a substantial percentage of their amino-acid residues that carry fixed anions in the form of β -, and γ -carboxyl groups. They also carry fixed cations in the form of ϵ -amino and guanidyl groups. As will be further made clear below, fixed β -, and γ -carboxyl groups are especially important for at least two reasons. First, they are carried on short side chains and thus close to the polypeptide chain serving as the highways of information and energy transfer. Second, β -, and γ -carboxyl groups are by far more numerous than any other functional group except the backbone NHCO groups. Add to all these, an abundance of water and the K^+ (and Na^+) and ATP, you have the chemical makeup of a typical nano-protoplasm.

In summary, the fundamental characteristics shared by all nano-protoplasm arise from their universal possession of (1) a long and a partially resonating polypeptide chain; (2) two kinds of proximal functional groups: the β -, and γ -carboxyl groups and the backbone NHCO groups and their access to alternative partners, K^+ , Na^+ or fixed cations (for the β -, and γ -carboxyl groups) and CONH groups belonging to the third amino-acid residues up and down the polypeptide chain or massive number of water molecules (for the backbone NHCO groups) and (3) the universal presence of principle, auxiliary and pseudo-cardinal sites and the right kind of cardinal adsorbent for each of them.

The dynamic structure of all nano-protoplasm is built upon a shared collection of chemical entities spelled out in the general formula given in equation 1 and by the shared spatial and energetic relationship among these basic components as diagrammatically illustrated in Figure 5. However, the underlying fundamental details that the images of Figure 5 can not tell us will be presented in sections to come. Before that, we need to look into some of the causes for the nano-protoplasm's diversity.

The distinction amongst different nano-protoplasms comes mostly from the type and sequential order of the amino-acid residues of their protein components. It also arises from the various attachments on the proteins (e.g., heme makes rbc nano-protoplasm red; chlorophyll makes chloroplast green.) Another source of diversity is the different location that a nano-protoplasm unit occupies in the cell. Still another source of diversity lies in the way these components *associate* with one another in space and in energy. Indeed, the difference between a *cooked* lobster and a *living* man who eats the lobster — as pointed out by the Scotch philosopher, James Stirling in his (historic) critique of Thomas Huxley's physical basis of life, — is the life-and-death question to be addressed in a following section. In the process, I shall spell out the new definition of life that I promised on an earlier page.

2.2 A definition of life at the nano-protoplasm level: as existence at the *resting living state* and reversible switching to the *active living state* (or irreversibly to the *dead state*)

I shall introduce this section on the energy and entropy profile of the nano-protoplasm with a simple inanimate model. First introduced in 1969 and illustrated with a figure that

is partly reproduced here as Figure 4, it is called the *nail-iron filing-magnet model* (Ling 1969, p. 37.)

The core of this model is a chain of soft-iron nails joined end-to-end with bits of string. Strewn around this chain of nails is a bed of iron filings. We now start the demonstration by bringing in the third component of the assembly, a horseshoe magnet. I then apply one end of this magnet to one terminal nail of the nail chain. As a result, the first nail would be magnetized, which in turn magnetizes the next one and this continues until all the nails in the chain will assume a more rigid magnetized state. Furthermore, these magnetized nails will have in the process picked up the randomly scattered iron filings, forcing them also to assume a less random but more orderly distribution.

In thermodynamic terms, the horseshoe magnet had brought about a spreading attractive (negative) energy among the neighboring nails and iron filings. In addition, it has also brought about a loss of the randomness or entropy of both the nails and iron filing. So, the overall consequence of the interaction with the horseshoe magnet is to change the whole system from a state of lower (negative) energy-higher entropy to a state of higher (negative) energy and lower entropy. Next, we compare this inanimate model with a diagrammatic illustration of a living nano-protoplasm unit shown in Figure 5.

The *nano- protoplasm* illustrated in Figure 5 and the nail-iron filing-magnet model shown in Figure 4, share basic similarities. Thus, like the horseshoe magnet, the controlling agent ATP (see p. 136 below for a more detailed description) also produces a



FIGURE 4. The nail-iron filings-magnet model. (from Ling 1969, by permission of Academic Press)

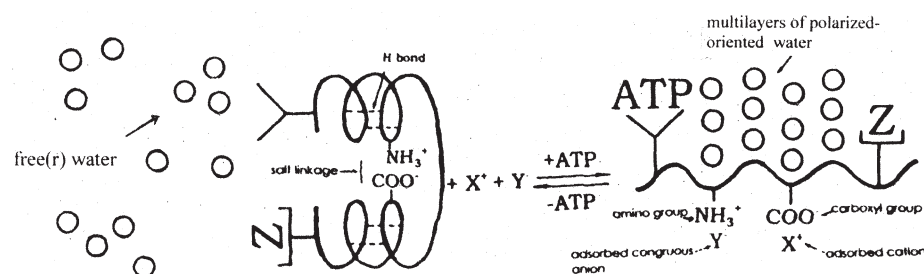


FIGURE 5. Diagrammatic illustration of all-or-none transition between the folded and the fully-extended state of a nano-protoplasm unit. (Modified version of Figure 44 in Ling 2001)

spreading (negative) energy and entropy impact on the surrounding water molecules and K⁺. Only here, we call the nano- protoplasm in the high (negative) energy-low entropy state, the *resting living state*. And we call the corresponding low (negative) energy and high entropy state either the *active living state* or the *dead state*, with reversibility characterizing the *active living state* and irreversibility characterizing the *dead state*.

Like that in its inanimate counterpart, the nail-filing-magnet model, the transition between the two alternative states is all-or-none, a phenomenon to be described more rigorously on page 140 below.

Existence in the resting living state is the definition of *living* or *being alive* in the AI Hypothesis. Reversible switches between the resting living state and the active living state constitute *life activity*. *Being alive* (or *living*) and engaging in *life activities* are the two aspects of life — a concept in fundamental harmony with earlier concepts traced all the way back to that offered by Aristotle, by Democritus, by Hippo and later by Lamarck and Lepeschkin (Ling 2001, p 271.)

In the following section I shall discuss in more detail the distance-spanning molecular structure that life alone produces, the *polypeptide chain*. I shall also briefly mention how the polypeptide chain plays the central role in maintaining the resting living state and in life activities.

2.3 The polypeptide chain — life's "highway" of information and energy transfer

The smallest molecule that contains a peptide bond (CONH) and thus may be seen as a model of the building block of all polypeptide chains and proteins is N-methylacetamide. In 1950, Mizushima and his coworkers showed that the bond joining the N and C atoms in this molecule is much shorter than a normal N-C single bond (Mizushima *et al.* 1950.) This bond-length shortening indicates that there is *resonance* or extremely fast changes between the two alternative structures shown below:



As a result of this resonance, the CN bond is 40% double bond and 60% single bond (and it assumes a flat or planar configuration.)

This partial double-bond nature of the peptide CN bond and the resonance that produces it contribute to the high polarizability of the polypeptide chain. In the AI Hypothesis, this high polarizability enables the polypeptide chain to serve its unique function in information and energy transfer over distances (Ling 1962, p. 93.)

Now, let us consider two nearest-neighboring β-, or γ-carboxyl groups on a polypeptide chain. They are separated from each other by a length of the polypeptide chain, plus two short segments of methylene (-CH₂-) groups. Transmission of inductive effect through methylene groups, (-CH₂)_n, is less efficient than transmission through the polypeptide chain, even though transmission through each methylene group is usually given as high as 0.333. Other investigators offer an even higher transmissivity of 0.48 (Taft 1953; Ling 1964a; Ling 1984, p.189.)

The high polarizability of the polypeptide chain provides the basis for what I suggested in 1962 of two kinds of transmission mechanisms along protein chains, called respectively

the *Direct F-effect* and the *Indirect F-effect* (Ling 1962, pp. 92-102.) A simple F-effect, on which these new terms are based, represents the combined inductive effect or I-effect transmitted through the intervening atoms and the direct or D-effect transmitted through intervening space (Hermans 1954.)

A direct F-effect is that between an agent that acts on one part of the protein chain and a target group on another part of the same (or different) protein chain a distance away. As such, the direct F-effect is static. So far, we have gathered at least four sets of independent evidence substantiating the far reach of the Direct F-effect. To wit, they could cover as far as a chain of three peptides and a short methylene groups on both ends of the chain.(See Ling 1992, p. 132; Ling 2001, p.161.)

The Indirect F-effect is built upon a sequence of Direct F-effects. Toward the end of Section 2.1, I pointed out the striking importance of the β -, and γ -carboxyl groups due to their ability to adsorb alternative ions, their abundance in physiologically active proteins (Figure 3) and their proximity to the polypeptide chain. It is now the time to remind the reader that like the β -, and γ -carboxyl groups, the backbone NHCO groups also serve as adsorption sites for different adsorbents but are even closer to the polypeptide chain — being parts of it. Now, we are ready for a brief introduction on how the Indirect F-effect achieves its goal of long-distance information and energy transmission.

Early theoretical analyses revealed that a long molecular chain of alternately positive and negative charges presents unusual capabilities. Thus, under suitable conditions, such a chain can transmit messages to infinitely far away destinations — not unlike an infinitely long train of falling dominos, only unlike the falling domino chain, which goes only in one direction, this transmission *via* the Indirect F-effect goes both directions.

In reality, the unique living structure, the polypeptide chain, is just such a system in which the alternatingly positive and negative sites are nothing other than the sequence of repeating NH and CO groups. Here, the adsorption of one pair of preferred positively- and negatively-charged adsorbents favors the neighboring pair of sites to adsorb a similar pair of adsorbents. To this kind of adsorption with favorable near-neighbor all-or-none interaction, I gave the name *auto-cooperative* interaction (Ling 1962, p. 102.) It is analogous to what is called *ferromagnetic cooperative* interaction in standard statistical mechanics language.

To understand how an auto-cooperative transition operates, we need to know first how electronic perturbation or induction can alter the preferred partner of a β -, or γ -carboxyl group — to be described next.

2.4 The c-value and selective adsorption of K⁺, Na⁺ or fixed cation on β -, and γ -carboxyl groups

In 1952 I made an iconoclastic suggestion. In contrast to the pervasive belief of full ionic dissociation everywhere, I suggested that virtually all the K⁺ in frog muscle and other cells are associated. More specifically, all the cell K⁺ are engaged in close-contact association with the β -, and γ -carboxyl groups (carried respectively on aspartic and glutamic acid residues) of the major muscle cell protein, myosin (Ling 1952, pp. 773–774; see also Ling and Ochsenfeld 1991.) Two new physical causes for this intense association were given and reproduced *verbatim* here next:

“(i) The force of attraction between ions of opposite sign in solution is opposed by the kinetic energy of the ions themselves. If one of the ions is rigidly fixed, half

of this energy is abolished, so that the ions stay on the average closer together than they would when the kinetic energy of both reacting charged particles is made negligible, as for example, in the macroscopic model of oppositely charged pith balls.

(ii) Fixation allows the close juxtaposition of a number of similarly charged ions, for the repulsive forces between them are less strong than the covalent bonds of fixation. Their individual fields thus overlap, and sum with respect to the force exerted collectively upon a free ion of opposite sign (Ling 1952, p.769.)

In years following this brief though landmark statement has been often referred to as the “principle of enhanced counter-ion association due to site fixation” (Ling 1960, p. 152; Ling 1962, p. 23; Ling 2001, pp. 48-49.) Very recently, the basic concept was expanded into a full-fledged — though still simple and easy to understand — statistical mechanics thesis and published with many illuminating experimental findings (Ling 2005.) Included is also a full analysis of how the mistaken notion of universal full ionic dissociation came into being. For readers of this paper, I strongly recommend this article, which is online and can be readily downloaded.

In consequence of (i) the full association with a fixed β -, or γ -carboxyl group and (ii) the phenomenon of *dielectric saturation* in the intense electric field immediately next to an ion (Debye and Pauling 1925,) which reduces the effective dielectric constant from 81 to near unity — the smaller (hydrated) K^+ would on the average experience a much stronger electrostatic attraction than the larger (hydrated) Na^+ (see Ling 2005, top of p.5.) The Boltzmann Distribution Law then dictates that K^+ becomes preferentially adsorbed on the fixed β -, and γ -carboxyl groups and thus selectively accumulated in the muscle (and other) cells.

The suggested electrostatic mechanism is diagrammatically illustrated in Figure 6 in Ling 1952 and reproduced in Figure 4.1B of Ling 1962, which in turn is reproduced in Appendix 1 at the end of a recently published article (Ling 2006b) in black and white and also on-line and can be downloaded without restriction

My next step was to show how selective K^+ adsorption and desorption play key roles in the information and energy transfer over distance and the information and the information and energy transfer, in turn, are essential to protoplasm functioning as a coherent system. To understand how this functional chain operates, we begin with a brief review of the classical examples of short-range *inductive effect* (Lewis 1923; Dewar 1949; Branch and Calvin 1941; Chiang and Tai 1963.)

It is well known that *acetic acid* ($CH_3 COOH$) is a weak acid, making vinegar pleasantly sour. However, no one will add *trichloroacetic acid* (CCl_3COOH) to his or her salads; it is too strong an acid for that purpose. This difference in acidity originates from the induction effect. Thus, even though both acids contain the same carboxyl group (-COOH), their acid dissociation constants or pK_a values are quite different because the remaining parts of the two acids are different. The methyl group (CH_3) of acetic acid is a strong electron donor (see Ling 1964, Figure 3 on p. 99.) As a result, the singly-charged carboxyl oxygen atom of acetic acid has a higher electron density, thus holding onto its proton (H^+) more tightly and a high pK_a . In contrast, the radical (CCl_3-) contains three highly electronegative chlorine atoms. As a result, the radical draws electrons more strongly toward itself and in consequence lowers the electron density of the singly charged oxygen atom. That, in turn, makes the oxygen atom more willing to give off its positively-charged proton (H^+), hence a lower pK_a (*ibid.*)

As such, the pK_a of an acidic group describes the *interaction* of an acidic group with a specific cation, H^+ . That interaction does not tell us much of the fundamental attributes of that acidic group — for the same reason that the knowledge that A loves B tells us little about the character of either. They could be *Tristan & Isolde* or *Bonne & Clyde*. To reach deeper into the underlying phenomenon, an *independent parameter* was needed and was introduced in 1962. It is called the *c-value*.

Rigorously defined elsewhere (see pages 120–121 including Figure 4.2 in Appendix 1 at the end of the recent paper, Ling 2006b,) the *c-value* is a quantitative parameter of the effective electron density of the singly-charged carboxyl (or other oxyacid) oxygen atom. A high pK_a value corresponds to a high *c-value*; a low pK_a value corresponds to a low *c-value*.

With the *c-value* defined, we proceeded to construct a theoretical model of a fixed oxy-acid group (like a β -, and γ -carboxyl group) and a monovalent cation (like K^+ or Na^+) plus varying number of water molecules found between them. Our purpose was to figure out how the *c-value* determines the relative adsorption energies of different monovalent cations on the fixed β -, and γ -carboxyl groups.

On first thought, it seemed more rigorous to construct a three-dimensional model. In fact, that would be at once difficult and pointless since so many *arbitrary* assumptions had to be made before one could even start. Thus, we settled for a linear model — as illustrated in Figure 6. Though the absolute numerical values eventually arrived at from this linear model cannot be taken too seriously, the *relative* values are useful and offer what all we really need.

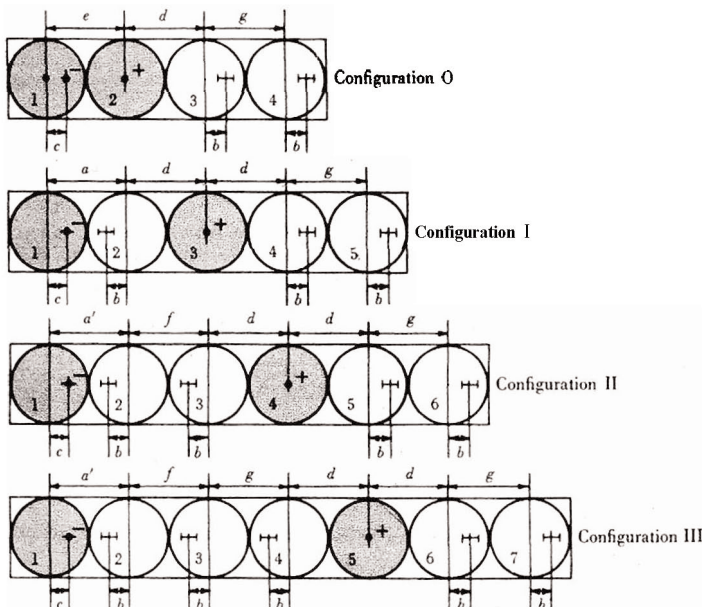


FIGURE 6. The linear model. The interaction energies were calculated from each of the monovalent cations in each of the four configurations of fixed anion and water. (from Ling 1962)

The first step in this effort was to list all the relevant laws or equations governing the theoretical components of the adsorption energies (and the numerical parameters associated with each.) All told, eight categories of energies were taken into account (see Equation 4-4 and Table 4-1 of Appendix 1 in Ling 2006b.) Thus armed, we then determined the total energies of each of the four assemblies. They each contain respectively zero, one, two or three water molecules between the interacting fixed oxyacid anion of a specific c-value and a specific cation. The specific ions studied are H^+ , Li^+ , Na^+ , K^+ , Rb^+ , Cs^+ and NH_4^+ , where NH_4^+ is also seen as a model of the fixed cation, the ϵ -amino group on a lysine residue and guanidyl group of an arginine residue and the α -amino groups at the end of a polypeptide chain. Finally, the adsorption energy of each cation at each c-value was computed by a Born-charging method described in text marked as Section B beginning on pages 134-141 of Appendix 1 in Ling 2006b.

Note that in the computations, I chose three different polarizability values for the fixed oxyacid (carboxyl) oxygen atom. Later information kindly brought to my attention by Dr. D. Reichenberg of London, led me to believe that $2.0 \times 10^{-24} \text{ cm}^3$ is the best choice and it was employed in the final result shown in Figure 7. This figure, providing the adsorption energy of each of the 7 ions at different c-values will be cited from time to time in the pages ahead. Our next task is to find out how c-value changes of the oxyacid group could be initiated at sites far away along a polypeptide chain.

However, before that story can be told, another parameter, called c'-value must also be introduced for the positive charge of a cationic group. Then we also have the equivalents of both the c-value and c'-value in dipolar groups like the CO and NH groups of the polypeptide chains. They do not carry *net* electric charge but are dipolar. Their polarity is seen only at short distances and at that range, the oxygen atom of a CO groups is negatively charged and its intensity described by what we call, a *c-value analogue*. Similarly, the H of the NH group at close range is cationic and its intensity described by a *c'-value analogue* (Ling 1962, p. 57; 2006b, p. 118.)

2.5 All-or-none shift of protein secondary structure between (i) the α -helical conformation and (ii) the water-polarizing-orienting, fully-extended conformation

Now, the incisive findings of Ambrose and Elliott — especially Elliott — have clearly established that, dissolved in a dilute water solution, each (synthetic) polypeptide assumes only one or the other of two alternative conformations. In one conformation, the NH and CO groups are oriented in the same direction as the polypeptide axis — as it should be in an α -helical fold. In the alternative conformation, the NH and CO groups are oriented perpendicular to the polypeptide axis, which can only be the fully-extended conformation (rather than the often erroneously assumed random-coil conformation.) (Ambrose and Elliott 1951; Elliott 1953; Bamford *et al* 1956, p. 101.) In broad terms, their findings lend strong support for the existence of two (all-or-none) alternative conformations of the nano-protoplasm in a water-rich environment as depicted in Figure 5.

With the advance of x-ray crystallography techniques, the three-dimensional structures of many crystalline proteins have been meticulously worked out. However, like a sharp sword, x-ray crystallography cuts both ways, good and not so good. Not so good, if one takes too seriously the “absolutes” it gives out in profusion (see p. 146 below for examples.) Good if one can extract the “relatives.” It is my best judgement that among the best “relatives” are three sets of what is known as the α -helical potentials of the different

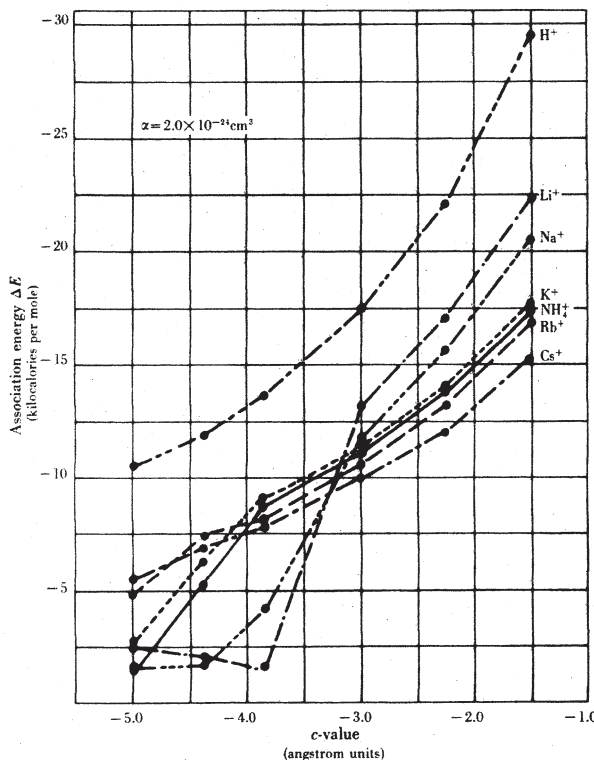


FIGURE 7. The theoretically computed association-energies in kilogram calories per mole of six mono-valent cations on a singly-charged oxyacid group with a polarizability of $2.0 \times 10^{-24} \text{ cm}^3$ and c-value as indicated on the abscissa. An ion, say K⁺, which shows a higher negative energy of association of -8.3 kcal/mole on a fixed oxyacid at a c-value of -4.0 Å is preferentially adsorbed over Na⁺, which at the same c-value shows a lower negative association energy of -3.3 kcal/mole only. However, at a higher c-value of -2.5 Å, the preference is reversed since at this point the negative association energy of Na⁺ at -16 kcal/mole is higher than that of K⁺ at -13 kcal/mole. Preference reversal at different c-values is important in physiological activities according to the association-induction hypothesis. (from Ling 1962)

amino acids published by Chou and Fasman (1978), by Tanaka and Scheraga (1976) and by Garnier *et al* (1978.)

Now, it is well known that on the peptide groups, the carbonyl (CO) group is highly polarizable while the imino (NH) group is much less so (Cannon 1955; Mizushima *et al* 1955.) Based on this knowledge, I postulated that the effective electron density of the carbonyl oxygen atom of an amino acid residue determines that residue's α -helical potential (Ling 1986.) This postulation paid off.

A positive linear correlation coefficient of +0.75 or even better has been established between each of the three (independent) sets of α -helical potential of the 20 amino-acid residues and the respective pK_a values of the corresponding carboxylic acids (e.g., acetic acid corresponds to glycine; n-propionic acid corresponds to alanine.) (Table 2)

TABLE 2. A study of the linear correlation between the α -helical potentials of 19 amino acid residues and the pK_a values of their corresponding carboxylic acids. (from Ling 1986)

	Chou and Fasman (P_α)	Tanaka and Sheraga (ω_{h,j^*})	Garnier et al. (j)	Corrected pK_a of Analogous Carboxylic Acids
Glu(-)	1.51	1.188	164	5.19
Ala	1.42	1.549	151	4.75
Leu	1.21	1.343	118	4.77
His(+)	1.00	0.535	98	3.63
Met	1.45	1.000	139	4.50
Gln	1.11	0.795	96	4.60
Trp	1.08	1.105	98	4.75
Val	1.06	1.028	100	4.82
Phe	1.13	0.727	102	4.25
Lys(+)	1.16	0.726	109	4.70
Ile	1.08	0.891	92	4.84
Asp(-)	1.01	0.481	91	4.56
Thr	0.83	0.488	60	3.86
Ser	0.77	0.336	47	3.80
Arg(+)	0.98	0.468	77	4.58
Cys	0.70	0.444	73	3.67
Asn	0.67	0.304	35	3.64
Tyr	0.69	0.262	41	4.28
Gly	0.57	0.226	0	3.75

What this positive correlation tells us is this. A strong electron donating side chain creates a higher *c-value analogue* of the residue's own carbonyl group on the polypeptide chain. The higher *c-value analogue* of the carbonyl groups in turn favors their formation of H Bonds with the third amide groups in either direction along the polypeptide chain, thereby forming the α -helical fold. On the other hand, a weak electron donating side chain creates a low *c-value analogue* of the residue's own carbonyl group. And, the low *c-value analogue* of the carbonyl group favors the assumption of the fully-extended conformation. A polypeptide in the fully-extended conformation, in turn, polarizes and orients multi-layers of water molecules — a phenomenon to be further discussed in the next section.

This successful correlation study thus shows that (a segment of) the polypeptide chain dominated by strong electron donating side chains would correspond to the left-hand side conformation of Figure 5. As such, it favors the formation of α -helical fold. In contrast, a segment of a polypeptide chain under the control of weak electron donating side chain would assume the right-hand side conformation of Figure 5. As such, it favors the assumption of the fully-extended conformation, which in turn polarizes and orients multi-layers of water molecules.

And, when the *c-value analogue* changes, the preferred conformation will change in consequence — in an all-or-none manner. This change is quite analogous to similar adsorption partner change of β -, and γ -carboxyl groups when their *c-value* change as illustrated in Figure 7 (and in the inset of Figure 11 to follow.)

In summary, we now have good evidence that the backbone NH and CO groups — like the β -, and γ -carboxyl groups — also have (two) alternative sets of partners. In one, they form α -helical H-bonds with their own backbone CO and NH groups three residues away

in either direction. In the other, they assume the *fully-extended* conformation, which polarize and orient multilayers of water molecules.

2.6 The polarized-oriented multilayer (POM or PM) theory of cell water

As mentioned earlier, how the protein chains can polarize and orient the bulk-phase cell water constitutes the last addition to the AI Hypothesis (Ling 1965; Ling 1972.) It was then called the polarized-multilayer (PM) theory of cell water. The original illustration of this theory is reproduced here without change as Figure 8. For historical and other reasons, I chose to do so even though the part of the diagram indicating the rate of declining polarization-orientation with distance away from the protein has proven too abrupt (see below.) A newer theoretical foundation of the POM theory will be presented immediately following the paragraph given in a smaller font.

In response to the introduction of a new theoretical foundation for the theory in 2003, the name of polarized multilayer theory has been changed to polarized-oriented multilayer theory of cell water — the acronym PM theory was left unchanged for a while (Ling 2003.) However, I then found out that this created confusion. So I have now decided to use the POM theory for the future. But if you should find the term PM theory, you would understand that it stands for the same theory. More recently, several reviews, all online, have been published (Ling 1965; Ling 1972; Ling 1992, pp. 69–110; Ling 2001, pp. 74–108; Ling 2003; Ling 2006, pp. 1–52.)

The new theoretical foundation of the POM theory is physics. Nonetheless, its usefulness lies mostly with biology, or more correctly, cell physiology (Ling 2003.) In the short cut I took, water molecules were considered as dipoles and were allowed to accumulate at near absolute zero temperature on what is called an *idealized NP surface* — with N standing for a negatively charged site and P standing for a positively charged site. Such an idealized NP surface represents an infinitely wide checkerboard of alternatingly positive and negative sites each uniformly 3.1 Å apart from its nearest neighboring site (Figure 9.) Results of computation show that as the distance from the idealized NP surface increases, *the water-to-water interaction energy* (E^n) does not taper off to zero. Rather, it approaches a constant value to be held from there on *ad infinitum*. That constant value (E^n) is expressed by the following equation:

$$E^n = (4\mu^2 r^3) / (r^3 - 8\alpha)^2, \quad (3)$$

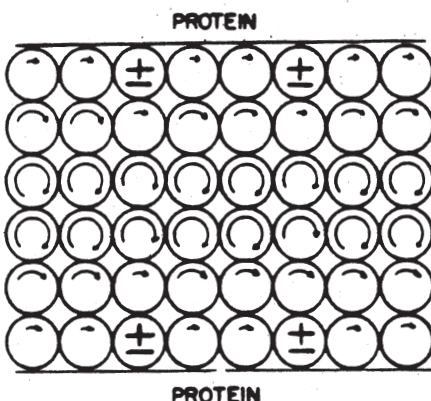


FIGURE 8. The original diagrammatic illustration of the translational and rotational motion restriction of deep layers of cell water molecules polarized and oriented by proteins. Later theoretical computations show that the relative motional freedom indicated by the size of the curved arrows in each water molecule is much flatter except at the first layer of water molecules in immediate contact with the protein polar groups. (from Ling 1965)

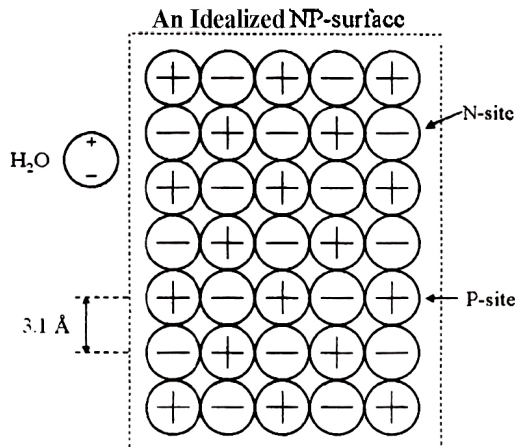


FIGURE 9. Diagrammatic illustration of an Idealized NP Surface. The distance between a pair of nearest-neighboring N (negative) and P (positive) sites is equal to the distance r between the average nearest neighboring water molecules in the liquid state at 3.1 Å. (from Ling 2003)

where μ is the permanent dipole moment of the water molecule; r is the diameter of the water molecule and α is its polarizability. Further elaboration shows that given this condition, the water cannot be frozen by any attainable low temperature. And it will not boil at a temperature as high as 451° C. Both of these theoretical predictions have been confirmed retroactively by work published fifty years ago, until now totally unexplained (Giguère and Harvey 1956; Hori 1956.)

Another important insight provided by the new POM theory is the recognition that with the exception of the water molecules in immediate contact with the NP sites (see Figure 8 in Ling 2003) the degree of polarization and orientation over longer distances are quite flat.

Now, there are no two-dimensional surfaces in living cells like the idealized NP surface or less idealized NP-surface of glass or polished AgCl prisms. Instead, it is what I call NP-NP-NP systems that function in living cells *in lieu of* an NP-NP surface (Ling 1980–1981.) Figure 10 shows diagrammatically both the top view and the side view of such an NP-NP-NP system of fully extended protein chains and water molecules they polarize and orient.

Since its introduction in 1965, the polarized (oriented) multilayer theory of cell water and model systems has been extensively tested by many investigators worldwide even though some of the work was done earlier and thus in ignorance of the theory.

A complete list of the eight physiological attributes investigated can be found on pp. 95–97 of Ling 2003, which is online and can be downloaded. Earlier summaries can also be found in Ling 1992, pp. 108–109, and in Ling 2001, p. 78. For the present review, only one physiological category of cell water will be discussed here, namely its solvency. (A recent review on a second topic, vapor sorption at near-saturation (physiological) vapor pressure can be found in pp. 25–33 in Ling 2006.)

It was first pointed out fully but briefly by Martin Fisher (Fischer 1909; Fischer and Suer 1935) and partially by Benjamin Moore and coworkers (Moore, Roaf and Webster 1912) and later elaborated in detail by A. S. Troshin (Troshin 1966, see also Equation 14 below), that a solute in a living cell can exist in two forms: (i) adsorbed on, or otherwise bound to the macromolecules, mostly proteins and (ii) dissolved in cell water. Dividing

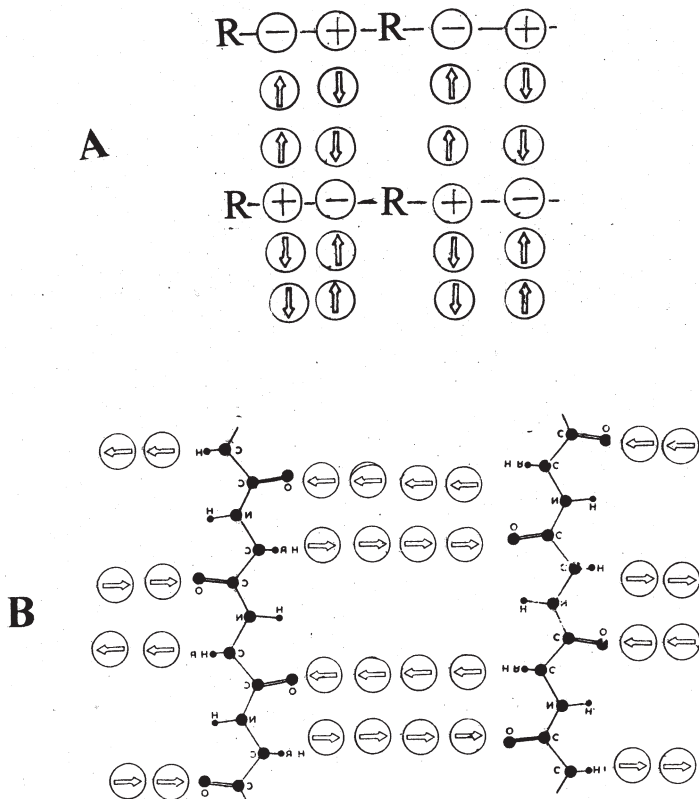


FIGURE 10. Diagrammatic illustration of what is called an NP-NP-NP system of water polarization-orientation by a matrix of fully-extended protein chains. Circles with hollow arrows inside are water molecules. A. side view; B. top view.

the total concentration of a solute in the cell by the equilibrium concentration of the solute in the surrounding medium, one obtains what is referred to in the AI Hypothesis as the *p-value* or *apparent equilibrium distribution coefficient* of that solute.

When the *p*-value of a solute is considerably higher than 1, most of the solute in the cell is adsorbed. On the other hand, when the *p*-value of a solute is near 1, most of the solute is probably dissolved in the cell water. In the latter case, the *p*-value would be close if not equal to the *true equilibrium distribution coefficient* or *q-value* of that solute.

Insight into the physical state of an intracellular solute can be obtained by plotting the intracellular (or intra-model) concentration of the solute against its corresponding equilibrium concentration in the bathing medium. If the plot appears as a straight line over a substantial concentration range, it would suggest that all or virtually all the intracellular or intra-model solute is dissolved in the intracellular water. The slope of such a rectilinear plot is then equal to the *q*-value of that solute. On the other hand, if the plot is not a straight line, most likely part of the solute is adsorbed. Section 3.2.1 below will deal with that subject in more detail.

In 1993, using Statistical Mechanical methods, I derived an equation for the q-value of a solute named the *i*th (q_i). As such, that equation is a little cumberson but it can be written in the following simpler form (Ling 1993):

$$RT \ln q_i = v_i (a \mathcal{U}_s - b \mathcal{U}_{vp}), \quad (4)$$

where R is the gas constant, T, the absolute temperature. v_i is the molecular volume of the *i*th solute in question in cubic centimeters or cc. \mathcal{U}_s is the *surface polarization energy* of one mole of water molecules in cal mole⁻¹. \mathcal{U}_{vp} is called the *exclusion intensity* for one mole of water molecules in cal mole⁻¹. a is a number in (cm)⁻¹, b is a pure number. $v_i \mathcal{U}_s$ represents the surface component of the q-value. $v_i \mathcal{U}_{vp}$ is the volume component of the q-value. The magnitude of both components depends on the molecular volume of the solute, v_i . The surface component, $v_i \mathcal{U}_s$ can be positive (favorable) or negative (unfavorable.) The volume component given as $-v_i \mathcal{U}_{vp}$ is always negative and thus acts to exclude a solute in proportion to its size. Hence the “size rule”, the larger the solute, the lower its q-value (Ling 1987.)

2.7 The AI Cascade mechanism for long range information and energy transfer

A microscopic mechanism for the long-range information and energy transfer over distance has been a part of the AI Hypothesis from its very beginning. At that time, this mechanism had been referred to off-and-on as an *indirect F-effect*. However, changes have been made in the ensuing years. To avoid confusion, I have decided recently to give it a new name, i.e., the *AI cascade mechanism*. The A and I are respectively the two first letters of the words, association and induction — acting in a reciprocating and non-attenuating cascading manner.

However, before plunging into the details, I would review briefly the classification of the controlling agents or *cardinal adsorbents*, which play key roles in the AI Cascade Mechanisms. I shall also look into the way the key cardinal adsorbent ATP controls auto-cooperative transitions.

2.7.1 Classification of cardinal adsorbents

In the AI Hypothesis, drugs, hormones, Ca⁺⁺, ATP, etc., that exercise powerful physiological activities at very low concentrations are called cardinal adsorbents.

There are three types of cardinal adsorbents. The first kind binds onto a cardinal site but produces no electronic impact and is called electron-indifferent cardinal adsorbent or EIC. The second kind binds and withdraws electrons toward itself and is called an electron-withdrawing cardinal adsorbent or EWC. The third kind binds and donates electrons and is called electron-donating cardinal adsorbent, or EDC.

As shown above in Figure 5, a very important cardinal adsorbent is ATP. This was pointed out since the very beginning of the AI Hypothesis in 1952 (Ling 1952, p. 777.) It is found in most nano-protoplasm and vital to its continued existence in the resting living state. Many nano-protoplasm units can break down ATP into ADP and inorganic phosphate. In these cases, the cardinal site for ATP might function at times as an ATPase. And by removing ATP, it could switch the nano-protoplasm from the resting to the active living state. Notwithstanding, the level of ATP in these and other cells is kept quite constant

by way of two regenerative mechanisms; (i) an enzyme, creatine kinase that can regenerates ATP at the expense of the large store of creatine phosphate in some cells (Ling 1992, p. 195); (ii) ATP is also regenerated as the end-product of glycolytic and oxidative metabolism (Ling 1977.)

(To avoid confusion, I want to mention here that once an erroneous idea called the high-energy-phosphate-bonds became widely taught (Lipmann 1941.) ATP does not contain packages of this high energy (Podolsky and Morales 1956.)

In other cases, like the ATP binding cardinal site on hemoglobin, the cardinal site does not have the latent capability of an ATPase. This fact offers a cause for the noted stability of the rbc cytoplasmic nano-protoplasm mentioned earlier.

2.7.2 A reproduced 2001 version of what is now called the AI cascade mechanism

The importance of the subject matter of this section — notwithstanding its still being in a very primitive stage of development — and the difficulty of condensing it without distorting it — led me to making a somewhat unusual decision. That is, the decision to present here an essentially unmodified model of long-range information and energy transfer that I published in my 2001 book, *Life at the Cell and Below-Cell Level*. This includes the key figure, reproduced here as Figure 11.

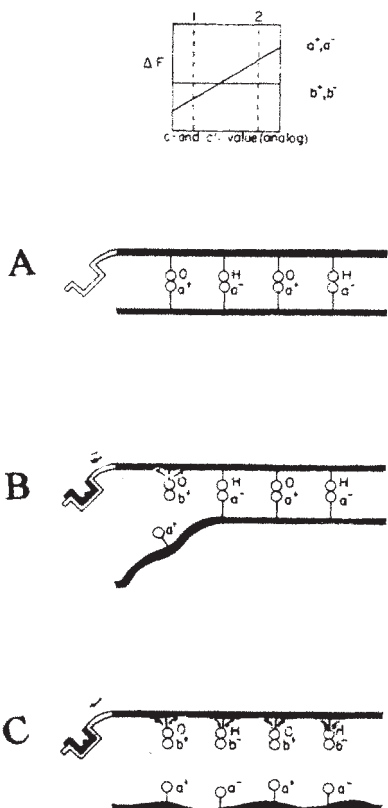


FIGURE 11. A theoretical model for the controlled auto-cooperative transition of a protein chain. The inset shows a simplified version of the relation between the association energies and the c -, c' - value analogues like those shown in Figure 7. The small arrows indicate the direction of electron migration and the counterion or H-bond partner exchanges initiated by the introduction of the cardinal adsorbent C^+ . The large arrow over the middle section shows the direction of propagated inductive changes. The middle figure indicates the intermediary steps in the auto-cooperative transformation from the initial metastable state (top) to the final metastable state (bottom.) Reversals of all steps follow removal of C^+ with intermediary steps shown in the middle figure but with all the directions of the arrows reversed. (modified from Ling 1964)

The single inset in Figure 11 illustrates the types of relationships between c-value analogue and c'-value analogue and the alternative adsorbents. At higher c- or c'-value analogue, a^+ and a^- are respectively preferred. At lower c- or c'-value analogue, b^+ and b^- are respectively preferred. Now, let us suppose that in Figure 11A, all the backbone CO groups shown as O and all the backbone NH shown as H are respectively at the high c-value analogue and a c'-value analogue of 2. In Figure 11B the adsorption of the EWC, W, at the cardinal site withdraws electrons from the nearest neighboring O site, decreasing its c-value analogue from 2 to 1. This decrease of the c-value analogue reverses the preference for a^+ over b^+ to b^- over a^- . As a result, the a^+ originally occupying the O site is replaced by a b^+ .

Now b^+ is a weaker electron-withdrawing agent than a^+ . In consequence, the displacement of a^+ by b^+ releases electrons. Some of the electrons released go back upstream toward the cardinal site-W couple, enhancing its electron-withdrawing effect. Other electrons released go downstream to the nearest H site, causing a decrease of its positive charge and hence a fall of its c'-value analogue from 2 to 1. A reversal of its preference for a^- over b^- to b^- over a^- follows, leading to the displacement of the a^- by b^- . Now b^- is a weaker electron-donator than a^- . In consequence, the displacement of b^- for a^- withdraws electrons. Some of the electrons withdrawn come from the O site upstream, further decreasing the c-value analogue of the O site upstream. Some of the electrons come from the next O site downstream, lowering the c-value analogue from 2 to 1. A b^+ for a^+ exchange follows. And the cycle repeats itself until all the a^+ and a^- are replaced by b^+ and b^- , respectively, as shown in Figure 11C.

In Figure 11 the side chains are not represented. In Figure 12 we deal with functional groups on short side chains also.

In Figure 11 we treated adsorption on the backbone O and H sites individually. In Figure 12, however, each pair of adsorbent a^+ and a^- in Figure 11, (adsorbed respectively on the CO and NH groups of peptide groups belonging to a single amino acid residue) is treated as a single entity and represented by a rectangular box **a**. Figure 12A then represents a protein segment before an EWC is taken up. Here, the electron-withdrawing power of the backbone cationic component (a^+) is represented as a downward arrow in the rectangular box, while the electron donating power of the anionic component (a^-) is represented as an upward arrow.

Figure 12B shows the same protein segment after an EWC, W, occupies the cardinal site. In consequence, the sequence of events described under Figure 11A to C takes place. As a result box B (which stands for b^+ and b^- together) displaces box A (which stands for a^+ and a^- together). Since the O site or carbonyl group (CO) is highly polarizable but the H site or imino group (NH) is less so, the electron withdrawing effect at the O site is strong and is represented as a long downward arrow in the b box. In contrast, the electron donating effect at the H site is weak and represents a short upward arrow. The net effect of displacing box a by box b is an electron-withdrawing effect. Since this electron-withdrawing effect is repeated at each CONH peptide group, every functional group on a short side chain experiences a similar electron-withdrawing influence as indicated by the downward arrow along each side chain as shown in Figure 12B.

Now a substantial number of these functional groups on short side chains are β -, and γ -carboxyl groups. A lowering of their electron density means a fall of their c-value (from an initial high value.) As a result, a monovalent cation A^+ may be replaced by B^+ . This B^+

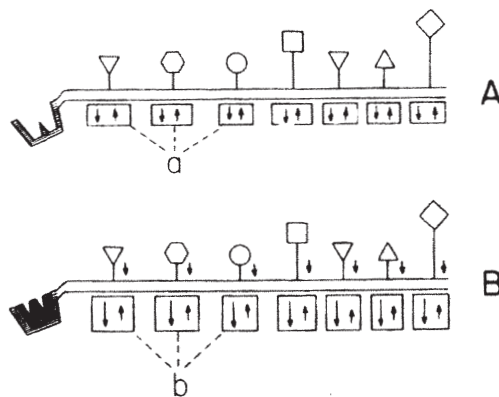


FIGURE 12. An alternative view of the model shown in Figure 11 of the controlled auto-cooperative transition between the two alternative states. Unlike the version seen in Figure 11, the side chains are shown. What are shown as individual O (OH-) and H (NH-) groups in Figure 11 are represented as a single unit and enclosed in a box. This makes it easier to understand that we can treat the pair of sites as one and their net electron-donating and electron-withdrawing activities lumped together as a net change. Thus, the boxes with equal-sized arrows pointing both upward and downward would have no influence on the side chain. After the cardinal adsorbent **W** has adsorbed on the cardinal site, the two arrows are no longer equal in size and the net result is electron-withdrawing indicated by the downward arrow on the stems of the side chains. Note that they are all of the same size, thus producing across-the-board uniform changes on all similar side chains as if they were one. (from Ling 2001)

for A^+ exchange in turn reinforces the b for a exchanges at the backbone as well as the adsorption of the EWC at the cardinal site. Taken together, the backbone sites and the functional groups on short side chains and their respective adsorption partners (a/ A^+ / etc. versus b/ B^+ / etc.) constitutes the alternative basic components of the autocooperative assembly diagrammatically illustrated in Figure 13B — and described formally in Equation 5. (Both Figure 13 and Equation 5 are to be presented below.)

In consequence of the interaction with the EWC, **W**, the backbone CO groups as well as the β -, and γ -carboxyl groups (and other functional groups on short side chains) undergo an across-the-board electron-density decrease from their initial higher values. And exchange of adsorption partners occur at both sets of sites. Conversely, with an EDC adsorbed onto the cardinal site of a protein segment, the backbone CO groups as well as the β -, and γ -carboxyl groups (and other functional groups on short side chains) may undergo an across-the-board electron density increase from their initial lower values. And exchange of adsorption partners follow at both sets of sites in the reverse direction.

On account of this coherence, one may say that the whole “gang” of cooperatively linked functional groups on short side chains and backbone carbonyl groups behave as if they were a single site. *By the same token, action at a distance and one-on-many impact of a cardinal adsorbent are achieved.*

That said, I must remind the reader that this is a prototype mechanism and as simple as one could make it. As such, it could under ideal conditions proceed *ad infinitum*. In reality, blockade of propagation might be halted by a gathering of side chains that could

absorb the electron density march. And as a result, the information and energy transfer would only be regional until other *bona fide* or pseudo-cardinal adsorbents are introduced to make the march continue (see Ling 2006b, Appendix I.) I add this little passage to prepare the reader for experimental findings that the simple prototype model does not directly predict. More important, those contradictory findings would quite likely open the door to new adventures lying around the corner.

2.8 Two types of initiation mechanisms for all-or-none transitions in adsorption

Figure 13 illustrates two types of initiation mechanisms for the all-or-none exchanges of two alternative adsorbents shown respectively as empty circles and solid circles. In the model labeled B, the relative abundance of the two adsorbents remains unchanged. The all-or-none exchange is then triggered by the binding of the cardinal adsorbent **W**. This type of adsorbent exchange is what was described in some detail in the preceding section and called a *controlled auto-cooperative transition* (Ling 1992, pp. 143–144.)

In the model labeled A, the all-or-none adsorbent exchange is triggered by an increase in the relative abundance of one of the two adsorbents in the surrounding medium. This type of exchange is referred to as a *spontaneous auto-cooperative transition*.

Note that while in the (idealized) spontaneous transitions, all sites are shown as regular sites and none as a cardinal site. Accordingly, the initiation of the propagated change could by chance start at any site. In contrast, in the controlled transition, the propagated change always begins at the cardinal site and its direction and path of propagation is thus predetermined.

In the following section, we will examine in quantitative fashion, these all-or-none changes in the more rigorous language of Statistical Mechanics.

2.9 The Yang-Ling cooperative adsorption isotherm

From its very inception, the objective of the association-induction hypothesis has been to explain the *macroscopic* cell physiological properties and behaviors in terms of the *microscopic* properties and behaviors of atoms, molecules and electrons (Ling 1962, Chapter 1.) Once you recognize this objective, you will understand why Ludwig Boltz-

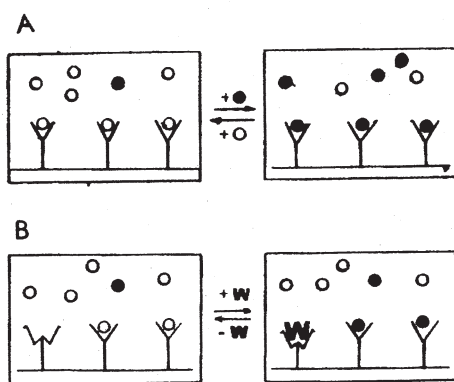
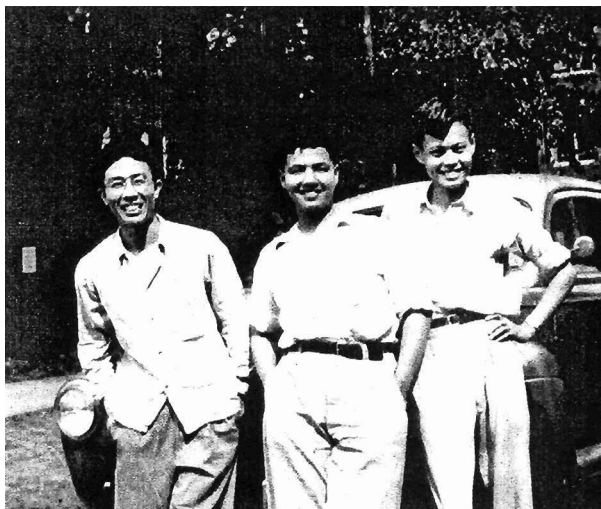


FIGURE 13. Two types of auto-cooperative transition of the system from its *i*th state in which all sites are occupied by the species *i* to the *j*th state in which all the sites are occupied by the species *j*. In the first model A, the all-or-none transition is created by increasing the ratio of the *j*th to the *i*th species in the surrounding medium. In this case, the initial exchange can happen anywhere along the infinitely-long chain. In the second model B, the concentrations of both the *i*th and *j*th species remain unchanged. It is the adsorption of the cardinal adsorbent **W** that triggered the auto-cooperative shift. Type B is what we have shown in models presented in Figure 5, 10 and 11. Unlike the first model A, the initial exchange happens at a site right next to the cardinal site and the propagation is directional in a predetermined fashion. (from Ling 2001)



C.N. Yang (far right), T.D. Lee and the author (far left) taken moments before we boarded our 1940 Ford and began our 9000-mile trip to the west on August 23, 1947.

mann and his work were of such vital importance to the development of the association-induction hypothesis.

Boltzmann was of vital importance to the understanding of life and its physical basis because he invented Statistical Mechanics — a new science further strengthened later by the American physicist, Josiah Willard Gibbs (1839–1903.) For the purpose of Statistical Mechanics is no other than to link the **microscopic** properties and behaviors of atoms, molecules and electrons to the macroscopic properties and behaviors of **macroscopic** matter in general (Boltzmann 1909.)

By then, the *Reductionist Four* had made it abundantly clear, that the macroscopic properties and behaviors of living matter, i.e., cell and below-cell physiology — are an integral part of the macroscopic properties and behaviors of matter in general.

In addition, I also profited a great deal from another theoretical physicist of comparable rank, Professor C. N. Yang. He was my room-mate at the Tsing Hua University Graduate School in Kun-ming, China between 1963 and 1965.

(C.N. Yang and T.D. Lee were awarded the Nobel Prize for physics of 1957 for their conjoint work on parity. For a brief vignette of Yang's contribution to statistical mechanics, particle physics etc., see Yang 1995.)

Yang was among the first to read and endorse my 1962 book, *A Physical Theory of the Living State: the Association-Induction Hypothesis* before it was published. Next thing you know, the Yang-Ling adsorption isotherm was born — based on the one-dimensional Ising method. As such, it was a quantitative extension of my simple model of a protein molecule seen as an infinitely long chain of equally spaced sites of similar nature, which could adsorb either an *i*th or a *j*th solute — as illustrated diagrammatically in Figure 13A.

It was planned originally that we would publish the work conjointly soon after. Due entirely to my fault, that day never came. Instead, I presented the isotherm in the first Symposium issue of the new journal, *Biopolymers* (Ling 1964a.) In 1980, Dr. George Karreman published his version of its derivation in the first Chapter of a monograph on *Cooperative Phenomena in Biology*, which he also edited (Karreman 1980.)

The Yang-Ling isotherm mentioned above reads as follows.

$$[\text{p}_i]_{\text{ad}} = \frac{[\text{f}]}{2} \left[1 + \frac{\xi - 1}{\sqrt{(\xi - 1)^2 + 4\xi \exp(\gamma / RT)}} \right] \quad (5)$$

where $[\text{p}_i]_{\text{ad}}$ and $[\text{f}]$ are respectively the concentration of adsorbed i th solute and $[\text{f}]$ the concentration of adsorption sites. ξ is defined as follows:

$$\xi = \frac{[\text{p}_i]_{\text{ex}}}{[\text{p}_j]_{\text{ex}}} \cdot K_{j \rightarrow i}^{\infty} . \quad (6)$$

$[\text{p}_i]_{\text{ex}}$ and $[\text{p}_j]_{\text{ex}}$ are respectively the equilibrium concentration of the i th and j th adsorbent in the bathing medium. $K_{j \rightarrow i}^{\infty}$ is the intrinsic equilibrium constant for the j th to i th adsorbent exchange and it is related to the intrinsic free energy of j th to i th adsorption exchange, $\Delta F_{j \rightarrow i}^{\infty}$ without creating a change in the number of nearest neighboring $i-j$ pairs, as in the case of a j -to- i exchange in a trio of nearest-neighboring sites: $ijj \rightarrow ijj$. On the other hand, for a j -to- i exchange in an alternative trio of sites: $jjj \rightarrow jij$, two new ij pairs are created. The creation of each new ij pair entails the addition of another energy term, called the *nearest neighbor interaction energy* equal to $-(\gamma/2)$. Thus, in this case of $jjj \rightarrow jij$ exchange, the total free energy change is not merely $\Delta F_{j \rightarrow i}^{\infty}$ but $\Delta F_{j \rightarrow i}^{\infty} + 2\{-(\gamma/2)\} = \Delta F_{j \rightarrow i}^{\infty} - \gamma$.

At this juncture, I want to mention that the j th alternative adsorbent may represent a vacancy. Its concentration is then presented as the total concentration of the adsorption sites minus those sites occupied by the i th adsorbent.

In cooperative phenomena, $-(\gamma/2)$, the nearest neighbor interaction energy, is of paramount importance. When $-(\gamma/2)$ is a negative number, the adsorption of an i increases the chance of adsorption of the alternative solute, j . This type of cooperative phenomena is given the name, *hetero-cooperative*. When $-(\gamma/2)$ is equal to zero, there is no cooperative interaction. The adsorption is then described by a Langmuir adsorption isotherm.

When $-(\gamma/2)$ is a positive number, the adsorption of one species favors the additional adsorption of that same species. This type of adsorption is given the name auto-cooperative as pointed out once already (Ling 1962, p. 103.)

Auto-cooperative phenomena are of critical importance in cell physiology because it is this type of interaction that holds a group of individual elements together and makes them function as if they were one. As an illustration of auto-cooperative adsorption, Figure 14B presents a linear plot of the mole fraction, X_i of the i th adsorption equal to $[\text{p}_i] / [\text{f}]$ against $[\text{p}_i]/[\text{p}_j]$. Note that in autocooperative adsorption, the plot is S-shaped or *sigmoid*.

Equation 5 can also be written in the following form:

$$\frac{[\text{p}_i]_{\text{ad}}}{[\text{p}_j]_{\text{ad}}} = \frac{\sqrt{(\xi - 1)^2 + 4\xi \exp(\gamma / RT)} + \xi - 1}{\sqrt{(\xi - 1)^2 + 4\xi \exp(\gamma / RT)} - \xi + 1} . \quad (7)$$

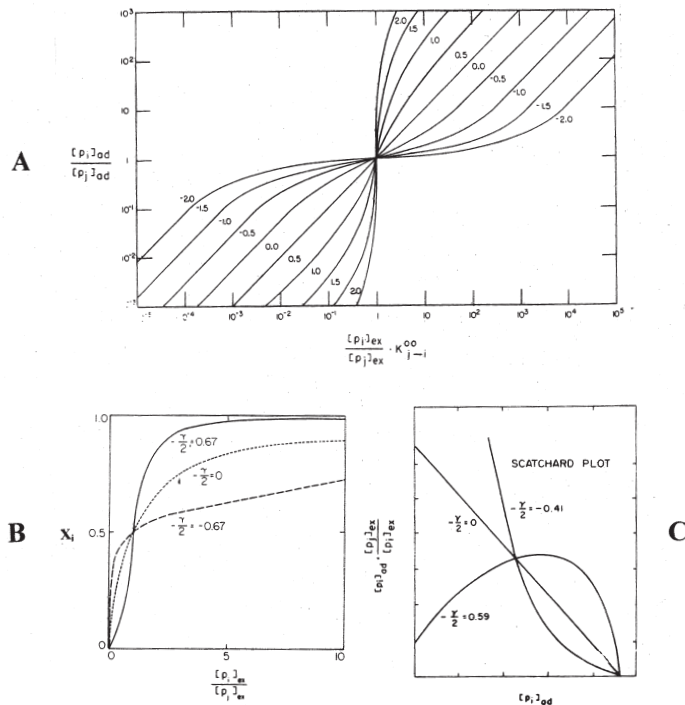


FIGURE 14. A. Log-log plot of the Yang-Ling cooperative adsorption isotherm. Number near each curve is the value of the nearest neighbor interaction energy, $-(\gamma/2)$. B. Linear plot of the same. C. Scatchard plot of same. (A, from Ling 1966 by permission of FASEB. C from Gulati 1973 by permission of NY Academy of Sciences)

A log-log plot of Equation 7 with different $-(\gamma/2)$ values is shown in Figure 14A. Figure 14C, on the other hand, presents the so-called Scatchard plot of the adsorption isotherm, which adds another method in diagnosing to which type of cooperative interaction, a set of data belongs. Note in particular, that in the Scatchard plot, the non-cooperative or Langmuir isotherm appears as a straight line whereas auto-cooperative adsorption concaves downward.

For easier presentation of more complex derivations of this equation to follow, I conclude this section by introducing a simplifying notation, Ω to represent one half of what lies inside the large bracket of Equation 5, i.e.,

$$\Omega = \frac{1}{2} \left[1 + \frac{\xi - 1}{\sqrt{(\xi - 1)^2 + 4\xi \exp(\gamma / RT)}} \right]. \quad (8)$$

As an example, Equation 5 would now take on the following simpler form:

$$[p_i]_{ad} = [f] \Omega, \quad (5a)$$

where $[p_i]_{ad}$ is the concentration of i th species adsorbed. $[f]$ is the concentration of fixed adsorption sites, both in units of moles per gram of fresh cells. Ω is as defined in Equation (8).

2.10 What joins a vast gathering of similar microscopic nano-protoplasm units into a coherent macroscopic structure of protoplasm?

A human being, like many other complex living organism, is made of a collection of organs. An organ is made of an assembly of similar and dissimilar cells. A cell is made of cytoplasm and organelles like the cell membrane, cell nucleus, mitochondria and so on. Cytoplasm and organelles are as a rule made of different kinds of protoplasm. Each kind of protoplasm is, in turn, made of a vast collection of nano-protoplasm (NP) units. The present section addresses the specific question how a large number of these *microscopic* NP units are joined together into their kind of macroscopic protoplasm.

We begin by examining how (macroscopic) protoplasm varies in its physical consistency. Thus we know that protoplasm can be a fluid of different viscosity which colloid chemists call a *sol*. On the other extreme, it can also be a solid of varying firmness that colloid chemists call a *gel*. That the same protoplasm within a unicellular organism can undergo reversible transformation between the sol and the gel state has fascinated cell biologists since mid-19th century when the invention of the microscope had made an invisible world suddenly visible.

As a sol, Felix Dujardin's sarcode could flow out of a crushed protozoon. Similarly, what von Mohl saw in plant cells and called protoplasm could also flow out from a cut giant alga cell. But an even more striking example to show how liquidy a protoplasm could be was provided by A.A. Lister in a slime mold (Mycetozoa.) Living in rotten oak this slime mold is usually full of dark brown spores of the fungus, upon which the slime mold feeds. However, when the slime mold was made to creep through a wad of wet cotton wool, the brown spores were all filtered out, leaving the emerging protoplasm crystal clear (Lister 1888.)

At the other end of the spectrum, the substance of a muscle cell is a firm gel. Since it is on record that mature human red blood cells can be cut into tiny pieces without losing its hemoglobin, clearly the red blood cell protoplasm is also a firm gel (Best and Taylor 1945, p. 48.)

Keeping in mind both the fluid slime mold and the solid red blood cell, one can draw a diagrammatic illustration like that shown as Figure 15, which shows the simplest dynamic sol state or gel state that an assembly of NP units could assume. Unfortunately, like all diagrams they illuminate some aspects and unintentionally misrepresent other aspects. The most significant inescapable misrepresentation is in the size of the protein moieties and the number of β -, and γ -carboxyl groups they carry. Take the rbc cytoplasmic NP units for an example.

As pointed out earlier, each liter of rbc contains 340 grams of hemoglobin. Since the average amino-acid-residue weight is estimated at 114, dividing this number into 340, we have a total of 2.98 or roughly 3 moles of amino acid residues per liter of fresh rbc. As also pointed out above, 11% of these residues carry β -, and γ -carboxyl groups, their total concentration is therefore 328 mmoles per liter of rbc. We know that in a living rbc, the concentration of K^+ in the cell is about 100 mmoles per liter of rbs. Virtually all of these ions are adsorbed on the β -, and γ -carboxyl groups (Ling 2005.) This leaves

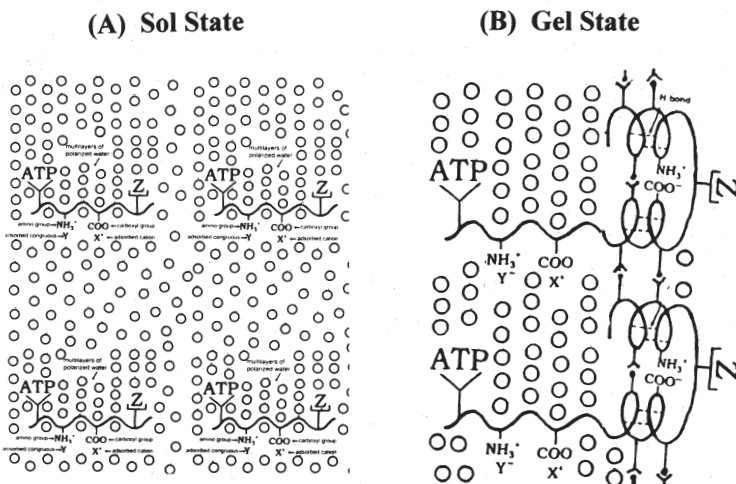


FIGURE 15. Auto-cooperative transition of a population of nano-protoplasm units (NPU) as part of a larger domain of protoplasm in the sol and gel state respectively. Diagram shows that polarized-oriented multilayers of water molecules belong to more than just one NPU, and are in fact a shared property of the entire domain of protoplasm and as such may provide the medium for temporal-spatial coordination in synchronous activities.

$328 - 199 = 228$ mmoles or roughly $28/328$ or 75% of the β -, and γ -carboxyl groups free to form salt linkages with fixed cations within the same hemoglobin molecules or with other hemoglobin and non-hemoglobin molecules nearby (see section 3.1.1.2 below for experimental verification.)

With these alternatives in mind, we would expect that in the real-world living cells, the basic nano-protoplasmic units are probably never linked together exclusively *via* the bulk-phase water molecules which they all participate in polarizing and orienting — as illustrated in Figure 15(A). For protoplasm like that in the slime mold, Figure 15(B) might be closer to the truth. As part of dynamic structures links form and break constantly.

More likely, the NP units also participate in some intra- and inter-molecular salt linkage formation though on a much smaller scale as in the real-world counterparts of Figure 15 (B). An important consequence is that this type of AI cascade mechanism can then in theory operate not only within the same NP units but between neighboring NP units as well.

However, a reader familiar with the vast amount of information we already have on protein structure could be alarmed by what he (or she) sees in Figure 15. It is all too familiar to him (or her) the three-dimensional representation of isolated proteins where every detail of the structure has been described with high level of precision. Yet what we see here in Figure 15 are connections of the most elementary kind. Why did I choose to do that?

I chose to do that for a good reason. In the truly natural state, the NP units are invariably associated with a large amount of water — as shown in Equation 1. And that cell water is in equilibrium with blood plasma (or Ringer's solution) containing water at a relative vapor pressure very close to saturation (99.6% saturation.) (Ling and Negendank 1970)

There is no denial that X-ray diffraction has made it possible to describe every little detail of a protein molecule. However, that description is only for hemoglobin in a crystalline form — made so by reducing the activity of water from near saturation to near zero with non-aqueous solvents like ethanol or high concentrations of salts. Therefore, the detailed data of hemoglobin crystals is relevant but only as a reference source of information. Crystalline proteins are in many ways like exquisitely-preserved Egyptian mummies. Both are dehydrated forms of something that are in their natural state highly watery.

That, however, does not mean that beside β -, and γ -carboxyl groups and backbone NHCO groups shown in Figure 15, other functional groups on the protein serve no physiological function. Of course, they do. The heme-heme interaction is one example and we are going to discuss it at some length below. That said, I must point out that we have just begun our new adventure and we believe in beginning with the simplest. At this moment, the theory predicts that β -, and γ -carboxyl groups and backbone NHCO groups play the central role in the coherence of protoplasm that makes life possible. And we will examine the results of experimental studies from both our own laboratory and from other laboratories to see how far our model can explain facts despite their utter simplicity.

3. Results of experimental testing of the AI theory of nano-protoplasm as the most basic unit of life

Part 1 describes experimental studies on an ultra-simple model of the nano-protoplasm. It is a model we created entirely out of pure components. That being the case, we know that if the model behaves in accordance with the prediction of the theory, it is produced by nothing other than what we put in — according to the formula of nano-protoplasm as given in Equation 1.

Part 2 describes results of investigations of nano-protoplasm in its natural setting as part of surviving cells. Some are located in the cell surface others located in different parts of the cell interior. Together they perform all four of the most fundamental physiological activities of the living cell: (i) selective accumulation of solutes, (ii) selective permeability, (iii) cellular electric potentials and (iv) cellular swelling and shrinkage.

The overall purpose of this section is to see how these widely different subjects of macroscopic cell physiology could be explained in terms of our theory of microscopic nano-protoplasm and its control by cardinal adsorbents as depicted diagrammatically in Figure 5 and quantitatively by variants of Equation 5.

3.1 Studies *in vitro*: a hemoglobin-salt solution as an ultra-simple model of nano-protoplasm

I chose to start our testing with a nano-protoplasm model made from a mature mammalian red blood cell, whose unusual simplicity we have examined in some details on p. 120 above.

By chopping a mature human red blood cell or rbc into smaller and smaller pieces, we finally obtain a vast number of similar nano-protoplasm (NP) units. Each one of these NP units contains a single hemoglobin molecule, about seven thousand water molecules, some twenty K^+ and even smaller numbers of ATP and 2,3-DPG. By taking advantage of the fourfold simplicity of the rbc, we are given the opportunity to put in a formula form as given on p. 120 above. It is the first nano-protoplasm given that name.

By analogy with an iron nail-filing-magnet model, I then suggested that in living protoplasm, the cardinal adsorbent, ATP would serve a similar function as the horse-shoe magnet in converting the low (negative) energy and high entropy autocooperative assembly of protein-water-K⁺ into a high (negative) energy low entropy autocooperative assembly in the resting living state. Remove the ATP and/or 2,3-DPG, we end up with an assembly of nano-protoplasm units in the active living (or dead) state.

The ultra-simple model of all nano-protoplasm could be produced by dissolving enough hemoglobin and salt in water to make a moderately concentrated solution of hemoglobin (and salt.) What is more, this perception not only allows us to perform new studies on this ultra-simple model of protoplasm; it also enables us to give new significance to old experimental findings performed on similar hemoglobin solutions. More specifically, we will examine the relevant old and new experimental data once more under two headings, (1) spontaneous auto-cooperative transition and (2) controlled auto-cooperative transition as represented respectively diagrammatically in Figure 13 A and B and more rigorously in Equations 5 (or Equation 8.)

3.1.1 Spontaneous auto-cooperative transition

3.1.1.1 Heme-Heme interaction

The primary physiological function of the red blood cell is to transport oxygen from the lungs or another respiratory organ to the tissue cells. To do so efficiently, the red cell must be able to load itself fully with oxygen on its passage through the lungs and discharge as much of its load as possible amongst the peripheral tissue cells in the second part of its cyclic journey. These dual contrasting requirements are admirably met in the S-shaped oxygen-binding curve of red blood cells as shown in the inset of Figure 16.

Thus, if the oxygen tension in the lung is equal to 80 mm Hg, the red blood cells will be according to the S-shaped curve shown in the inset of Figure 16, 90% saturated with oxygen on its passage through the lung. If the tissue oxygen tension is, say 20 mm of Hg, 80% of the oxygen carried by the blood would be unloaded to the peripheral tissues. Taken together, the circulating red blood cells have thus effectively carried out their primary physiological function.

To further emphasize how important is the S-shaped oxygen uptake curve of the hemoglobin, one compares it with the hyperbolic oxygen dissociation curve of myoglobin. Myoglobin is a protein found in stationary muscle cells and it does not transport oxygen. Its oxygen binding curve is also shown in the same inset of Figure 16. Here at 20 mm Hg among the peripheral tissues, the protein is still fully loaded with oxygen. If hemoglobin behaves like myoglobin, it would not be able to deliver the oxygen that the peripheral tissues need.

Now, according to the definition given on a previous page, the bulk of a red blood cell is at the most basic level an auto-cooperative assembly of a vast number of nano-protoplasm units. Each of these NP units contains one hemoglobin molecule and associated water and K⁺, with or without the cardinal adsorbent ATP (and/or 2,3-DPG or IHP) as shown in Figure 5. And, as just pointed out above, a model of rbc cytoplasmic protoplasm in its *living state* could be produced by simply dissolving enough isolated pure hemoglobin and salt in the right amount of water. And, in theory, it too should be able to produce an S-shaped oxygen-binding curve.

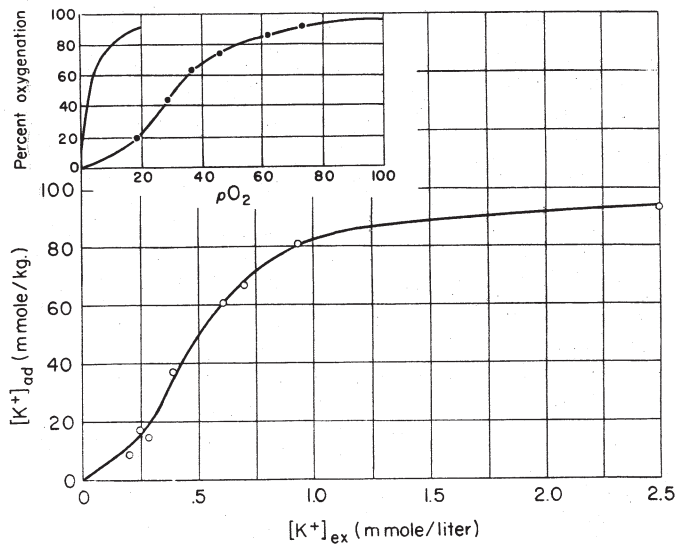


FIGURE 16. A composite presentation showing the similarity of the oxygen uptake of a population of intact human red blood cells (curve with solid dots in inset) and the uptake of K^+ in frog muscle exposed to a constant concentration of Na^+ (at 100 mM) and increasing concentration of K^+ . The non-cooperative oxygen uptake of myoglobin is also shown in the inset. (from Ling 1966 by permission of FASEB)

That brings to fore the unusual advantage enjoyed by a late-coming theoretical prediction. Just such a hemoglobin solution had been prepared and shown to demonstrate the (now) predicted S-shaped oxygen-binding curve a little over a century ago (Bohr 1903.) But that is not all.

Seven years after the discovery of the S-shaped oxygen binding curve of hemoglobin by Bohr, British physiologist, A. V. Hill introduced an equation that describes the steep part of the oxygen binding curve of hemoglobin (Hill 1910.) Representing the mole fraction of binding sites occupied by oxygen as y and that of vacant sites as $1-y$, what has become widely known as the Hill equation emerged in the following form:

$$\log \{y / (1-y)\} = n \log p O_2 + n \log K, \quad (9)$$

where pO_2 is the partial pressure of oxygen measured in mm of Hg. The symbol, n , known as the Hill coefficient, is equal to the slope of a log-log plot of $\{y / (1-y)\}$ against pO_2 . When n is larger than 1, the empirical curve simulates the middle portion of an S-shaped, or sigmoid-shaped oxygen binding curve. For this reason, n has been used to measure the "sigmoidity" of an oxygen-binding curve. Not to be mistaken is the fact that n is a purely *empirical* constant and the Hill equation a purely *empirical* equation. As such, neither the Hill equation nor the Hill coefficient tells us anything about the underlying causes of the S-shaped oxygen binding phenomenon. However, the Yang-Ling adsorption isotherm has changed that.

For n is according to the Yang-Ling model, related to the *nearest neighbor interaction energy*, $-\gamma / 2$, by the following simple relationship (Ling 1964a, p. 93):

$$n = \exp (-\gamma / 2). \quad (10)$$

Table 3 lists the quantitative relationship between the two parameters: n and $(-\gamma / 2)$. As partly pointed out earlier, when $n > 1$, $(-\gamma / 2) > 0$, and the adsorption is auto-cooperative. When $n = 1$, the adsorption is non-cooperative and as such, Equation 6 becomes a simplified version of a Langmuir adsorption isotherm, which describes the hyperbolic type of oxygen binding of myoglobin mentioned earlier (see Ling 2005, p. 18.)

Now, we are ready to compare in depth the Hill equation and the Yang-Ling adsorption isotherm in their respective ability to describe the real-world oxygen binding of a solution of hemoglobin — as an ultra-simple model of rbc cytoplasmic nano-protoplasm. To do so, we must first find an accurate and complete set of data on the oxygen binding of a reasonably concentrated solution of pure hemoglobin in a dilute salt solution.

Luckily, I soon found such a set of highly accurate data in the Ph.D. thesis of Dr. R. L. J. Lyster, completed under Professor F. J. W. Roughton's tutelage at the Cambridge University of England. I then re-plotted the data points in a log-log format shown in Figure 17. Immediately, we can see that while the Hill equation as such can only describe the data points near half oxygen saturation point, the solid line in the figure is a theoretical plot of the Yang-Ling adsorption isotherm as given in Equation 5. As such, it contains

TABLE 3. The relation between the Hill coefficient, n , and the nearest neighbor interaction energy $(-\gamma / 2)$.

n	$-(\gamma / 2)$ (kcal/mole)
1.0	0
1.25	0.132
1.5	0.239
1.75	0.331
2.0	0.409
2.25	0.479
2.5	0.541
2.75	0.597
3.0	0.649
3.25	0.695
3.5	0.739
3.75	0.780
4.0	0.818
4.25	0.854
4.5	0.888
4.75	0.919
5.0	0.949
5.25	0.978
5.5	1.006
5.75	1.032
6.0	1.057

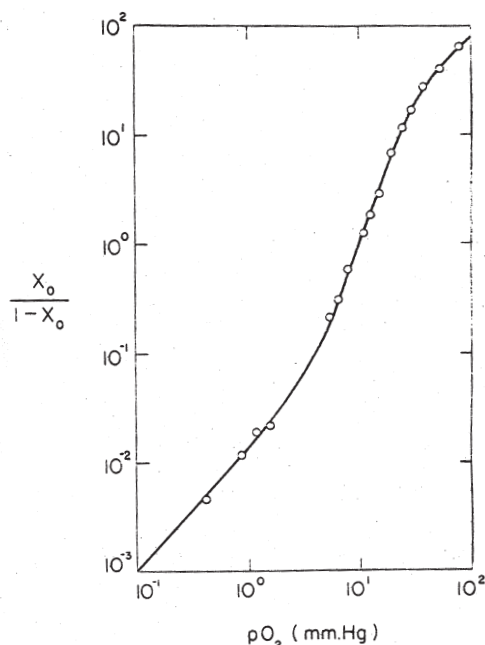


FIGURE 17. A log-log plot of the uptake of oxygen by human hemoglobin at pH 9.1, 19° C and in the presence of 0.6 M phosphate. Data from Lyster as presented by Rossi-Fanelli *et al* (1964.) Points are experimental, line is theoretical according to the Yang-Ling adsorption isotherm given in Equation 5 with $K_{j \rightarrow i}^\infty = 5.88 \times 10^{-6}$ M and $-(\gamma/2) = 0.67$ kcal./mole. (from Ling 1969, by permission of the Academic Press)

just two variables $K_{j \rightarrow i}^\infty$ equal to 5.88×10^{-6} M and $(-\gamma/2)$ equal to 0.67 kcal/mole. Nonetheless, all the data points fall on or very near the entire theoretical curve.

In 1925, G.S. Adair produced a theoretical curve that also fits the entire S-shaped oxygen binding curve of hemoglobin then available. He did this by assuming that each of the oxygen binding constants of the four heme groups is different. However, attempts to isolate the intermediate products failed (Conant and McGrew 1930.) Then, what became known as the Crevice theory was proposed, according to which the weak oxygen binding heme sites are on the surface of the hemoglobin molecule while the stronger binding heme sites are buried inside crevices of the hemoglobin crystals. Perutz's definitive work on hemoglobin molecules revealed that all four heme groups are located on the surface of the molecule and none is buried (Perutz 1969.) For comments on the later theoretical models of Monod, Wyman and Changeux (1965), Atkinson, Hathaway and Smith (1965) and Koshland, Nemethy and Filmer (1966), see Ling (1969, p. 52; 1981, p. 62.)

Lyster's data and their theoretical backing illustrate how by increasing the oxygen tension in the environment, a point will be reached when in an all-or-none manner, the hemoglobin switches from the deoxygenated state to the fully oxygenated state. The high positive value of $(-\gamma/2)$ raises the effective free energy of oxygen binding from that of $\Delta F_{j \rightarrow i}^\infty \{ = RT \ln K_{j \rightarrow i}^\infty = 0.596 \times \ln (5.88 \times 10^{-6}) \} = -7.18$ kcal./mole to $(\Delta F_{j \rightarrow i}^\infty - \gamma) = -7.18 - 2 \times 0.67 = -8.52$ kcal/mole.

Next, we look deeper into what lies behind this all-important $-\gamma/2$. In classical statistical mechanics dealing with the phenomenon of ferromagnetic cooperativity, a nearest neighboring activation energy is that between atoms sitting right next to one another. Not so are the nearest neighboring heme sites we dealt with above. In fact, physically speaking

they are “miles” apart. But instead of empty space, each pair of nearest neighboring heme sites are joined by a stretch of the polypeptide chain and short side chains carrying the imidazole functional groups on which the heme are attached. And, two years before the introduction of the Yang-Ling isotherm, the AI hypothesis has already provided an answer to this apparent dilemma. It is what was then called the indirect F-effect, now renamed the AI cascade mechanism, that turns distant sites to acts as if they were in close contact.

Nor does the AI cascade mechanism limit its bridging impact to similar functional groups like the four heme sites. It could also involve other types of functional groups but especially those on short side chains. In the following, I shall discuss two types of responses to oxygenation of the heme groups of that protein. One is known as the Bohr effect, which I shall discuss first. The other is what I call the R-T transformation also initiated by the oxygenation and deoxygenation of the heme groups. (For still other types of prior findings that fit our model most of the time but not always, see Ling 1992, pp. 154–155.)

(i) *The Bohr effect* Now oxygenation involves the withdrawal of electrons from the heme sites of hemoglobin (see Weissbluth 1974, p. 14.) According to the AI model, oxygenation would create an across-the-board decrease of c-value of prototropic groups (e.g., β -, and γ -carboxyl groups) and hence their pK_a value. The net result is a change of some weak acidic groups to stronger ones. Since stronger acids hold their H^+ less tightly, some of the bound H^+ is liberated and released into the medium lowering its pH. This is of course the phenomenon first described in 1904 by Danish physiologist, Christian Bohr and known as the Bohr effect (Bohr *et al.* 1904.)

(ii) *The R-T transformation* As already mentioned, oxygenation withdraws electrons from hemoglobin (see Weissbluth 1974, p. 14.) According to the AI hypothesis, this electron withdrawal lowers the respective c-value of the β -, and γ -carboxyl groups and the c-value analogue of the backbone carbonyl groups. Since high c-value favors the formation of salt linkages and the formation of salt linkages in turn reduces the motional freedom or flexibility of the protein chains, oxygenation should reduce this rigidity and make the protein more relaxed.

(Retroactive) experimental confirmation of this prediction has also been known long before. Thus, the oxygenated hemoglobin has been often referred to as in the R or relaxed state and that of the deoxygenated hemoglobin as in the tense or T state (see Weissbluth 1974, p. 23.)

By the same token, a rise of the c-value analogue as a result of deoxygenation should cause the liberation of polarized-oriented water molecules with a gain of the entropy of the system. This, too has been known for a long time (Manwell 1958) and interpreted on the basis of the AI Hypothesis (Ling 1984, p. 519.)

As mentioned earlier, 11% of the total amino acid residues of hemoglobin are (the sum of) aspartic and glutamic acid residues carrying respectively β -, and γ -carboxyl groups on their respective short side chains. There are also an approximately equal percentage of fixed cations. The simple law of electrostatic attraction predicts that in the absence of a high concentration of competing salt ions in the medium, these fixed cations and fixed anions would be fully engaged in “salt linkages” (Speakman and Hirst 1931.)

With this in mind, the T to R transition brought on by oxygenation requires in theory the participation of salt ions. In other words, the AI cascade mechanism which underlies

a positive nearest neighbor interaction energy ($-\gamma/2$) requires — in the case of the NP units of rbc cytoplasmic protoplasm — free ions in the medium. If that is a correct theoretical prediction, one would expect the magnitude of ($-\gamma/2$) to be related to the concentration of salt ions in the medium.

In fact, this was precisely what Enoki and Tyuma (1964) discovered and is shown in two graphs reproduced here as Figures 18A and 18B. Figure 18A shows Hill plots of oxygen uptake of human hemoglobin in the presence of increasing concentration of NaCl in the medium. Note that the slope of the plots, which equals the Hill coefficient n , increases with the NaCl concentration. But the impact of salt ions is not limited to NaCl. Other monovalent and divalent ions exercised similar influence (Figure 18B.) As pointed out repeatedly above, n is a function of the nearest-neighbor-interaction energy ($-\gamma/2$) as shown in Equation 10.

In terms of the AI Hypothesis, the oxygenation-induced changes of heme sites described above belong to the category of spontaneous autocooperative transition as illustrated in Figure 13 A. Next we turn to another kind of spontaneous autocooperative transition. This too occurs in the model of rbc cytoplasmic NP units in the form of a moderately concentrated solution of mammalian hemoglobin. But instead of prosthetic groups like the oxygen-binding heme sites, we will be dealing with β -, and γ -carboxyl groups. And, in place of oxygen molecules, the solute taken up by these β -, and γ -carboxyl groups would be the alkali-metal ions, including Na^+ .

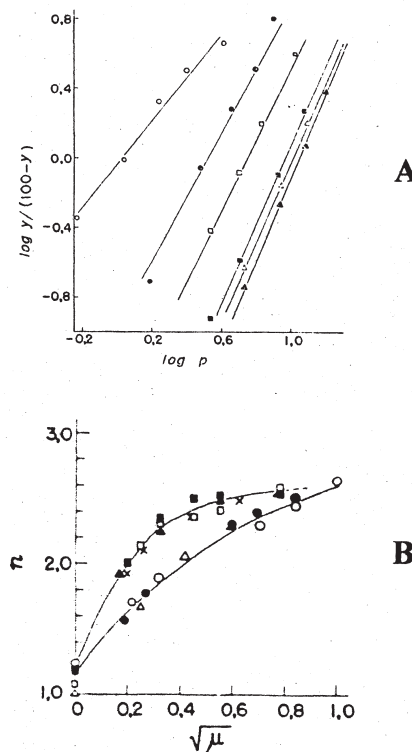


FIGURE 18. Effect of salt concentration upon the oxygen binding of human hemoglobin. Hemoglobin concentration was 1.5×10^{-3} M or 10% (w/v). **A.** Log-log plot of oxygen binding in the presence of increasing concentration of NaCl. The left-hand most line with open circles was obtained in the absence of NaCl. NaCl concentration increased progressively toward the right, reaching 1 M at the right-hand most curve with open triangles. Note that the slope of these curves equals the empirical Hill coefficient. **B.** Plot of the Hill coefficient, n , with increasing ionic strength of the different salts present in the hemoglobin solution studied.
 o-o NaCl; •• KCl; Δ-Δ K_2SO_4 ; □-□ MgCl_2 ; ■-■ CaCl_2 ; ▲-▲ MgSO_4 ; ×-× KH_2PO_4 K_2HPO_4 (from Enoki and Tyuma 1964, by permission of The Japanese Journal of Physiology)

3.1.1.2 Auto-cooperative Na^+ binding on β -, and γ -carboxyl groups

There was once a strong taboo against the salt linkages idea (For details, see Ling 2005, top of p. 12.) Max Perutz produced powerful evidence for their existence (Perutz 1969.) In 1984 another set of evidence for their existence appeared in print (Ling and Zhang 1984.)

Ling and Zhang titrated a 10% solution of bovine hemoglobin with an increasing amount of NaOH. They recorded step by step both the pH and the free Na^+ concentration in the hemoglobin solution respectively with a pH and a Na^+ -specific glass electrode. By subtracting the free Na^+ remaining at each point from the total amount of Na^+ added in the form of NaOH, they determined the amount of adsorbed Na^+ at each point.

First, they confirmed earlier repeated reports of very low Na^+ binding in solution of untreated native hemoglobin (Ling and Zhang 1984, Table 1 on p. 224.) What came after the introduction of NaOH was an altogether different story. From here on, for each fixed cation (α -, ϵ -amino groups and guanidyl groups) neutralized by the OH^- added, one Na^+ would become bound to one of the newly liberated β -, and γ -carboxyl groups from the salt linkages — as illustrated diagrammatically in Figure 19.

In theory, the (combined) titration curves of all the fixed cationic groups should match quantitatively the Na^+ -binding curve. Figure 20 shows that this is exactly what was found. The points represent the different amounts of bound Na^+ experimentally measured at different pH. The solid line going through or near these points is the *combined theoretical titration curves of all the α -amino groups, the ϵ -amino groups and the guanidyl groups* in this pH range. (The imidazole groups of the histidine residues are partly engaged in anchoring the heme groups and do not participate in salt-linkage formation.)

We now return to Figure 19, which illustrates the theoretical predictions we have just confirmed experimentally. In addition, it also shows how close this diagram resembles the diagram in Figure 5, describing the transition between the resting and active living state of the nano-protoplasm. Only, instead of OH^- anions that split the salt linkages, it is the

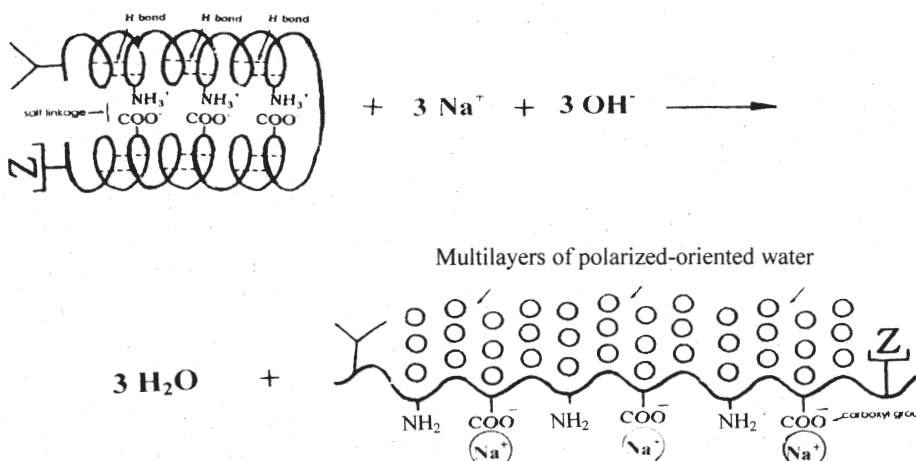


FIGURE 19. Diagrammatic illustration of the titration of hemoglobin with NaOH and its projected (and affirmed) consequences of twofold unfolding of the α -helix by multilayers of water molecules and of the salt linkages by Na^+ .

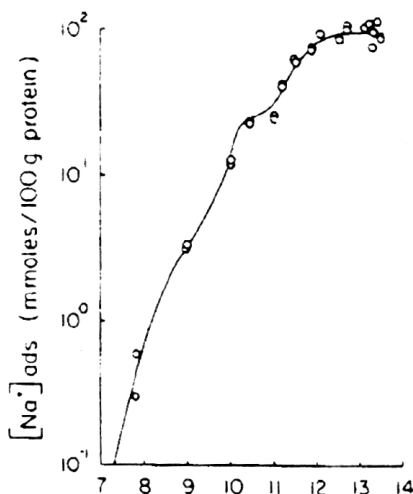


FIGURE 20. Quantitative accord between the number of neutralized fixed cations (α -amino groups, ϵ -amino groups of lysine residues and guanidyl groups of arginine residues) and the number of Na^+ taken up by the (newly) liberated β -, and γ -carboxyl groups in the titration of a 10% (w/v) bovine hemoglobin — as depicted in the preceding figure (Figure 19.) Points are experimentally determined Na^+ taken up by the hemoglobin at different pH. Line going through or near most of the experimental points is computed titration curve in an above neutral range based on the known number of α -amino groups and ϵ -amino groups and guanidyl groups in 100 grams of bovine hemoglobin. (from Ling and Zhang 1984)

combined activity of ATP and “congruous anions” and cation together that splits the salt linkages and liberates the β -, and γ -carboxyl groups for K^+ (or Na^+) adsorption.

Now we ask if the Na^+ -titration curve is also auto-cooperative as in the heme-heme interaction? After all, both occur in the same hemoglobin molecule.

We can get the answer readily by first determining the ratio of the mole fraction of β -, and γ -carboxyl groups binding Na^+ over the mole fraction of the β -, and γ -carboxyl groups not binding Na^+ . We can then make a log-log plot of this ratio against the free Na^+ concentration in the medium according to Equation 5 and Figure 14A. If the transition is auto-cooperative, one should find a curve with a midpoint slope (or Hill coefficient n) higher than 1 and accordingly a nearest neighbor interaction energy $-(\gamma/2)$ above 0. The same data can also be put in the form of a Scatchard plot (see Figure 14C.) If the data are autocooprative, the data points should follow a course concaving downward.

The answers to both questions are positive. But only the Scatchard plot is shown here (as Figure 21.) The pronounced concavity of the plot indicates strong auto-cooperativity of the binding of Na^+ on the liberated β -, and γ -carboxyl groups of the hemoglobin. Like in the case of heme-heme interaction, the observed $-(\gamma/2)$ is also a positive equal to 0.824 kcal/mole, corresponding to an even higher Hill coefficient of 4.0.

There are two more sets of valuable insights that the Ling-Zhang study described above have revealed:

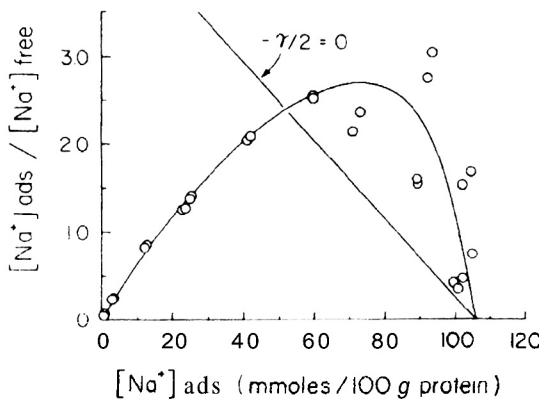


FIGURE 21. Scatchard plot of the adsorption of Na⁺ on bovine hemoglobin in a 10% (w/v) solution titrated with NaOH. The strong downward concavity shows highly auto-cooperative adsorption. $-\gamma/2 = 0.824$ kcal/mole. Straight line indicates a non-cooperative adsorption with $-\gamma/2 = 0$ kcal/mole. (from Ling and Zhang 1984)

(i) the one-on-one, close contact adsorption of Na⁺ on the β -, and γ -carboxyl groups

To make certain that the Na⁺ taken up by hemoglobin (and thus becoming “invisible” to the Na⁺-sensitive electrode,) is indeed engaged in one-on-one close-contact adsorption according to the AI Hypothesis, we studied the influence of four other alkali-metal ions, Li⁺, K⁺, Rb⁺ and Cs⁺ on the binding of Na⁺. Now, these four alkali metal ions differ from each other and from Na⁺ only in their respective *short-range attributes* (e.g., size), which cannot be perceived unless they are in close-contact. Thus, if the Na⁺ taken up exists not in close-contact adsorption but only as part of an ion cloud hovering around the fixed anion, then the displacements by each one of four alkali-metal ions exercise on the adsorbed Na⁺ would be identical, since the respective *long-range attributes* of the four cations as (hovering) univalent cations are identical.

The data actually obtained show that the effectiveness of the four alkali metal ions tested in displacing Na⁺ from binding is all different. This leaves no doubt that each of these alkali metal ions is adsorbed on the β -, and γ -carboxyl groups in a one-on-one close contact manner. In addition, the data show that the rank order of preference in their adsorption follows the sequence Li⁺ > K⁺ > Rb⁺ > Cs⁺ — indicating that the the β -, and γ -carboxyl groups on which they are adsorbed are in a state of high c-value. Keep this in mind, because we are going to come back to it below.

(ii) the maximum number of β -, and γ -carboxyl groups liberated from salt linkages by NaOH

Figure 20 shows that as pH increased, the number of Na⁺ bound eventually reached a plateau. That maximum plateau number of Na⁺ bound per hemoglobin molecule matches the total number of β -, and γ -carboxyl groups that the (bovine) hemoglobin molecule possesses, i.e., 64 per hemoglobin molecule or 100 mmole per 100 gram of hemoglobin as shown in Figure 20 or 1 mmole per gram (Dayhoff 1972, p. D-61.)

In the next section, we return to Figure 19 once more to witness another global change in a solution of hemoglobin brought about by the addition of NaOH.

3.1.1.3 Multilayer adsorption of water molecules on the exposed NHCO groups of hemoglobin

According to the AI Hypothesis, side by side with the auto-cooperative binding of Na^+ on the OH-liberated β -, and γ -carboxyl groups, there should be (i) an auto-cooperative transition of the polypeptide chain. As a result, (ii) the polypeptide chain should switch from its original α -helical folded conformation to the fully-extended conformation. (iii) That switching in turn should bring about the polarization and orientation of the bulk-phase water. (iv) And the polarized-oriented water would then demonstrate size-dependent solute exclusion (Ling 1993.)

All these predictions, too, have been confirmed.

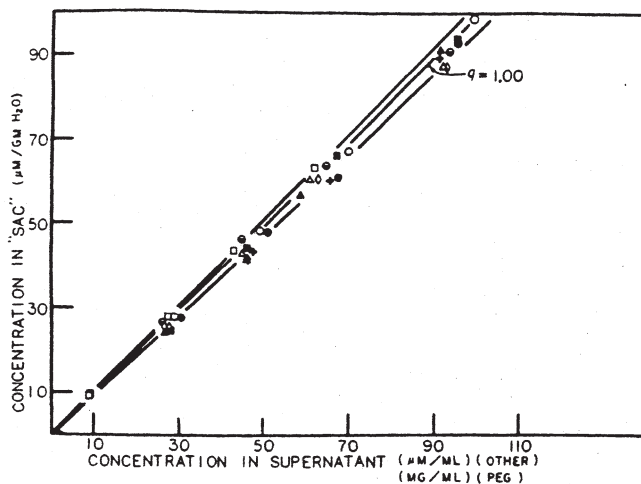
Figure 22A shows the equilibrium distribution of solutes of different molecular size between a 30% native-bovine-hemoglobin solution inside dialysis sacs and the surrounding medium of buffered water. Without exception, the plot for each solute is a straight line, indicating that all, or virtually all of the solute is dissolved in the water within the dialysis bags and none, or virtually none, adsorbed on the hemoglobin. The slope of each of these straight lines, which equals the q-value of that solute, is uniformly close to 1. This unity q-value shows that for solutes as large as raffinose and smaller, the water in a 36% native hemoglobin solution is not significantly different from that of normal liquid water. (However, see p. 173 below.)

In contrast, Figure 22B shows the equilibrium distribution of similar solutes between NaOH-denatured hemoglobin solution in the dialysis sacs and the surrounding water at a pH close to 12. These plots are also straight lines but with slopes (and hence the q-values of each solute) as a rule different from unity. Taken as a whole, these data follow the “size rule”. That is, the larger the molecular volume of the solute, the lower the slope and hence q-value — in accordance with the subsidiary theory of solute exclusion of the POM theory, nicknamed the *size rule*.

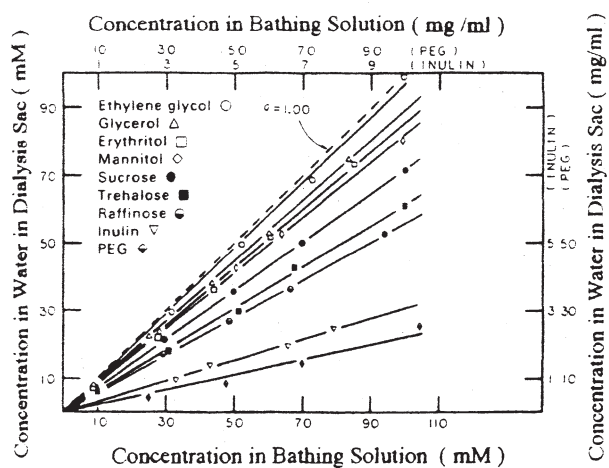
The two sets of data presented in detail in Figure 22 are presented a second time in an inset (Inset A) of Figure 23 under the respective labels of “native Hb” and “NaOH Hb.” Here, the format of the plots is different. The ordinate now represents the q-value of each solute obtained from the slopes of the individual (straight) lines of Figure 22. The abscissa here represents (the logarithm of) the molecular volumes (in units of cm^3 or cc) of the solutes under study. The top curve of the inset shows in a different way the more or less constant q-value near 1 for all the solutes investigated in a neutral native hemoglobin solution. In contrast, each solute in the study of NaOH- denatured hemoglobin has a different q-value and when viewed together as in Figure 23 Inset A, the plot is Z-shaped, indicating size-dependent exclusion.

Inset B of Figure 23 shows a different mechanism — than exposure to high pH — that can also produce water polarization-orientation and size dependent solute exclusion in a protein as well as non-protein polymer solution.

Here it is molecular structural reasons that make both gelatin and polyethylene oxide (PEO) stay in the fully-extended conformation. The PEO chain does not carry positively-charged sites like the NH groups of the normal polypeptide bond and therefore cannot form α -helical folds. Gelatin, on the other hand, contains a large percentage of proline and hydroxyproline. These exceptional amino-acid residues also do not possess the positively charged H groups on the N atom of the unusual peptide groups. In addition, gelatin also contains a large percentage of glycine residues which have a low “ α -helical



A



B

FIGURE 22. A. Equilibrium distribution of various solutes in a neutral solution of bovine hemoglobin (39%) after a 5-day incubation at 25°C. Solution contained 0.4 M. NaCl. Ethylene glycol ●, glycerol △, erythritol □, D-xylose +, sorbitol ▲, mannitol ◇, trehalose ■, raffinose ○. B. The equilibrium distribution of various solutes in an alkaline solution containing 20% bovine hemoglobin and 0.4 M. NaOH. Incubation time and temperature same as in A. (from Ling and Hu 1988)

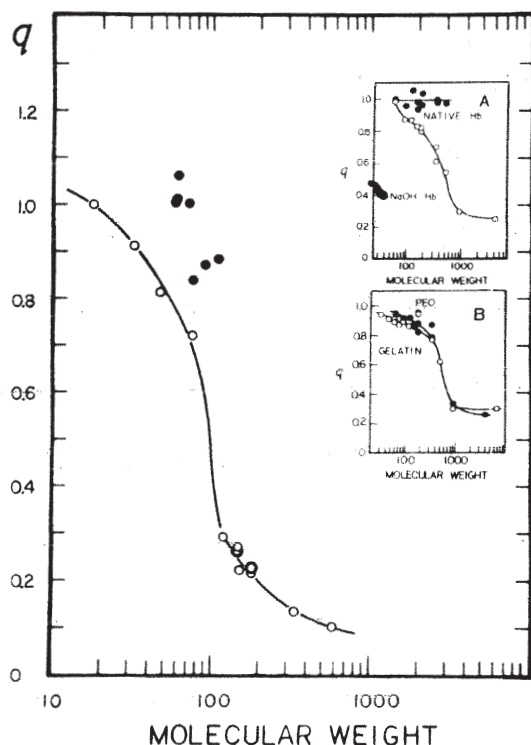


FIGURE 23. The (true) equilibrium distribution coefficient or q -value of 21 nonelectrolytes in frog muscle cells plotted against the logarithm of their respective molecular weights. Insets show similar q - w plots in native and NaOH-denatured bovine hemoglobin (top inset) and of solutions of gelatin and polyethylene oxide (PEO.) (from Ling, Niu and Ochsenfeld 1993)

potential" (see p. 132) and thus prefer not to form α -helical folds. Together, they make gelatin stay mostly if not entirely in the fully-extended conformation (Ling 1978, 1985; Ling and Ochsenfeld 1991; Ling *et al* 1980, 1980a;.) For all these reasons, both PEO and gelatin polarize and orient the bulk phase water which then show size dependent solute exclusion. In each of these cases, the q -values of large solutes reach values substantially below unity.

All three cases (solutions of NaOH denatured hemoglobin, gelatin and PEO) cited thus far belong to what I call the NP-NP-NP system as discussed on p. 134 with the help of Figure 10.

Figure 24 shows what I call the case of the marching microspheres. Here, instead of studying aqueous solutions of linear oxygen-containing polymers like PEO and polyvinyl alcohol (PVA) (Ling *et al* 1980), Zheng and Pollack (2003) studied polyvinyl alcohol (PVA) in the form of a solid PVA-gel surface. The five snapshots shown in Figure 24 were taken at time intervals indicated. Together they show these giant probes of coated microspheres as large as 1 micrometer in diameter marching away resolutely from the PVA gel surface as a result of a similar exclusion mechanism that operates in a PEO solution (NO-NO-NO) system.

On the basis of the very limited information available, I have come to the conclusion that this exclusion of the coated microspheres is not entirely due to the volume factor, represented by $v_i \mathcal{U}_{vp}$ in Equation 4. To a substantial extent, this exclusion could be due to an unfavorable surface factor described by the $v_i \mathcal{U}_s$ in that same equation.

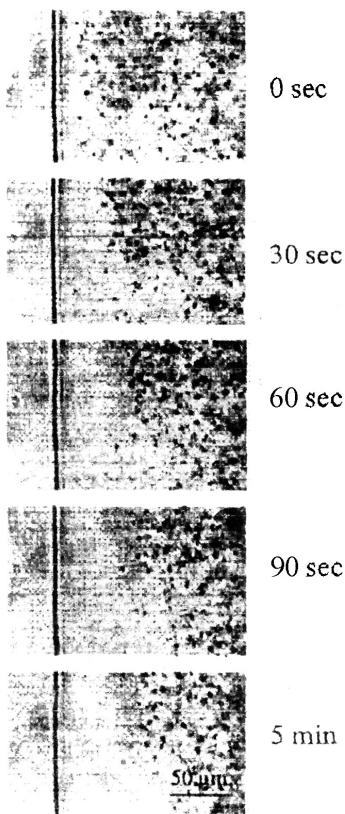


FIGURE 24. Time lapse photography of the emergence and progressive widening of a clear, exclusion zone away from the NP-NP (or NO-NO) surface of a polyvinyl alcohol gel — for the gigantic 2 μm -wide carboxylate-coated latex microsphere probes. (from Zheng and Pollack 2003, by permission of The American Physical Society)

These pictures of the marching microsphere offer a most dramatic visual verification of the POM theory of solute exclusion in particular and the AI Hypothesis in general. In parallel with this, there were also new theoretical development of the theory of long-range, indeed *ad infinitum*, water polarization and orientation mentioned above on p. 133 as well as the technological advance in vapor sorption studies of biological systems at saturation vapor pressure (Ling and Hu 1987) that led me to write the review entitled; “The Convergence of Theoretical and Experimental Breakthroughs Affirms the PM Theory of Dynamically Structured Cell Water on the Theory’s 40th Birthday” as the first chapter of a book on *Water and the Cell* edited by Pollack *et al.* (Pollack *et al* 2005.)

I conclude this section with a table (Table 4.) It is introduced here to serve three purposes.

First, it shows yet another way of producing fully-extended protein chains by the action of concentrated urea, which unravels the α -helical folds.

Second, it shows that all ten proteins studied, including hemoglobin, responded to high urea concentration by undergoing an all-or-none transformation from the “native” folded conformation to a fully-extended conformation, which in turn, makes the bulk-phase water exhibit size dependent solute exclusion. As an example, radioactively-labeled urea with a (small) molecular volume of 49.6 cc (and possibly a favorable surface structure that

TABLE 4. A comparison of the D-values of ^3H -labeled urea and that of ^{14}C -labeled sucrose in the same water in solutions of ten different proteins all denatured by the presence of 9 M urea in the solution. The numbers in the parenthesis following the p-values of urea are from left to right: the number of individual assays made, the total number of sets of experiments performed, the percentage of water in the urea-denatured protein solution and the pH of the solution. (from Ling and Ochsenfeld 1989)

	ρ_{urea}	ρ_{sucrose}
Albumin (serum)	1.02 ± 0.010 (20,5;41;7.0)	0.697 ± 0.010
Albumin (egg)	1.00 ± 0.015 (24,4;40,6.9)	0.710 ± 0.010
α -chymo- trypsinogen	1.02 ± 0.030 (12,3;44;6.7)	0.707 ± 0.012
Edestin	1.00 ± 0.013 (8,2;41;6.7)	0.759 ± 0.007
Fibrinogen	0.964 ± 0.012 (12,3;43;8.1)	0.771 ± 0.014
γ -globulin	1.05 ± 0.015 (14,3;40;7.8)	0.660 ± 0.013
Hemoglobin	0.984 ± 0.008 (32,8;41;6.9)	0.685 ± 0.020
β -lacto- globulin	0.972 ± 0.010 (20,5;40;7.2)	0.670 ± 0.010
Lysozyme	1.01 ± 0.014 (12,3;43;7.3)	0.855 ± 0.015
Trypsin	1.04 ± 0.022 (12,2;47;5.7)	0.809 ± 0.016
Mean \pm S.E.	1.006 ± 0.008 (10)	0.732 ± 0.019 (10)

fits well into the surrounding polarized-oriented water structure), shows an average p-value of 1.002 while in the water of the very same solution, the p-value of sucrose — with a molecular volume of 342.3 cc. — is only 0.732.

Third, this set of data has also an important historical significance. It has reversed the world-shaking conclusion of A.V. Hill made in 1930 that cell water is normal liquid water because it does not exclude urea. It was this conclusion of Hill that had put to rout the protoplasm-oriented cell physiologists worldwide, who believed that at least some cell water is bound and thus “non-solvent.” (Hill 1930; Hill and Kupalov 1930.) Now we know better. (For more details, see Ling 2001, pp. 38–39, 100–101.)

Indeed, the main curve to the left of Figure 23 shows the solute distribution in the same kind of tissue Hill studied, frog muscle. As such, it at once confirms the near unity q-value(s) of urea (and ethylene glycol) and the size-dependent exclusion of sucrose and a host of probes of larger sizes within the same or similar cell water.

3.1.2 Controlled auto-cooperative transition

3.1.2.1 Control of heme-heme interaction by cardinal adsorbents including ATP

From way back, investigators of the oxygenation and deoxygenation of hemoglobin had noticed a profound difference in the affinity for oxygen of isolated pure hemoglobin in solution from that of hemoglobin in living red blood cells. Comparing the oxygen binding of isolated hemoglobin shown in Figure 17 with the oxygen binding curve of hemoglobin in intact human red blood cells shown in the inset of Figure 16, you will quickly reach the same conclusion. Thus, in Figure 17, the oxygen tension that produces half saturation of the heme sites is 10 mm Hg. The corresponding oxygen tension that produces half saturation in intact red cells is three times higher at 30 mm, Hg.

Put in a different way, a solution of purified hemoglobin would not be able to deliver oxygen from the lungs to the peripheral tissues for the same reason that myoglobin would not be able to deliver oxygen to the peripheral tissues: both hold onto the oxygen too tightly and would not release it where it is needed. Thus, a hemoglobin solution is not in the normal living state to operate physiologically. To maintain the nano-protoplasm in the normal living state, it requires the binding of a suitable cardinal adsorbent in the form of ATP (or its equivalents, like 2,3-DPG) as shown in Figure 5. Of course, we know that human red blood cell in its resting living state does contain ATP and 2,3-DPG, but to make sure that it is indeed the ATP or 2,3-DPG (binding) that brings about the reduced affinity of the heme sites for oxygen, we need precise quantitative experimental data again.

Once more, we are lucky in having access to another set of very accurate data of Benesch and Benesch (1969) on both the impact of 2,3-DPG and of inosine hexaphosphate (IHP) on the oxygen binding of human hemoglobin. Soon we discovered that both sets of data fit our theoretical curves well. To save space, only the set with IHP as the cardinal adsorbent is reproduced here as Figure 25. Again the points are experimental and the lines theoretical computed on the basis of the following equation:

$$[p_i]_{ad} = \{g/2\} [C]_{ad} \Omega_c + \{g/2\} \{[F] - [C]_{ad}\} \Omega_o, \quad (11)$$

where $[p_i]_{ad}$ is the concentration of the i th solute (oxygen in the present case.) g is the number of cooperatively linked regular adsorption sites (heme sites). $[C]_{ad}$ is the concentration of cardinal sites occupied by the cardinal adsorbent. Ω_c and Ω_o are basically as defined in Equation 8 on p. 143. The subscripts C and O indicate that the regular adsorption sites for the i th solute in gangs under the domination of the cardinal adsorbent C and those not under the dominance of a cardinal adsorbent. Other relevant information can be found in the legend of Figure 25.

The most striking revelation of these first-rate data is that (the adsorption of) inosine hexaphosphate (IHP) dramatically reduces the affinity of hemoglobin for oxygen. Given as the free energy of binding, the free energy of oxygen binding falls from -6.63 Kcal/mole to only -4.71 Kcal/mole. We will return to this issue below.

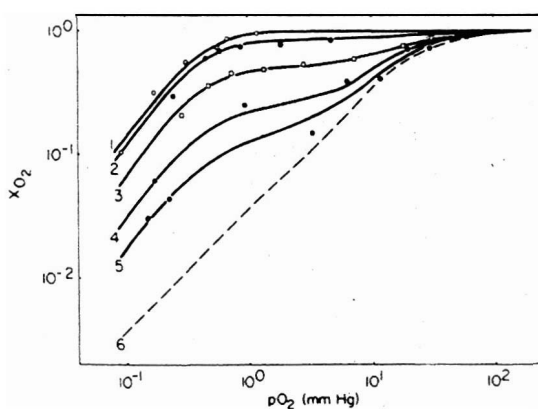


FIGURE 25. Oxygen uptake by human hemoglobin in the presence of different concentrations of inosine hexaphosphate (IHP). Points are experimental from Benesch and Benesch (1969). Lines are theoretical based on the Yang-Ling adsorption isotherm. Number at the ends of different lines refer to concentration of IHP: (1) no IHP; (2) 1.2×10^{-5} M; (3) 2.4×10^{-5} M; (4) 3.5×10^{-5} M; (5) 4.8×10^{-5} M; (6) ∞ IHP. Values of parameters used are as follows: $K_0 = 3.33$; $K_c = 0.67$ (mm Hg) $^{-1}$; $-(\gamma_0/2) = 0.39$ kcal/mole; $-(\gamma_c/2) = 0.21$ kcal/mole; $\mathcal{K}_c = 4.2 \times 10^{-4}$ (M) $^{-1}$; $-(\Gamma/2) = 0.68$ kcal/mole. (from Ling 1970)

Of equal, or perhaps greater importance, is the finding of ATP's similar ability to reduce the affinity of hemoglobin for oxygen (Benesch and Benesch 1967; Chanutin and Curnish 1967.) However, so far I have not been able to locate quantitative data like those of the Benesch's on DPG and IHP. Nonetheless, there is no doubt that ATP performs the same function as an electron-withdrawing cardinal adsorbent or EWC as illustrated for (2,3-DPG and) IHP in Figure 13B.

As pointed out before, hemoglobin does not possess ATPase activity. This makes ATP and 2,3-DPG coequals, both serving the same basic function of a cardinal adsorbent — without the complication of the ATPase activity of some more specialized cardinal sites in other more complicated forms of protoplasm.

3.1.2.2 Control of the dynamic structure of bulk-phase water

The work referred to in the above title has not been published yet. For this reason, only a short summary of the essence of this work will be given on p. 222 under the concluding section entitled Discussion.

3.2 *In vivo* studies of the nano-protoplasm as a part of a living cell

Thus far, the studies of the binding of oxygen and of Na^+ were carried out in solutions of salt and hemoglobin as an ultra-simple model of the rbc cytoplasmic nano-protoplasm in specific and protoplasm in general. Furthermore, in the presence of suitable cardinal adsorbent, be it ATP, 2,3 DPG or IHP, they can carry out their major physiological function of oxygen transport, matching that observed in a population of intact human red blood cells. Indeed, in more than one way, this concordance between theory and experimental facts went far beyond our fondest hopes.

From here on, our studies would move to normal protoplasm as part of living cells. Since according to the association-induction hypothesis, the cardinal adsorbent ATP is an integral part of the living nano-protoplasm, a study of normal living cells is a study of the protein-salt ion-water assembly under the domination of ATP. In other words, *all the study of living cells, regardless of which cell physiological activity is studied, is a study of the equivalents of the 2,3-DPG-, or IHP- or ATP-dominated hemoglobin-salt ion-water system as a whole — rather than the equivalent of an assembly of hemoglobin-salt ion-water system by itself in the absence of the controlling cardinal adsorbent.*

Ideally, the theory of protoplasm as an auto-cooperative assembly of similar or dissimilar nano-protoplasm units should be tested on all living phenomena. In a limited sense, that has been what I and my associates here and abroad have been doing from 1952 on. And the results have been presented in my four books (Ling 1962, 1984, 1992 and 2001) but especially in the first two. The reader can also get a glimpse of the list of topics addressed from the reproduced tables of contents in the websites: <www.gilbertling.org/lp7a.htm> and <www.bioparadigma.narod.ru/ling.htm>

In an article like the present, my review would be limited to the four classic cell physiological topics: (i) solute distribution, (ii) solute permeability, (iii) cellular electric potential and (iv) cell volume control. It should be pointed out that these four subjects have been the foci of the thinking of most cell physiologists since the cell was first discovered as the basic unit of life.

In addition, I shall demonstrate also the following: (i) the concordance between theory and experimental observations is not limited to a specific kind of cell but among cells or

even organelles of widely different origin and specific chemical makeup; (ii) the overwhelming dominance of the role of β -, γ -carboxyl groups and the backbone NHCO groups in all the physiological activities investigated; (iii) in all cases, the Yang-Ling adsorption isotherm is used to check and verify the concordance between theory and facts and as a way of extracting critical quantitative data from the raw experimental findings.

Each of these sections begins with a list of key review articles that describe the historic background of the subject and preferably in articles that are also reachable online with no restriction. Following this list, there would be a section on the quantitative theoretical formulations for that specific physiological phenomenon. Details of experimental studies and their analysis then follow.

3.2.1 Distribution of solutes in the living cell and its control

Reviews: Troshin 1966; Ling 1962 Chapt. 9; 1984 Chapt. 11, 1992 Chapt. 8; 2001 Sect. 15.1; Ling 2005.

3.2.1.1 Theory

In 1965, I introduced a general equation for solute distribution in living cells (Ling 1965b, p. 99.), given as Equation A6 on page 284 of Ling 2001. In this general equation I assumed the existence of n different types of adsorption sites for the ith solute. (However, see p. 220 in Discussion to follow, for final verdict on the validity of this assumption.)

$$[p_i]_{in} = \alpha q_i [p_i]_{ex} + [f]_1 \Omega_1 + [f]_2 \Omega_2 + \dots + [f]_n \Omega_n . \quad (12)$$

The first term of the right-hand side of Equation 12 refers to free solute dissolved in the cell water; the second and succeeding terms refer to adsorbed solute on each of the n types of adsorption sites. $[p_i]_{in}$ and $[p_i]_{ex}$ are respectively the equilibrium intracellular and extracellular concentration of the ith solute. α is the water content of the cell in weight percentage. q_i is the equilibrium distribution coefficient of the ith solute between the cell water and that in the surrounding medium. $[f]_1$, $[f]_2$, ... $[f]_n$ are the concentration of the first, second and nth adsorption sites. The Ω 's are the corresponding symbols as defined in Equation 8 on page 143.

In the case, where the living cell under study contains only one type of adsorption site for the ith solute, Equation 12 would be reduced to a two term equation as follows:

$$[p_i]_{in} = \alpha q_i [p_i]_{ex} + [f] \Omega . \quad (13)$$

When the only existing type of the adsorption sites demonstrates no site-to-site interaction, Equation 13 reduces to a form first introduced by A.S. Troschin (Troschin 1951.) Known as the Troschin equation (See Ling 2001, Equation A1 on page 282,) it can be written in the following form:

$$[p_i]_{in} = \alpha q_i [p_i]_{ex} + \frac{[f][p_i]_{ex} K_i}{1 + K_i [p_i]_{ex}} , \quad (14)$$

where K_i is the adsorption constant of the i th solute on the (only one type of) adsorption site in units of (moles/liter) $^{-1}$. The second term on the right hand side is the Langmuir adsorption isotherm. When there are two types of solute competing for the single type of adsorption sites, Equation 14 can be written as

$$[p_i]_{in} = \alpha q_i [p_i]_{ex} + \frac{[f][p_i]_{ex} K_i}{1 + K_i [p_i]_{ex} + K_j [p_j]_{ex}}. \quad (15)$$

which , in turn, can be also written in the reciprocal form:

$$\frac{1}{[p_i]_{in}} = \frac{K_i}{[f]} \left(1 + \frac{[p_j]_{ex}}{K_j} \right) \frac{1}{[p_i]_{ex}} + \frac{1}{[f]}. \quad (16)$$

A plot of $1/[p_i]_{ad}$ as ordinate against different values of $1/[p_i]_{ex}$ as abscissa would yield a straight line with its slope determined by the concentration of the j th competing ion and the adsorption constants of both the i th and j th solutes. In form, this reciprocal plot is identical to what is familiar to many readers as the Michaelis-Menten plot in enzyme kinetics. From the slopes and intercepts all the unknown quantities can be determined.

3.2.1.2 Results of experimental studies on the distribution of water and solutes

a. Water

Historically speaking, the mature plant cell is a red herring. Its possession of a large amount of ordinary liquid water contained in its huge central vacuoles misled Theodor Schwann into the belief that all living cells are membrane-enclosed puddles of salty but otherwise perfectly normal liquid water. As mentioned above, and as an integral part of the association-induction hypothesis, the POM (or PM) theory of cell water was introduced in 1965 (Ling 1965.) However, not until 2004 was it made explicitly clear that the only theory of cell water that meets all three sets of decisive findings is the polarized-oriented multilayer (POM, PM) theory of cell water (Ling 2004.)

Now, according to the POM theory of cell water, it is a matrix of fully extended protein chains that provide the alternately negative oxygen atoms of the CO groups and the positive H atom of the NH groups that polarize and orient the cell water in the dynamic structure of polarized-oriented multilayers. The excess water-to-water interaction energy is relatively speaking weak but highly (auto-)cooperative. As such, one would expect that in an environment of increasing vapor pressure, the living cell would take up little water until the vapor pressure reaches a very high value. This expectation was confirmed in 1970 by Ling and Negendank (1970.)

Figure 26 shows the vapor sorption isotherm of surviving frog muscle cells reported by Ling and Negendank (1970.) It is an unusually steep-rising curve. Indeed, fully three fourths of the water taken up occurs at relative vapor pressure above 95%. The tragic irony is that the vast amount of fine water vapor sorption data on isolated proteins in the literature were limited to relative vapor pressure below 95%. That is so with one striking exception: the extensive study of water sorption of proteins and other bio-materials by

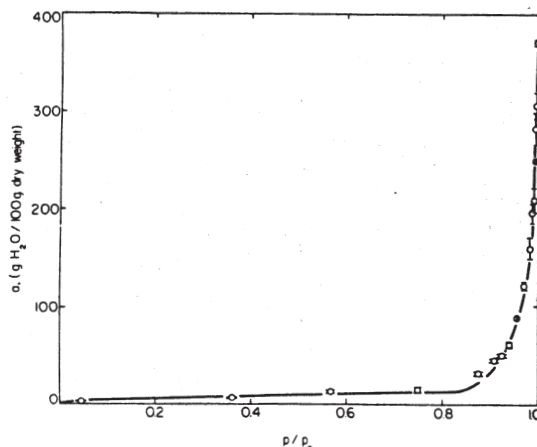


FIGURE 26. Water vapor sorption of strips of intact frog muscle cells from relative vapor pressure of 0.043 to 0.996. Sterilely isolated muscle strips hung in vapor phase of stoppered glass tubes, which were entirely immersed in a constant temperature water bath maintained at $25^\circ \pm 0.05^\circ\text{C}$ for five days. (Ling and Negendank 1970)

J.R. Katz (Katz 1919.) His data cover relative vapor pressure all the way to 100% saturation. In admiration, I reproduce in Table 5 two sets of his original reported findings. They are respectively on hemoglobin and on gelatin. And what striking difference in the water vapor sorption the pair of proteins has revealed — only to be largely ignored by most later workers.

In hemoglobin, there is a small additional gain from 0.500 gram of water per gram of protein to 0.710 g/g when the relative vapor pressure rose from 0.965 to 1.000. In sharp contrast, the gain for gelatin rose from 0.641g/g to 4.0 g/g from the same increase of relative vapor pressure from 0.965 to 1.000.

In years after, most investigators of protein hydration followed the lead of the hemoglobin data, which showed little additional uptake of water vapor at relative vapor pressure higher than 0.95 in the belief that crystalline hemoglobin represents the good,

TABLE 5. J. R. Katz's original data on the water vapor sorption of oxyhemoglobin and of gelatin at from 0 to 100% vapor saturation. (from Katz 1919)

Oxyhämoglobin		Gelatine.	
h	i	h	i
0,—	0,—	0,—	0,—
0,020	0,014	0,020	0,033
0,048	0,020	0,122	0,095
0,122	0,038	0,306	0,168
0,208	0,063	0,420	0,232
0,306	0,085	0,525	0,298
0,420	0,101	↑ 0,620	0,793
0,525	0,124	0,718	0,328
↑ 0,620	0,140	0,793	0,376
0,718	0,173	0,857	0,442
0,793	0,221	0,915	0,442
0,857	0,296	0,965	0,641
0,915	0,390	1,000	+ 4,6
0,965	0,500		
	0,720		
1,000	0,700		
	0,710		

"native" protein and that gelatin, which they believed to be bad or denatured is ignored. However, a comparison of the data of Table 5 with the data shown in Figure 26 shows that it is just the opposite. The (denatured) gelatin is in a state much closer to the water-sorbing proteins in living cells.

There is another reason that very few studied water vapor sorption at near saturation vapor pressure as J. R. Katz did almost two centuries ago. That is the extreme slowness in reaching vapor diffusion equilibrium. It took months of incubation for J. R. Katz to get the data he published. However, he was not sure that that was long enough. So he put a \pm sign in front of his figures for gelatin at 100% vapor pressure.

Eventually, Ling and Hu introduced a new method called "the Null Point Method" which shortens the time of equilibration to only five days (Ling and Hu 1987.) Using this method, they studied not only the water sorption at near saturation of gelatin — proving that Katz was right in putting a big \pm sign in front of his number of 4.6. For in our studies with the null-point method, the water uptake of gelatin at near saturation reached 5.50. As a model of the living protoplasm, gelatin shows that it is in a fully-extended conformation under most circumstances. That gives it the high level of water vapor uptake at physiological vapor pressure (0.996), matching that seen in living frog muscle cells.

Using the Null Point method, Ling and Hu also studied other simple models beside gelatin, including various oxygen-containing linear polymers like polyvinylpyrrolidone (PVP), polyethyleneglycol (PEG), polyvinyloxide (PEO.) As also shown in Figure 27, the water uptake of these polymers can be even higher than either gelatin or frog muscle cells. Then at the lower part of the graph, we see hemoglobin and another so-called native protein, γ -globulin. Both take up much smaller amounts of water — again in full harmony with our model of nano-protoplasm as depicted in Figure 5.

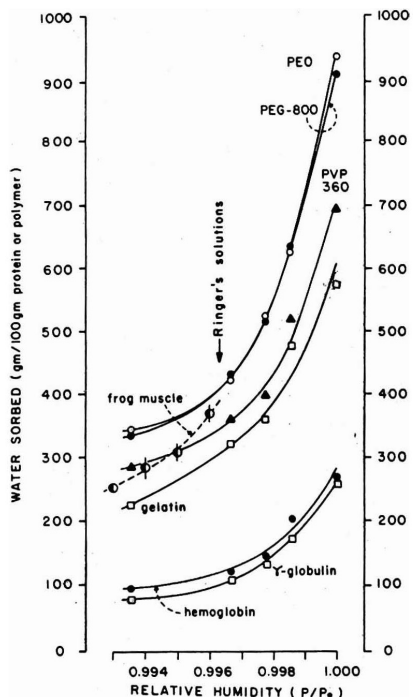


FIGURE 27. Equilibrium vapor sorption of three proteins (gelatin, hemoglobin and γ -globulin) and three linear oxygen-containing polymers (PEO, PVP 360 and PEG-800.) In addition, a stretch of the vapor sorption data of frog muscle from the preceding figure and the vapor pressure of frog Ringer's solution are also included for comparison. Data obtained with Ling and Hu's new Null Point Method. (from Ling and Hu 1987)

b. Ions

A striking feature of the living cell is its ability in maintaining in itself a very high level of K^+ but a low level of (the highly similar) Na^+ — from an external environment containing little K^+ but an overwhelming abundance of Na^+ . It is no surprise that the well known (and less well known) theories of the living cell were all built around this outstanding physiological attribute.

As examples, both the atomic sieve version and the pump version of the membrane theory were designed to cope with this asymmetry in ion distribution. In addition, the association induction hypothesis also began in 1952 with a non-energy consuming mechanism for this K^+ over Na^+ selectivity under the title of Ling's fixed charge hypothesis. The more up-to-date model of the nano-protoplasm as illustrated in Figure 5 prescribes at once a mechanism of selective adsorption for K^+ accumulation and bulk-phase water polarization-orientation to produce a low q -value for the partially excluded Na^+ (Cl^-).

By the same token, nano-protoplasm in its resting living state contains the principle cardinal adsorbent ATP, which is the final product of energy metabolism. So much for a general introduction for the subject of selective K^+ accumulation in living cells.

Next, we begin our more focused discussion on selective ionic accumulation with the main figure of Figure 16 on p. 148, a plot of the equilibrium distribution of K^+ in frog muscle at varying external K^+ concentration shown on the abscissa and a constant concentration of Na^+ at 100 mM. It is obviously also an S-shaped curve very much like the oxygen-binding curve of hemoglobin in intact red blood cells shown in the inset and to which we have referred to repeatedly above. This similarity in two totally different physiological manifestations in two totally different kind of living cells affirms the concept of a shared fundamental physical basis of all life, the nano-protoplasm. Actually, the similarity goes even deeper as what follows demonstrates.

Figure 28 shows a log-log plot of the K^+/Na^+ distribution in isolated frog muscle, which too bears striking similarity to the oxygen binding curve in a similar log-log plot as shown in Figure 17 on p. 150.

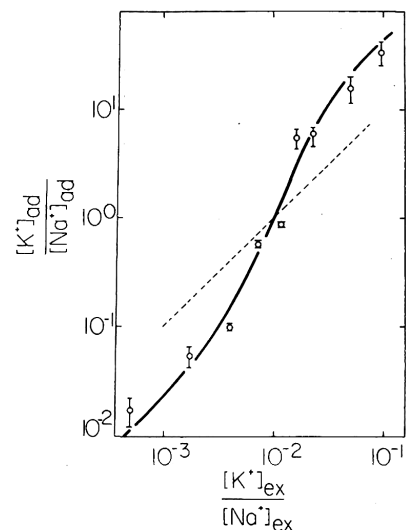


FIGURE 28. Log-log plots of the equilibrium distribution of K^+ and Na^+ in isolated normal frog muscle. External Na^+ concentration in the bathing medium was held unchanging at 100 mM while the K^+ concentration was varied. Points are experimental. The distance between the two horizontal bars is equal to twice the standard errors of the mean, each point representing at least four determinations. Solid line going through or near most of the points is theoretical, calculated according to the Yang-Ling isotherm with $K^\infty_{Na \rightarrow K} = 100$ and $-\gamma/2 = 0.62$ kcal/mole. Dashed straight line shows a non-cooperative adsorption. (from Ling and Bohr 1970, by permission of the Biophysical Journal)

Like Figure 17, the points in Figure 28 are experimental and the line is theoretical — indeed, it is the same Yang-Ling isotherm (Equation 5) that describes the oxygen binding data of Lyster shown as Figure 17. Here, the $K_{Na \rightarrow K}^\infty$ is equal to 100 equivalent to a $\Delta F_{Na \rightarrow K}^\infty$ of 2.74 kcal/mole. The $-(\gamma / 2)$ is equal to 0.62 kcal/mole, equivalent to a Hill coefficient n of 2.9 — to be compared with the $-(\gamma / 2)$ of 0.67 kcal/mole and a Hill coefficient of 3.1 in the binding of oxygen on human hemoglobin shown in Figure 17.

The auto-cooperative adsorption of K^+ and Na^+ in protoplasm that makes up the frog muscle cells has also been repeated in other types of protoplasm making up other types of living cells. They include the smooth muscle cells of canine carotid arteries (Gulati 1973), guinea pig taenia coli — a narrow bundle of smooth muscle running along the length of the intestine (Reisin and Gulati 1973) and human lymphocytes (Negendank and Shaller 1979.) All can be quantitatively described by the same Yang-Ling adsorption isotherm. Furthermore, the $K_{Na \rightarrow K}^\infty$ and $-(\gamma / 2)$ values derived from the data are not far from those obtained from the frog muscle (Figure 28); nor from the ultra-simple model of red blood cell nano-protoplasm under the control of 2,3-DPG, IHP and ATP.

There are extensive evidence that the adsorption sites for the K^+ or Na^+ described are β -, and γ -carboxyl groups. And these evidence have been reviewed repeatedly in recent publications (Ling and Ochsenfeld 1991; Ling 2005, pp. 42-44.) Only one set is reproduced here as Figure 29A.

But before discussing the data, I need to remind the reader that data already shown in Section 3.1.1.2 and yet to be shown below in Section 3.2.1.2.2 have established the basic fact that both K^+ and Na^+ occupy the same sites, only their binding energies differ. Thus, one can investigate the nature of their common binding sites, with either K^+ or Na^+ as the probe. At the time we did this study we only had on hand some long-lived ^{22}Na but no access to short-lived ^{42}K . For this reason, we used the labeled Na^+ for our study of the adsorption sites that in normal cells are as a rule occupied by K^+ .

Figure 29A is a plot of the number of μ moles of labeled Na^+ bound to each gram of frog muscle nano-protoplasmic proteins at different pH's. This curve shows that all the binding sites for Na^+ (or K^+) have a uniform pK_a of 3.85 and a total concentration above 70 μ moles/g. β -, and γ -carboxyl groups alone exist in high enough concentration in this (and other) type of living cells and all have the matching pK (3.65–4.7) (Stecher 1968, p. 107; Edsall & Wyman 1958, p. 534) to fill this role. This agreement affirms the basic postulation of the AI Hypothesis that β -, and γ -carboxyl groups are the adsorption sites for K^+ and Na^+ found in most if not all living cells.

c. Nonelectrolytes

Figure 30 presents linear plots of the equilibrium concentrations of 9 nonelectrolytes in living frog muscle cell water against those in the bathing medium. Like its *in vitro* counterpart, shown in Figure 22, these and 12 other plots of still other solutes studied are all straight lines. The slopes of these straight lines yield the q -values of the solute studied. In Figure 23, the data points are plotted against the molecular weights of the nonelectrolytes. In this case, the Z-shaped curve that fits part of the data points are by visual inspection. Seven points apparently are too high to be consigned to the same curve.

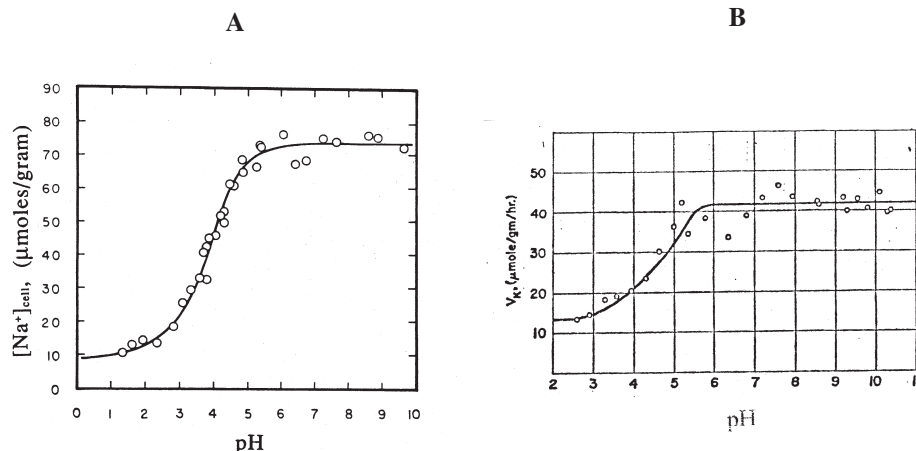


FIGURE 29. Identifying as β -, and γ -carboxyl groups, both the sites in muscle cytoplasm that adsorb K^+ (and Na^+) and the sites on muscle cell surface that mediate K^+ entry. A. Equilibrium uptake of labeled Na^+ at different pH by 2 mm wide muscle cell segments with open ends. After due corrections had been made the titration curve shows an inflection point at a pH of 3.86. This led to the conclusion that the β -, and γ -carboxyl groups belonging mostly to myosin offer the adsorption sites. B. Effect of pH on the rate of entry of labeled K^+ into intact frog muscles. Corrected titration curve shows an inflection point at a pH of 4.6, again suggesting β -, and γ -carboxyl groups of cell surface proteins mediate K^+ entry. (A from Ling and Ochsenfeld 1991. B from Ling and Ochsenfeld 1965, by permission of the Biophysical Society)

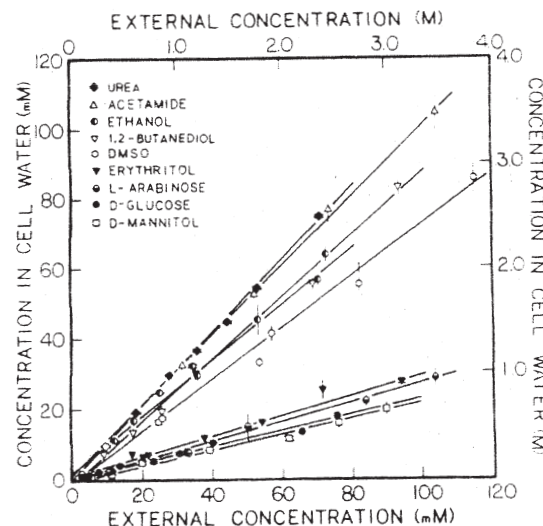


FIGURE 30. Equilibrium distribution of nine nonelectrolytes in frog muscle cell water against their respective concentration in the bathing medium. Names and symbols of each of the nonelectrolytes are given in the graph. (Ling, Niu and Ochsenfeld 1993)

In Figure 31, on the other hand, the same set of all the data points are presented in the inset on the left lower corner of the graph. Here the q -values are plotted against the respective molecular volume of each solute, but there are two theoretical curves both based on Equation 4 on p. 136.

Only here, the seven seemingly aberrant points of Figure 23, prove to be not aberrant at all. Instead, they demonstrate the same U_{vp} value of 126 cal/mole but different U_s values. The U_s of the curve that fits the lower groups of points is 119 cal/mole but the curve that fits the higher group of points has a U_s of 156 cal/mole. Five of these seven nonelectrolytes with the higher U_s are established *cryoprotectants*. That is, chemicals when added to the freezing mixture of living tissues to be preserved at liquid-nitrogen temperature, protects the tissue from freezing or thawing injury. A sixth chemical (urea) could also be a cryoprotectant if it were not also a protein denaturant

3.2.1.3 Results of experimental study on the control of solute distribution

3.2.1.3.1 Control by ATP

a. Ions

Figure 32 shows the linear relationship demonstrated by Gulati *et al* (1971) between the K^+ and ATP concentration in the same slowly dying frog muscle cells. Note that it does not matter what poison was used to bring about the slow death. Essentially the same linear relation between ATP and K^+ concentration holds. This indifference to the nature of the poisoning step emphasizes that the deprivation of ATP — the end-product of all energy metabolism — is the critical cause of the decline of K^+ adsorption — in full support of the role of ATP as the critical cardinal adsorbent depicted in Figure 5.

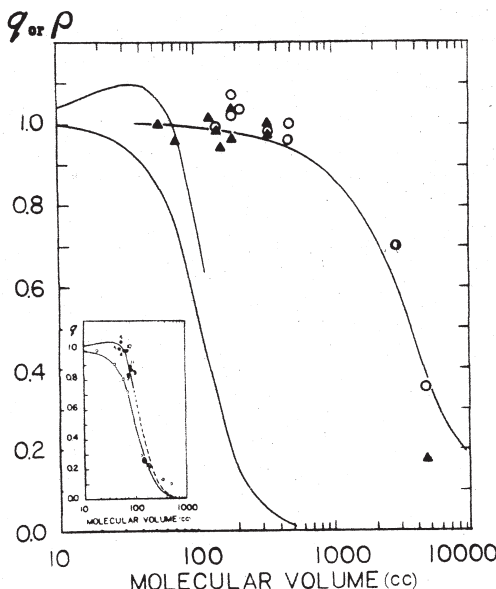


FIGURE 31. The equilibrium distribution coefficients (q , ρ , and ρ -values) of various nonelectrolytes in a neutral solution of 36% bovine hemoglobin (solid triangles) and in the water of killed Ehrlich ascites cells (open circles) against the molecular volumes of the respective nonelectrolytes. The solid line going through or near most of the experimental points are theoretical according to Equation 4 on p. 136, with an U_{vp} equal to 3.8 cal/mole. The inset shows q - v plot of living frog muscle cells. The solid lines going through or near most data points are theoretical according to Equataion 4 with U_{vp} equal to 126 cal/mole, as are their outlines also drawn on the main graph. (from Ling 2005a)

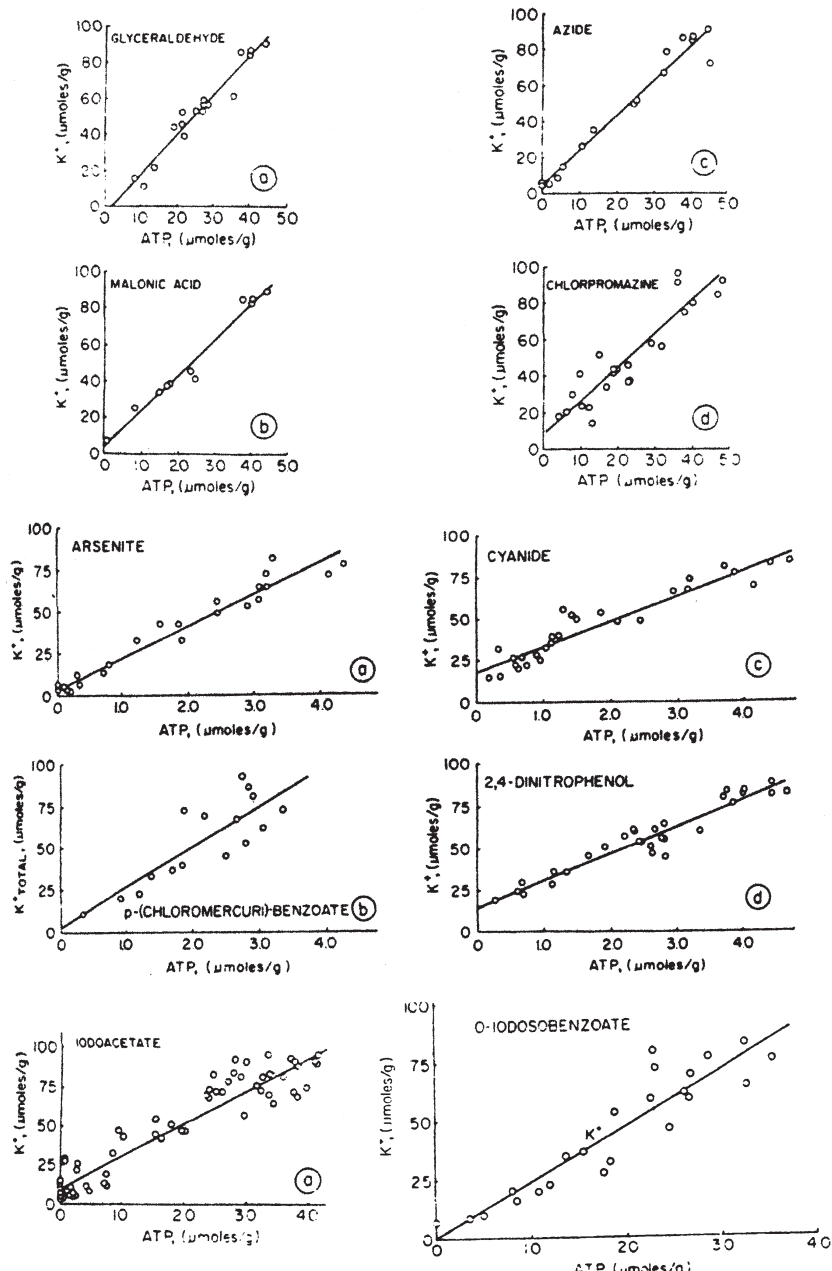


FIGURE 32. The relationship between the equilibrium concentration of K^+ and that of ATP in frog muscle cells exposed to a wide variety of poisons at 25° C. To insure the attainment of diffusion equilibrium the muscles were transferred after varying length of time in the 25° C solution to a 1° C solution for 2 to 4 hours before being readied for analysis. The simple straight line relationship between K^+ and ATP concentrations seen here may be dependent on this second incubation. (For other results obtained without this second trip to 1° C, see Figure 8.19 on p. 193 of Ling 1992.) (from Gulati, Ochsenfeld and Ling 1971, by permission of Biophysical Journal)

Figure 33 shows the parallel time courses of change of ATP and K^+ — which confirms what has already been shown in Figure 32. In addition, Figure 33 also shows an anti-parallel time course of Na^+ -concentration change. There are two alternative interpretations of the anti-parallel Na^+ concentration change.

In the first interpretation, all the extra Na^+ gained with time is adsorbed, displacing an equivalent amount of K^+ normally adsorbed on the β -, and γ -carboxyl groups. In the second interpretation, the Na^+ gained is free Na^+ dissolved in the cell water in consequence of a steady increase of the q -value of Na^+ (as chloride) in a depolarizing and disorienting cell water. This increasing depolarization and disorientation of the cell water parallels the time course of ATP depletion.

The fact that sucrose, also shows a rising time course in parallel with the Na^+ time course favors the second interpretation. That is, the binding of ATP controls both the selective adsorption of K^+ and the exclusion of Na^+ (and sucrose.) In poisoned muscle cells, ATP depletion causes the concomitant loss of cell K^+ and gain of dissolved cell Na^+ by at once lowering the c -value of the β -, and γ -carboxyl groups and the c -value analogue of the backbone carbonyl groups.

Both Figure 32 and Figure 33 also show that with the total disappearance of ATP, the muscle cells no longer selectively accumulate K^+ , nor do they exclude Na^+ or sucrose. In addition, they also lost their normal softness and flexibility as they enter into the state of *rigor mortis* by forming salt linkages as also indicated by the left-hand side figure of Figure 5.

b. Nonelectrolytes

According to the earliest version of the AI Hypothesis, rigor mortis of (dead) muscle is the consequence of the formation of extensive inter- and intra-molecular salt linkages (Ling 1952.) Now, the so-called “native” hemoglobin also does not bind Na^+ (or K^+) but does so when its fixed cations are neutralized with OH^- (Figure 19 and 20.) This OH^- -induced Na^+ -binding confirms that salt-linkage formation is the underlying cause why native proteins do not adsorb, or adsorb little K^+ or Na^+ (Ling 1952, Figure 8 on p. 778.)

The recognition of the wide-ranging impact of salt-linkage formation in cell physiology also opened the door to other productive new ideas. As an example, it led one to suspect something exists in common between what we call “native” proteins like store-

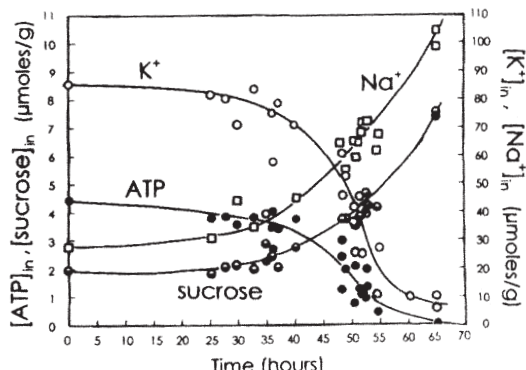


FIGURE 33. Time courses of changes in the concentrations of K^+ , Na^+ , sucrose and ATP in frog muscles incubated in a Ringer's solution containing initially 1 mM of Na-iodoacetate and 10 mM labeled sucrose and maintained at 0°C. Symbols used are as follows: K^+ o, Na^+ □, sucrose ⊖, ATP ●. (from Ling and Ochsenfeld in Ling 2001)

bought crystalline hemoglobin and proteins in dead cells. This suspicion metamorphosed into reality by the demonstrated quantitative similarity of water in a 36% native hemoglobin solution and in dead (Ehrlich ascites cancer) cells to accommodate the same concentration of large probe molecules as shown by the figure on the extreme right of Figure 31.

Here, the data points in the form of solid triangles were obtained from a 36% native bovine hemoglobin solution in dialysis bags. In contrast, the data points represented as empty circles were from killed Ehrlich ascites cancer cells. Water in both systems, though showing no detectable exclusion for probes as large as raffinose with a molecular volume of 550 cc., strongly exclude polyethylene glycol (PEG 4000) with a molecular volume of 4717 cc. Both sets of data points fit the same theoretical curve based on Equation 4 with a volume factor of exclusion, \mathcal{U}_{vp} equal to 3.4 cal/mole. For comparison, the two curves to the left in the same figure are from living (frog muscle) cells. There, the corresponding \mathcal{U}_{vp} is more than 30-times higher at 126 cal/mole.

I have on more than one occasion expressed my marvel at the extreme sensitivity of the q -value studies to reveal a minute excess of water-to-water interaction energy of only 3 to 4 cal/mole, when the total normal water-to-water interaction energy is 10,000 cal/mole. As a commentary, I also pointed out that this phenomenon finds a parallel in an analytical balance where pans weighing hundreds of grams in weight, do not hamper the instrument from revealing the true weight of a sample at a fraction of a milligram. It is all a balancing act.

3.2.1.3.2 Control by ouabain

Ouabain, also known as G-strophanthin, is a water-soluble cardiac glycoside. It has been widely used by investigators testing the validity of the sodium pump hypothesis in their belief that ouabain is a specific inhibitor of the hypothetical Na pump — but in vain (see Ling 1997a.) Nonetheless, there is no question that ouabain at extremely low concentration dramatically increases the level of Na^+ in living cells at the expense of accumulated K^+ . Therefore, it is imperative to find out if the AI Hypothesis can offer a more plausible alternative explanation why this drug can do what it does and to test and verify this explanation experimentally. The answer is an emphatic yes.

In anticipation of what is to follow, I may mention that in the AI Hypothesis, ouabain acts as an electron-donating cardinal adsorbent (EDC) whose binding onto *bona fide* or pseudo-cardinal sites (see Ling 2006b, p.110) initiates an across-the-board rise of the c -value of the cell's β -, and γ -carboxyl groups so that the selectivity ratio of K^+/Na^+ is reduced. As a result, Na^+ displaces most of the K^+ normally occupying these β -, and γ -carboxyl groups. Next, I describe results of our experimental testing.

Figure 34 shows two pairs of X-shaped pair of curves. In each, the concentration ratio of (adsorbed) K^+ over (adsorbed) Na^+ of frog muscles is plotted against the different concentration ratios of the two ions in the bathing medium. Since all the bathing medium uniformly contains 100 mM Na^+ , so a concentration ratios, $[\text{K}^+]_{\text{ex}} / [\text{Na}^+]_{\text{ex}}$ equal to 10^{-2} indicates an external K^+ concentration of 1 mM.

The left set of X-shaped curves was obtained from normal frog muscles. The theoretical curves for both the K^+ data points and for the Na^+ data points are based on Equation 13 and a $K_{\text{Na} \rightarrow \text{K}}^\infty$ equal to 100 and a $-(\gamma/2)$ equal to 0.67 kcal/mole ($n = 3.0$).

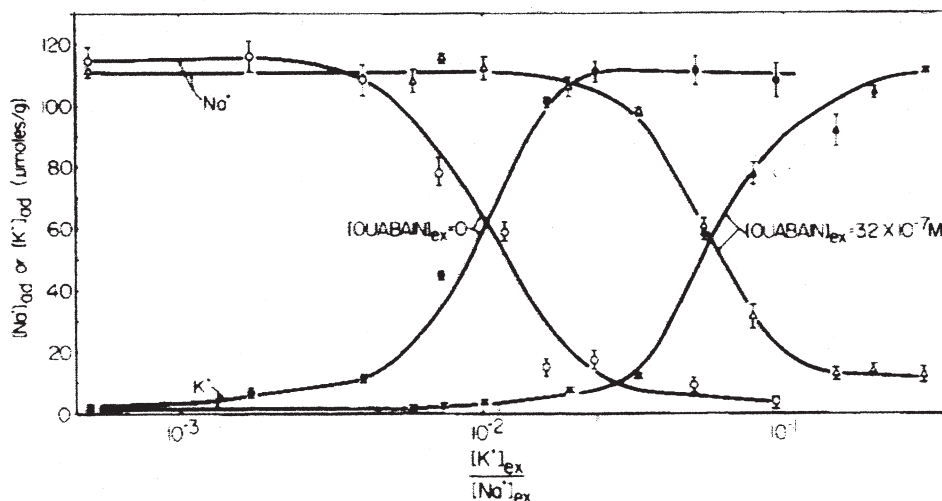


FIGURE 34. Effect of ouabain (3.26×10^{-7} M) and the concentration ratios of K^+ over Na^+ in the bathing medium upon the adsorbed K^+ (●) and Na^+ (○) concentrations in the frog muscle. Points are experimental. The solid lines going through or near the data points are theoretical according to Equation 5. Ouabain changes $K_{Na \rightarrow K}^\infty$ from 100 to 21.7 with no change in $-(\gamma/2)$. (from Ling and Bohr 1971)

Exposure of similarly treated muscle to ouabain at the (extremely low) concentration of 0.326 micromolar (or 3.26×10^{-7} M) moved the theoretically computed X-shaped pair of curves to the right by reducing $K_{Na \rightarrow K}^\infty$ from 100 to 21.7 with little or no change in $-(\gamma/2)$.

As pointed out earlier, extensive evidence now exist that virtually all K^+ in frog muscle cells are adsorbed one-on-one, close contact on β -, and γ -carboxyl groups (see Ling 2005, pp 38-45.) There are also strong NMR as well as electron-microscopic-autoradiographic evidence that the Na^+ gained by frog muscle in response to ouabain is adsorbed on similar β -, and γ -carboxyl groups (Ling and Bohr 1971; Edelmann 1986; for review of both, see Ling 2001, pp.186-190.) So what ouabain does to frog muscle is to change the relative preference of the β -, and γ -carboxyl groups from highly preferring K^+ over Na^+ to moderately preferring K^+ over Na^+ — such as one would expect if a rather small change of the c-value of the β -, and γ -carboxyl groups has occurred in response to ouabain. The much higher concentration of Na^+ than that of K^+ in the bathing medium did the rest: virtually all the (adsorbed) cell K^+ is replaced by (adsorbed) Na^+ .

Our next figure, Figure 35, is shown here to emphasize the basic similarity in the way cardinal adsorbents work. This figure shows how the equilibrium concentration of K^+ in frog muscle cells changed when both the concentration ratio of external K^+ / Na^+ and the concentration of ouabain were changing. Compare this set of data with those shown earlier in Figure 25, where it was a simultaneous change in the external oxygen tension and the concentration of IHP that produced the family of oxygen binding curves on hemoglobin. The similarity is striking. It affirms the notion that all life phenomena are based on the fundamentally similar behaviors of all nano-protoplasm units.

From the highly uniform fall of the relative affinity for K^+ over Na^+ of such a vast number of β -, and γ -carboxyl groups and the minute amount of ouabain that has created all

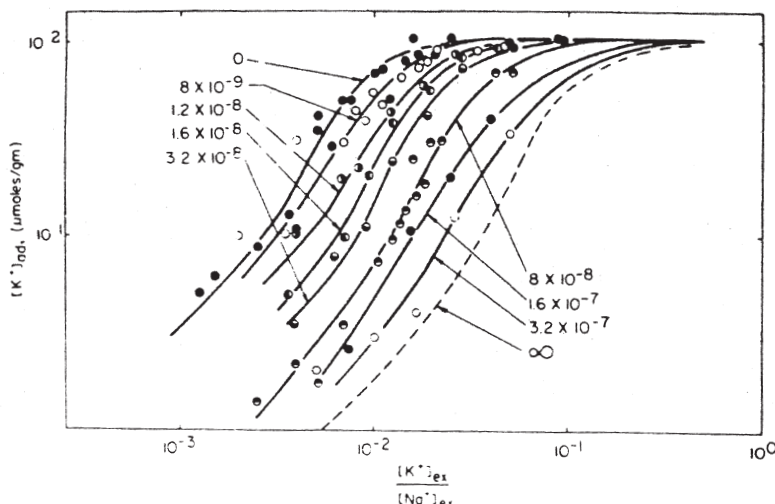


FIGURE 35. Effect of different concentrations of ouabain as shown near each curve and the concentration ratio of K^+ over Na^+ in the bathing medium upon the equilibrium concentrations of adsorbed K^+ in frog muscle cells. Each point is the average of four determinations with SE similar to those shown in Figure 34. (Ling and Bohr 1971)

this change, there is only one rational theoretical explanation known to me at this time. And that is, ouabain has created an across-the-board uniform fall of the c-value of all the β -, and γ -carboxyl groups involved through the operation of the AI cascade mechanism given above on p. 136 and illustrated in Figure 11.

Since we knew exactly how much ouabain we introduced into each flask containing several muscles of known total weights and hence the number of K^+ -adsorbing β -, and γ -carboxyl groups , it was possible to calculate precisely the (average) number of β -, and γ -carboxyl groups in the frog muscles we studied that a single ouabain molecule occupying a cardinal site controls. The number is 1042 or roughly, one thousand. This shows you why a mechanism like that described as the (*ad infinitum*) AI Cascade mechanism is absolutely necessary for living protoplasm to achieve its physiological functions. (For details, see Ling 2001, pp. 259–262.)

In the immediately following section in smaller print, we cite confirmatory work on the effect of ouabain on other kinds of living cells. That they do indeed show a similar response, supports the thesis that fundamentally similar nano-protoplasm exists in all types of living matter.

Gulati showed that ouabain at 10^{-7} M produced a similar autocooperative shift of K^+ to Na^+ adsorption in the smooth muscle of canine carotid arteries (Gulati 1973.) Negendank (1982) also showed that in human lymphocytes, exposure to ouabain at 5×10^{-8} M produced a similar shift from high preference of the adsorbing β -, γ -carboxyl groups for K^+ over Na^+ to a much reduced preference of K^+ over Na^+ . Thus, the presence of a large amount of DNA in the nucleus of a large fraction of the lymphocytes does not make the protoplasm of human lymphocytes behave differently toward the pair of alkali metal ions, K^+ and Na^+ .

Next, I shall introduce another set of studies by Ling and Bohr (1971) that offers still more quantitative insight on the ouabain-induced c-value change in these β -, and γ -carboxyl groups. But before that can be done, I need to introduce Figure 36, which is derived from the theoretical data presented in Figure 7 given on p. 131 but represents the relative adsorption constants of various monovalent cations (K_x) in comparison with that of K^+ (K_K) on oxyacid groups at varying c-value. Of course, in our present case, the oxy-acid groups are mostly if not exclusively β -, and γ -carboxyl groups.

Ling and Bohr equilibrated at 25° C steriley isolated frog muscles in modified Ringer solution called Solution 731 (for composition, see Ling and Bohr 1969) containing 1 mM each of K^+ , Rb^+ and Cs^+ and 5 or 10 mM Li^+ and 100 mM Na^+ . Figure 37A shows the time course of uptake of Rb^+ , Cs^+ and Li^+ at the expense of K^+ as well as Na^+ . Equilibrium was reached on the fourth day of incubation.

After correcting for contributions from the extracellular fluid, the "connective tissue elements" and free ion in the cell water, the equilibrium *selectivity ratio* of the *i*th (adsorbed) cation given as $[p_i]_{ad}$ (over $[p_i]_{ex}$) is expressed as a ratio over a similar ratio for K^+ , namely $\{[p_i]_{ad} / [p_i]_{ex}\} / \{[K^+]_{ad} / [K^+]_{ex}\}$ — and shown as the left-hand graph in illustration B in Figure 38.

A comparable set of data was also obtained from frog muscle in which the bathing solution contained exactly the same K^+ , Na^+ , Cs^+ , Rb^+ and Li^+ concentrations that gave rise to the data of Figure 37A but also ouabain at the same concentration that gave rise to the data shown earlier in Figure 35A, i.e., at 3.26×10^{-7} M. A different set of time courses was obtained and shown as Figure 37B. In this case, equilibrium was reached a little earlier at about the end of the third day. Here, there were much smaller gains of Rb^+ and Cs^+ but an overwhelmingly greater gain of Na^+ and a modest gain of Li^+ .

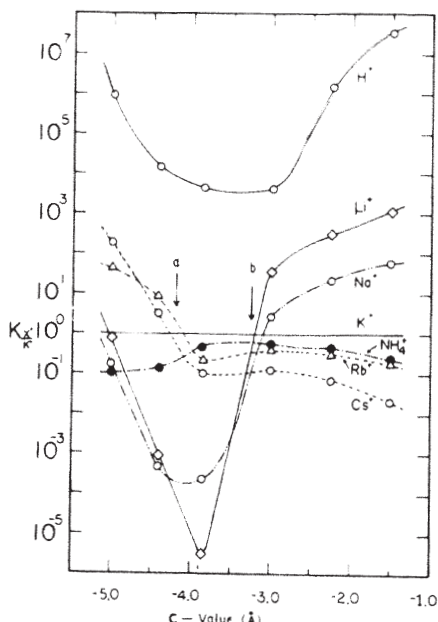


FIGURE 36. The relation between the selectivity ratios of various cations in comparison with K^+ and the c-value. Calculations based on the same set of theoretical computations given as Figure 7 above. The letters a and b point to c-values of -4.20 and -3.25 Å respectively. (from Ling 1992)

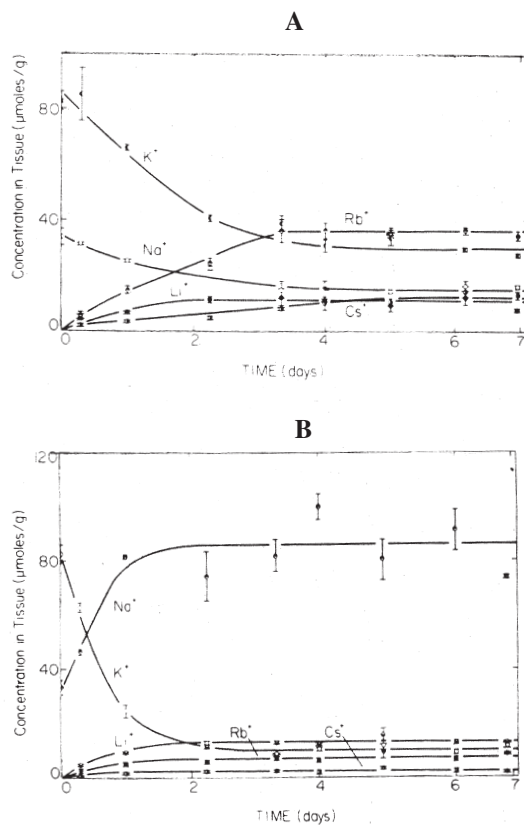


FIGURE 37. Time courses of changes in the ionic concentrations in normal frog muscle (A) and in muscle treated with 3.26×10^{-7} M ouabain (B), both at 25° C. The final external equilibrium concentrations of the five ions in A are in millimolarity: Cs⁺ (0.83), Rb⁺ (0.88), K⁺ (1.35), Na⁺ (99.9) and Li⁺ (8.20); those in B are: Cs⁺ (0.98), Rb⁺ (0.95), K⁺ (1.38), Na⁺ (99.0) and Li⁺ (7.81.) (from Ling and Bohr 1971)

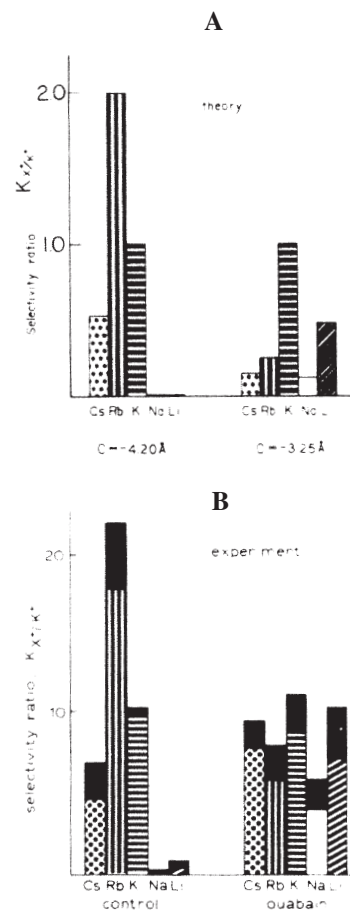


FIGURE 38. The selectivity ratio of the *i*th ion given as the ordinate is equal to $\{[p_i]_{ad}/[p_i]_{ex}\}/\{[K]_{ad}/[K]_{ex}\}$. In A, these selectivity ratios are theoretical and computed from the values given in Figure 36 at the *c*-value of -4.20 Å and -3.25 Å respectively for the normal muscle on the left and the ouabain-treated muscle on the right. In B, these ratios are experimental based on the data shown in Figure 37 after corrections have been made for non-adsorbed ions. (from Ling 1992)

The equilibrium selectivity ratios for the five ions in the ouabain-treated muscles are shown as bar graphs at the right-side bar-graph of Figure 38B. In contrast, the two other sets of bar graphs in Figure 38A were theoretical values obtained from Figure 36 at two different c-values, -4.2 \AA and -3.25 \AA as marked by arrows. Although the agreement between theory and observations is far from perfect, it is by and large good agreement. Thus, ouabain at the minute pharmacological concentration of $3.26 \times 10^{-7} \text{ M}$ had brought about an across-the-board uniform rise of the c-value of all the β -, and γ -carboxyl groups from -4.2 \AA to -3.25 \AA . Once more, this affirms our earlier conclusion that ouabain is an electron-donating cardinal adsorbent or EDC. And as such, it has brought about an one-on-many, over-the-distance control.

3.2.1.3.3 Control by Ca^{2+}

Figure 39 from Gulati (1973) shows that the concentration of Ca^2 at 2.5 mM is essential for the maintenance of the high K^+ -low Na^+ ion distribution seen in this (smooth muscle of dog carotid arteries) and likely all other types of living cells. Reduction of Ca^{2+} concentration produces a disturbance in the pattern of alkali-metal ion distribution similar to the deprivation of ATP and addition of ouabain. Off the bat, one may regard this divalent cation as an EWC. But it is possible that at extremely low Ca^{2+} concentration (i.e., initial concentration labeled as zero), ATP decrease could also be involved. Again, the points are experimental and the lines theoretical according to the Yang-Ling isotherm with the constants given in the legend.

3.2.1.3.4 Control by insulin

D-glucose is the principal energy source of many living organisms including ourselves. Through the enzymatic action of pancreatic amylase and maltase, we convert the ingested (polymeric) starch back to its (monomeric) D-glucose and release the D-glucose into our blood stream.

Part of this glucose would be used by tissues like voluntary muscle. Yet, a careful look at Figure 30 reveals that D-glucose has a very low q-value in the muscle cell water, i.e.,

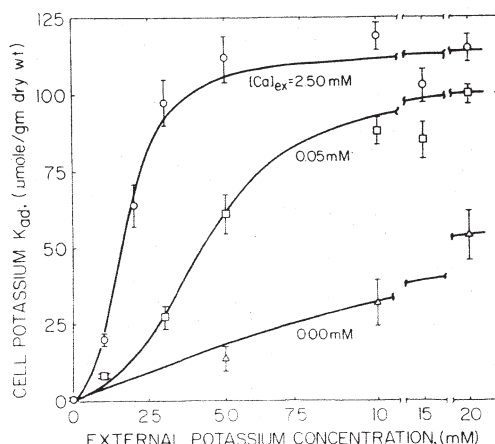


FIGURE 39. The effect of Ca^{++} on concentration of K^+ in canine carotide arteries. Points are experimental; solid lines are theoretical calculated according to Equation 5. $K_{\text{N} \rightarrow \text{K}}^{00}$ are for each of the external Ca^{++} concentrations indicated on the graph: 85 (2.5 mM); 35 (0.05 mM) and 5 (0 mM); the Hill coefficient, n are respectively in the same sequence: 2.7, 2.7 and 1.0. (from Gulati 1973 by permission of NY Academy of Science)

0.227. Thus the total amount of D-glucose that the muscle cell water can accommodate is very limited. That being the case, how can the muscle cells get enough energy during sudden intense muscle activities needed to fight or flight? The answer lies in insulin.

In our early attempt to understand how insulin works, we had our first break. That is, we discovered that isolated frog muscle can take in D-glucose at 0°C but it cannot metabolize it. This made it possible to study the mechanism of D-glucose accumulation without interference from its metabolic conversion to something else. Unfortunately, low temperature also stops insulin activity in promoting the entry of D-glucose into muscle cells.

Then came our second break. That is, we can let insulin act on muscle cells at a higher temperature before studying D-glucose accumulation at 0°C. A satisfactory routine was worked out.

We first pre-incubate at 25°C with shaking two groups of isolated frog muscles, each group in one of the two large volumes of Ringer's solution for 6 hours. The solution bathing the first group of isolated muscles contains both insulin and D-glucose. The solution bathing the second groups of muscles contains neither. At the conclusion of this pre-incubation, the muscles were transferred to cold Ringer's solution containing different concentrations of non-labeled D-glucose and ^{14}C - or ^3H -labeled D-glucose and incubated for another 16 hours at 0°C. After that, the muscles were analyzed for their labeled D-glucose contents.

The results show that in the absence of both insulin and D-glucose in the pre-incubation solution (bottom curve in Figure 40A) the labeled D-glucose taken up in the subsequent incubation at 0°C falls on a straight line just like those in Figure 30 on page 169.

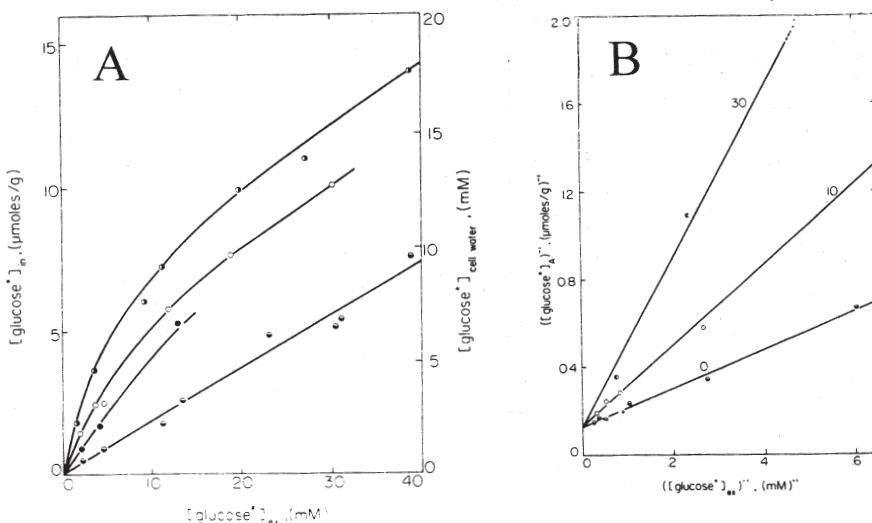


FIGURE 40. The equilibrium distribution of labeled D-glucose at 0°C in insulin-treated frog muscle (top three curves in A) and in insulin-depleted frog muscle (bottom line in A.) B is a reciprocal plot of the additional gain of labeled D-glucose obtained by subtracting data given in the bottom curve of A from each of the top three curves in A. For more details see text. (Ling and Will 1969)

This rectilinearity, of course, indicates that all or virtually all the labeled D-glucose taken up by the muscle is found in the cell water. The slope of the straight line, which equals the *q*-value of D-glucose in the muscle cell water, averages 0.25 — to be compared with a *q*-value of 0.227 from data shown in Figure 30.

When both insulin and D-glucose or another *primer* (for definition and list, see Ling and Will 1976) were included in the warm (25°C) pre-incubation solution, the total uptake of labeled D-glucose in the subsequent 0° C incubation was substantially increased in the form of *adsorbed* labeled D-glucose. Meanwhile, the rectilinear fraction in the cell water stays the same as that in the insulin-free muscles. Indeed, by subtraction, the adsorption fraction can be isolated and shown to follow Equation 15. As such, it can be plotted reciprocally according to Equation 16 and the results given as Figure 40B. The set of converging straight lines affirms the one-on-one adsorption on a fixed number of D-glucose adsorption sites opened up by the cardinal adsorbent, insulin with the assist of the primer. The relevant quantitative numbers are given in the legend of the figure.

By 1984, it was all too clear that the once dominant concept that the cell membrane is permeable to some solutes but absolutely and permanently impermeable to others is wrong. Accordingly, the hypothesis that a bacterial protein called *lactose permease* can make the microbial cell membrane permeable to this sugar needs rethinking. In 1984, I suggested an alternative. That is, these *permeases* are low-molecular-weight intracellular hormones. Acting like insulin on muscle cells, the so-called “permease” causes all-or-none conformation change of the relevant intracellular protein(s), making them adsorb the specific sugar, like lactose. For details and supporting evidence, see Ling 1984, pp. 371–375.

3.2.2 Permeability and its control

Reviews: Ling 1962 Chapt.11; 1984 Chapt.12; 1992 Chapt. 9; 2001 Sect.15.2

3.2.2.1 Theory

3.2.2.1.1 Theory of surface-limited permeation

As mentioned above, I introduced in 1952 the concept that *spatial fixation* of β -, and γ -carboxyl groups of intracellular proteins produces one-on-one, close-contact preferential association of these anionic sites with K^+ (over Na^+ .) Selective K^+ accumulation in the cells is thus achieved. It was also pointed out that similar β -, and γ -carboxyl groups borne on cell surface proteins also selectively associate with K^+ (over Na^+) providing a molecular mechanism for another major physiological attribute of the living cell: selective (K^+) permeability.

The concept that there are fixed charges in the cell membrane and cell membrane models was not new even then. However, up to 1952, the fixed charges and their counterions had been traditionally regarded as fully-dissociated as shown in two diagrammatic illustrations reproduced here together as Figure 41.

In contrast, Figure 42 illustrates the new vision of a submicroscopic part of the living cell surface I introduced in the early 1950's. Here, a K^+ enters the cell (mostly) by first engaging in close-contact association with a fixed surface anion before entering into the cell interior *via* what is called the *adsorption-desorption route* (Route 2 in the illustra-

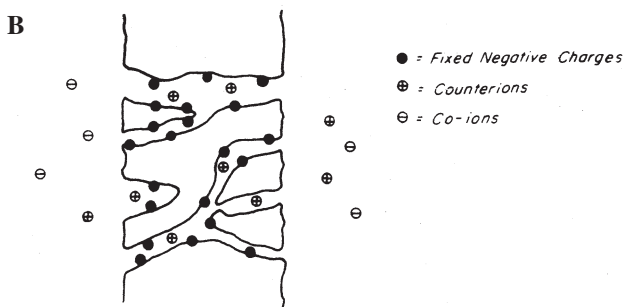
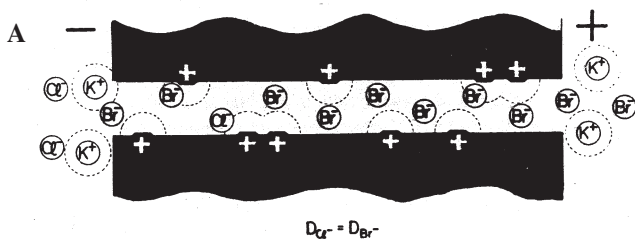


FIGURE 41. Two sets of figures demonstrating the prevailing belief (before the publication of Ling's Fixed Charge Hypothesis in 1952 and even after) that counter ions are fully dissociated from fixed ions in colloid (A) and in perma-selective membrane, (B.) (A) from Sollner 1949, by permission of Journal of Physical Chemistry; B, from Hills 1961, by permission of Academic Press)

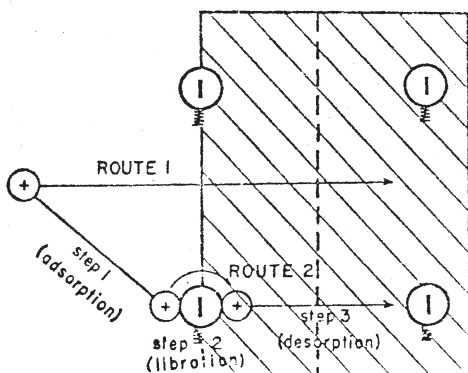


FIGURE 42. Two alternative routes of entry for an external cation into a cell carrying predominantly fixed anionic sites. Saltatory route (Route 1) entails leaping through polarized-oriented water domain of surface nano-protoplasmic units. Adsorption-desorption route (Route 2) entails three steps indicated on graph. (from Ling and Ochsenfeld 1965, by permission of the Biophysical Journal)

tion.) Less frequently, the K^+ enters the cell by leaping through the (polarized-oriented) water domain of the cell surface *via* what is called the "saltatory route" (Route 1.) Combining the two mechanisms, the rate of ion permeation is described by a general equation for permeability:

$$v_i = A_i [p_i]_{ex} + v_i^{\max(1)} \Omega_1 + v_i^{\max(2)} \Omega_2 + \dots v_i^{\max(n)} \Omega_n, \quad (17)$$

where A_i is a rate constant in units of cm/sec; $A_i [p_i]_{ex}$ represents the rate of entry of the i th ion *via* the saltatory route. It is assumed that there are all told n types of surface anionic adsorption sites. $v_i^{\max(n)}$ is the maximum rate of the i th ion entry *via* the n th type of

adsorption sites, The Ω 's are as defined in Equation 8 on page 143. $v_i^{\max (1)} \Omega_1$, $v_i^{\max (2)} \Omega_2$ and $v_n^{\max (n)} \Omega_n$ are the rate of the ith ion entry via the first, second and nth adsorption site respectively. (For the final verdict on the assumed mutiplicity of sites, see p. 220.)

In the case, where there is only one type of adsorption site mediating the ith solute entry via the adsorpton-desorption route, Equation 17 simplifies into:

$$v_i = A_i [p_i]_{\text{ex}} + v_i^{\max} \Omega_1. \quad (18)$$

On the other hand, if that adsorption site does not show nearest neighbor interaction, Equation 18 further simplifies into the following form where Ω_1 is replaced by the simpler Langmuir adsorption isotherm:

$$v_i = A_i [p_i]_{\text{ex}} + \frac{v_{\max} K_i [p_i]_{\text{ex}}}{1 + K_i [p_i]_{\text{ex}}}. \quad (19)$$

Now, if a jth ion is also present in the external medium, it will compete for the same adsorption site at the cell surface, Equation 19 then takes on the following form:

$$v_i = A_i [p_i]_{\text{ex}} + \frac{v_{\max} K_i [p_i]_{\text{ex}}}{1 + K_i [p_i]_{\text{ex}} + K_j [p_j]_{\text{ex}}}, \quad (20)$$

For an ion like Na^+ that exists at high concentration in the external medium but is weakly adsorbed on the surface adsorption site, it will enter the cell mostly by way of the saltatory route. For an ion like K^+ that as a rule exists at low concentration in the bathing medium but is strongly adsorbed on the surface adsorption sites, it will as a rule enter via the adsorption-desorption route. In this latter case and as a first approximation, the saltatory entry can be ignored. The ith ion entry can then be described by the adsorption-desorption route alone and:

$$v_i = \frac{v_{\max} K_i [p_i]_{\text{ex}}}{1 + K_i [p_i]_{\text{ex}} + K_j [p_j]_{\text{ex}}}. \quad (21)$$

Plotted reciprocally, (21) now appears as:

$$\frac{1}{v_i} = \frac{K_i}{[f]} \left(1 + \frac{[p_j]_{\text{ex}}}{K_j} \right) \frac{1}{[p_i]_{\text{ex}}} + \frac{1}{v_{\max}}. \quad (22)$$

This Equation (22) shows that if one plots $(1/v_i)$ against $(1/[p_i]_{\text{ex}})$ at a constant $[p_j]_{\text{ex}}$, one obtains a family of straight lines all converging on the ordinate at $\{1/[p_i]_{\text{ex}}\} = \text{zero}$. From the slopes and intercepts, all the unknown parameters can be assessed.

3.2.2.1.2 Theory of influx profile analysis of bulk-phase (and surface) limited permeation

According to the association-induction version of the (redefined) protoplasmic theory, the cellular organelles and the cytoplasm all contain polarized-oriented water as the largest component of their makeup. Nonetheless, within limits, the precise proportion of water versus solids and the intensity of excess water-to-water interaction energy vary. As a result, the rate of diffusion through the bulk-phase protoplasm and through the (cell or organelle) membranes may be different for different ions and other solutes and for (labeled) water. Since the mathematics of simple and complex diffusion have all been worked out in the past, it is easy to construct a kind of diagnostic pictorial analysis like that shown in Figure 43.

Each one of the three figures in Figure 43 represents a plot of the fractional uptake of a substance at time t as a percentage of the maximum uptake at equilibrium (M_t / M_∞) against the square root of the time, t . For the rate of diffusion into say, a living cell, that is slowest at the surface and thus designated as *surface-limited*, the profile is S-shaped as shown under A. For diffusion that is uniform throughout the bulk phase of the target space (including the surface) and designated *bulk-phase limited*, the profile assumes the shape of a curve consistently concaving downward as shown under B. Then, there is the third figure under C, which represents a (complex) bulk-phase limited diffusion. That is, the substance becomes either partially adsorbed onto certain intracellular sites or enters into some intracellular particles after it has entered the cell *via* a bulk-phase limited migration. To determine which mode of diffusion applies, one needs highly accurate data. Fortunately, with the availability of high activity radio-isotope-labeled chemicals, this degree of accuracy was within reach. A second requirement is an unusually large cell. Both mature frog ovarian eggs and giant barnacle muscle cells meet this requirement.

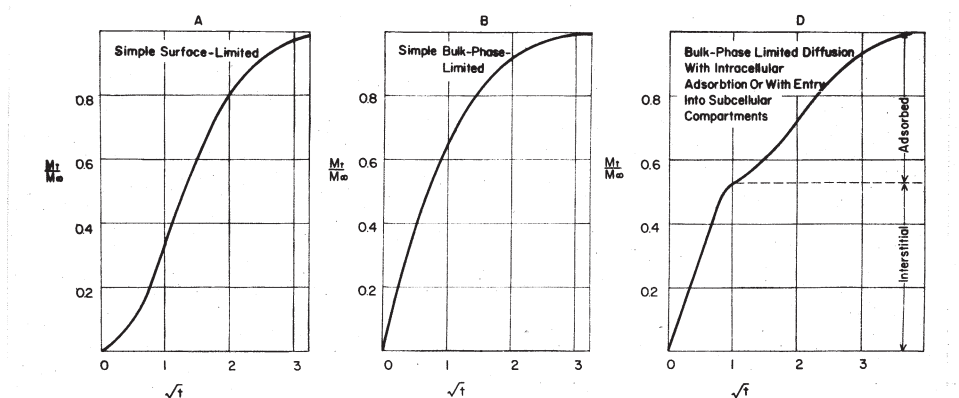


FIGURE 43. Influx profile analysis, showing how different rate-limiting steps in the migration of a labeled substance into a living cell or model system can be clearly revealed visually from a plot of the fractional uptake (M_t / M_∞) at time t against the square root of t . See text for additional details. (from Ling *et al* 1967, by permission of the Rockefeller University Press)

3.2.2.2 Results of experimental study of permeability

a. Ions

In the 19th International Physiological Congress held in Montreal, I showed that the rate of permeation of Rb⁺ into frog muscle cells was competitively inhibited by K⁺ present in the bathing medium (Ling 1953.) I demonstrated this in a converging double reciprocal plot of the rate of permeation of Rb⁺ ($1/v_i$) against the concentration of Rb⁺ ($1/[p_j]_{ex}$) in the presence of varying concentrations of competing K⁺ ($[p_j]_{ex}$) according to Equation 22. (A converse experiment showing Rb⁺ inhibiting K⁺ permeation is shown in Figure 44A to follow.)

However, this was not the first time, competition (and saturability) was demonstrated in the rate of permeation among entrant alkali-metal ions. Thus, a year before, Epstein and Hagen (1952) demonstrated similar competition between alkali-metal ions in their permeation into barley roots. But, in theory, they (and virtually all others demonstrating similar behaviors in ionic permeation) invoked what is known as carrier hypothesis. That is, the entrant ion is ferried across the cell membrane by a hypothetical “ferry boat” or carrier. The discovery that the antibiotic, valinomycin could selectively transport K⁺ across man-made phospholipid membranes, stimulated an extensive search for Nature-made counter parts in live cell membranes. All failed as Dr. Paul Müller, a one-time vigorous proponent of the idea, ruefully concluded in 1975: “A lot of us have spent a wasted ten years or so trying to get these various materials into the (phospholipid) bilayers...” (Müller 1975.)

In contrast to the failure of the carrier model cited above in smaller prints, the association-induction model of ion permeation has been uniformly successful. As an example, Figure 44 shows that Equation 22 quantitatively describes not only the competitive inhibition of ion entry into *living* frog muscle cells (A), it also describes the competitive inhibition of ion entry into *non-living* systems. They include cation exchange resin sheet (B) and sheep’s wool (C). While the cation exchange resin sheet carries fixed sulfonic acid groups, both frog muscle and sheep’s wool carry fixed β -, and γ -carboxyl groups.

That each alkali-metal ion reduces to a different degree the rate of permeation of another alkali-metal ion into exchange resin sheet (Figure 44B) is not exceptional. On the contrary, it is the rule and observed in ionic permeation into all types of cells and models investigated. Since the various alkali-metal ions differ only in their respective short-range attributes, which cannot be perceived without close contact, these studies offered yet more support for the AI model. As pointed out earlier, in this model, one-on-one, close contact adsorption on surface anionic sites is the rate-limiting step in the permeation of ions like K⁺ and Cs⁺.

A more comprehensive thesis for ion permeation was presented in the Appendix of Ling and Ochsnerfeld (1965.) From that thesis, we were able to derive altogether four types of influence that one mono-valent cation can exercise on the rate of permeation of another mono-valent cation. All four types have been demonstrated experimentally on living cells. Three of the predicted types of interaction are shown on the left side of Figure 45. They are respectively labeled A (competition), B (facilitation) and C (initial competition changing into indifference at higher inhibitor concentration.) Corresponding experimental confirmations of each are shown as D, E and F on the right side of the same figure.

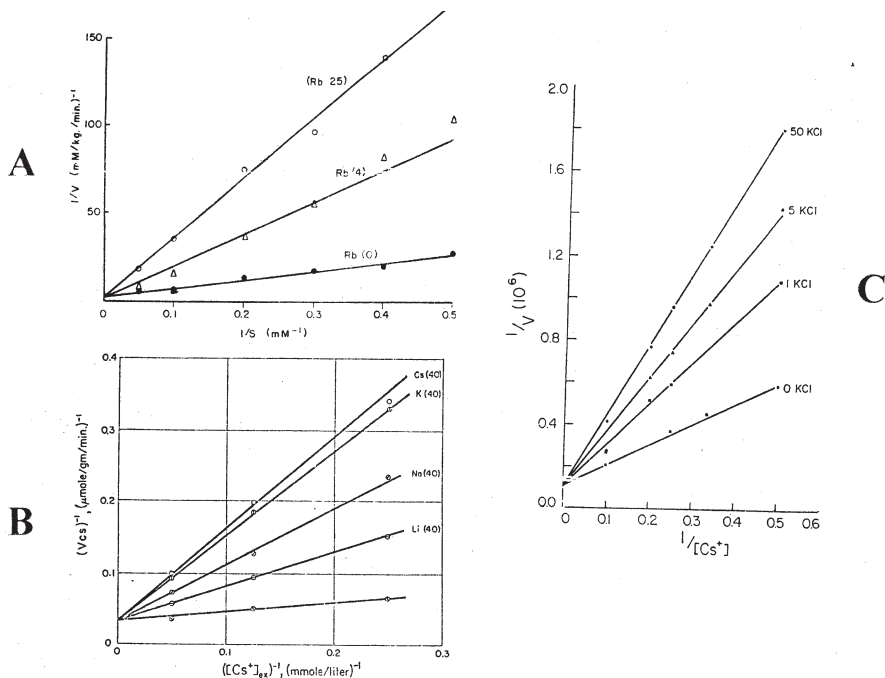


Figure 44. Demonstration of competitive inhibition of a second monovalent cation upon the rate of entry of the first one into a living frog muscle (A), a piece of cation exchange resin sheet (B) and defatted sheep's wool, (C). (A and C from Ling 1960, by permission of the J. Gen. Physiol.; B from Ling and Ochsenfeld 1965, by permission of Biophysical Journal)

Taken together, these findings affirm the equations of ionic permeability based on the idea that the cell surface is covered with nano-protoplasm similar to the protoplasm filling the inside of the living cell. Both exist as assemblies of nano-protoplasm units described in Equation 1. That said, we move on to focus on the finer similarity between the anionic groups that selectively adsorb and thus accumulate alkali-metal ions in bulk-phase cytoplasm and the anionic groups that mediate the entry of alkali-metal ion entry into living cells.

Now, according to Equation 1, these anionic groups cannot be anything other than β -, and γ -carboxyl groups. The reason could not be simpler. β -, and γ -carboxyl groups are the only anionic groups which all proteins carry in large enough number (Figure 3.)

One set of confirmatory experimental came from a study of the effect of pH on the rate of entry of labeled K $^{+}$ into frog sartorius muscles. As shown in Figure 29B, the mid-point of inflection of this "titration" curve occurs at pH between 4.6 and 4.7, which is characteristic of the pK_a of β -, and γ -carboxyl groups — see p. 168 above for sources of typical pK's of β -, and γ -carboxyl groups (3.65-4.7). The second "titration curve" labeled A deals with alkali-metal ion accumulation in the cytoplasm of similar frog muscles. Its mid-point of inflection occurs at a pH of 3.8, which is also characteristic of β -, and γ -carboxyl groups but on the lower end of the spectrum. Small differences notwithstanding, there is

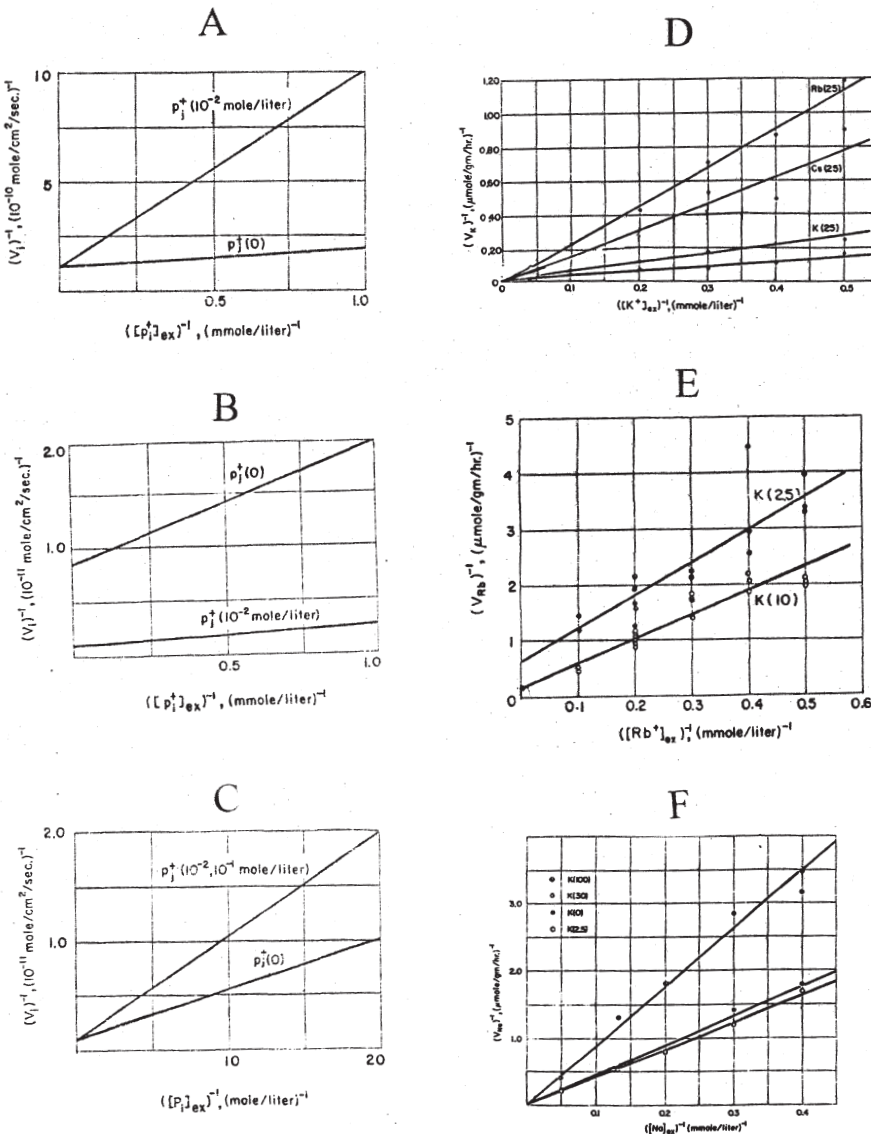


FIGURE 45. Three types of influence a second monovalent cation may have on the rate of entry into a nano-protoplasmic surface or model system. A, B, C are theoretical. D, E, F are experimental confirmation of the theoretical predicted changes. (Ling and Ochsenfeld 1965, by permission of the Biophysical Journal)

no question that these pK's observed indicate β - and γ -carboxyl groups in both cases. Having made this main point clear, let us now direct our attention to the minor differences in the pK's observed.

In fact, there is a plausible interpretation for this small difference. It could have come from the different locations where the β - and γ -carboxyl groups are found in the cell. The bulk-phase K^+ accumulation occurs in the cytoplasm within the cells. Ionic permeation occurs only at the cell surface. This difference in location could produce a difference in the pK_a as observed for the following reason:

In the cell interior, there is as a rule an equal number of fixed cations and fixed anions. On the basis of the polarity of the electric potential difference at the cell surface — to be discussed in the following section —, the surface of muscle and nerve cells is covered predominantly with anionic β - and γ -carboxyl groups (and few if any fixed cations.) The overlapping of the electric field due to neighboring β - and γ -carboxyl groups discussed on p. 128 may cause the cell surface β - and γ -carboxyl groups to bind H^+ more strongly than those in the cell interior, hence a higher pK_a of the cell surface β - and γ -carboxyl groups.

b. Nonelectrolytes

Figure 46 shows the time course of entry of seven nonelectrolytes into isolated frog muscles at $10^\circ C$ from an initial external concentration of 20 mM for each solute. The final levels reached in the cells follows the "size rule", the larger the solute, the lower its p - or q -value. — as I have shown earlier in Figures 22, 23 and 28. An even more important reason I chose to include Figure 46 here is to emphasize that in typical living cells like frog muscle (i) just how rapidly all these nonelectrolytes reach diffusion equilibrium and

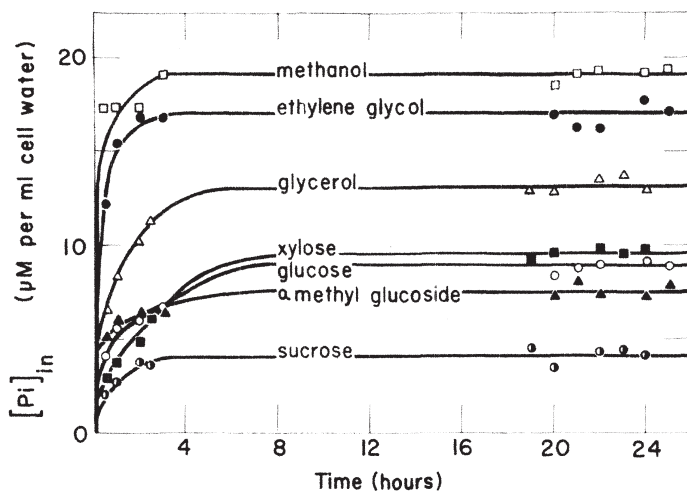


FIGURE 46. Time course of permeation and equilibration of seven nonelectrolytes into frog muscles at $10^\circ C$. Initial concentration of each solute was 25 mM . Data indicate rapid attainment of equilibrium for all solutes studied big or small. (from Ling *et al* 1973. by permission of the New York Academy of Sciences)

(ii) how little difference there is among the lengths of time different solutes take to reach their final equilibrium levels in the muscle cells.

Thus, a closer look at the time courses reveals that it took only twice or, at most, three time longer for D-glucose to reach diffusion equilibrium than for methanol to do the same. Is it not astonishing that the diffusion coefficient of methanol in *normal liquid water* at 18°C is 1.37×10^{-5} cm²/sec. (Gerlach 1931) and thus also between 2 to 3 (or more precisely, 2.4 times) faster than that of D-glucose in normal liquid water at the same temperature, 0.57×10^{-5} cm²/sec (Thovert 1914)? It is. What this comparison demonstrates is that judging from the relative rates of diffusion of D-glucose and methanol, the frog muscle cell membrane behaves as if it were not far different from a layer of normal liquid water.

This rapid rate of permeation of sugars and other nonelectrolytes into most living cells is entirely reasonable. After all, the cells constantly need D-glucose as the energy source for all their activities. Like a busy store, it would be suicidal if the doors to the store are kept locked. Further confirmation of this “open door policy” will be described in the section right after the one immediately following.

True. Fast passage through the cell surface nano-protoplasm is vital for the survival of the animal. However, if this rule holds for all cells, it would present a problem — especially for aquatic animals like frogs, which spend their lives in pond containing a large quantity of water. So, D-glucose that goes in and out of muscle cells with ease would also go out of the animals into the pond water with ease. Continued, it would kill the frog. To prevent that from happening, the nano-protoplasm of the external covering skin of frogs must be different from the nano-protoplasm covering internal body cells like muscle. To find out if this is true, we studied the permeation of sugars and other nonelectrolytes through the outermost covering of a frog, its skin.

Results of our studies of the permeability of (inverted) frog skin to sugars and other nonelectrolytes are presented along the ordinate of Figure 47. It shows an entirely different picture as that given in Figure 46. For example, the permeability of the (inverted) frog skin for L-glucose (which diffuses like D-glucose but is not steadily vanishing due to metabolism) is not 2 or 3 times slower than for methanol, it is 5000 times slower than methanol. Despite this great spread in the permeability among the different solutes, the collection of data as a whole follows rigorously the size-rule: the larger the solute, the slower it permeates. We will return to this subject shortly.

The main conclusion from this study is that the nano-protoplasm making up the outer skin of a frog acts as a strong barrier to the loss of vital ingredients like the sugars while the surface membranes of ordinary internal body cells like muscle hardly act as a diffusion barrier at all.

However, Figure 47 tells us much more than the striking difference in the permeability to small methanol and to larger glucose, it also presents a parallel study on an inanimate model of the frog skin that in as far as permeability to non-electrolytes is concerned, acts as if it were an exact copy of the frog skin.

For the wide-ranging permeation rates of the inverted frog skin shown in Figure 47 are almost exactly duplicated by a non-living “water membrane” in the form of a water-loaded cellulose acetate sheet, which Eastman Kodak marked for water purification purposes. In Figure 47, the frog skin permeability for each solute at a specific temperature (0°, 4° or 25° C) is plotted as ordinate against the cellulose-acetate-sheet permeability to

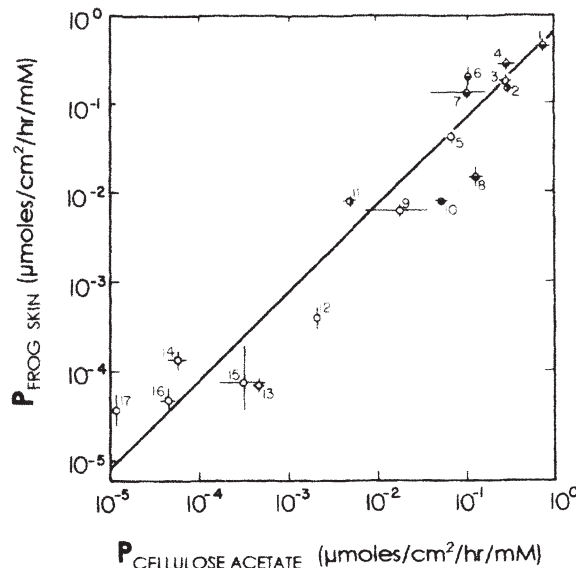


FIGURE 47. The permeability of labeled water and 10 nonelectrolytes at up to three different temperatures (0° C, 4° C and 25° C) through inverted living frog skin — plotted against the permeability of the same substances at the same temperatures across water-loaded cellular acetate membrane. 1, THO, 25° C; 2, THO, 4° C ; 3, THO, 0° C; 4, methanol, 25° C; 5, methanol, 0° C; 6, ethanol, 25° C; 7, n-propanol, 25° C; 8, ethylene glycol, 25° C; 9, ethylene glycol, 0° C; 10, glycerol, 25° C; 11, glycerol, 4° C; 12, glycerol, 0° C; 13, erythritol, 0° C; 14, xylitol, 0° C; 15, sorbitol, 0° C; 16, L-glucose, 0° C; 17, sucrose, 0° C. (from Ling 1973, by permission of Biophysical Journal)

the same solute at the same temperature as abscissa. The linear correlation between the two sets of data is 0.96. By the method of least square, the straight line going through or near the full set of data points is described by the following equation:

$$\log (P_{\text{frog skin}}) = 0.9901 (P_{\text{cellulose acetate membrane}}) + 0.16959. \quad (23)$$

Since the two sets of data are in the same units, what this equation shows is not just good correlation but near-perfect correspondence. Thus, not only do the two sets of data share the same complete obedience to the size rule, they also share the same temperature coefficients for the rate of permeation of each one of the solutes studied.

The “pore size” of the cellulose acetate membrane has been estimated with electron microscopy by Schultz and Asunmaa (1969) to give an average diameter of 44 Å and thus about five times wider than the diameter of sucrose, (9 Å) to which the cellulose acetate membrane is virtually impermeable (See also Ling 2007, Table 1 on p. 23.) Only the POM theory of cell and nano-protoplasmic water can explain this because functionally, the polarized-oriented water acts as it were a sieve but is not a mechanical sieve. That said, we tackle the question, why does cellulose acetate membrane act as if it were inverted frog skin?

First, because the cellulose acetate — like the fully-extended polypeptide chain of nano-protoplasm shown on the right-hand side figure of Figure 5 — also exists in a fully-extended form (see Pigman 1957, p. 662, line 22, p. 692.) Second, like the anionic dipolar (CO) groups and cationic dipolar (NH) groups that the fully extended polypeptide chain carries, the cellulose acetate model also carries anionic dipolar (CO) groups and cationic dipolar (OH) groups. Third, like (fully-extended) poly(glycine-D,L-alanine) and living frog muscle, cellulose acetate membrane also sorbs a vast amount of water but only at near saturation vapor pressure (Ling 1972 Figure 14; Ling 2006 Figure 14.) Thus, there is good reason to expect that like nano-protoplasm in its resting living state, the heat-

activated cellulose acetate membranes also polarize and orient water in deep layers and accordingly, show similar permeability when the other defining condition prevail (see below).

The next question to address is how can similar nano-protoplasm offer virtually no resistance to glucose permeation in the frog muscle cell membrane but enormous resistance to glucose permeation in the frog skin epithelial cells? The answer lies in the extreme sensitivity of membrane permeability to the degree of excess water-to-water interaction energy that determines the q -value of glucose. To understand this, we need to introduce another equation relating the permeability, P of a solute through a membrane to the q -value of that solute in the permeation rate-limiting part of that membrane:

$$P = k (q / r \eta), \quad (24)$$

where r is the average radius of the diffusing particle and η is the viscosity of the diffusing medium (polarized-oriented water.) At unchanging temperature, k is a constant equal to $(RT) / 6\pi N$, where N is the Avogadro number and RT has the usual meaning. Since the excess water-to-water interaction energy, U_{vp} and U_s , are exponentially related to the q -value as shown in Equation 4 on p. 136, a small change of the value of these parameters would accomplish all that is needed to turn the frog skin into a vastly stronger permeability barrier than the membranes of internal body cells like frog muscle. In the following section, we will see more evidence that the frog muscle cell surface is almost as free as normal liquid water for the permeation of another chemical, water itself.

c. Water

Figure 48 shows the influx profiles of the diffusion of radioactively labeled water into single frog ovarian eggs (D, E and F) and clusters of a few similar eggs (A, B and C.) There is no discernible difference between these two groups. In all six cases (and many others not shown) the diffusion of labeled water is *bulk-phase limited*. A similar influx profile study has also been conducted by Reisin and Ling (1973) on giant barnacle muscle cells, leading to the same conclusion that water diffusion into these cells is also *bulk-phase limited*. What these findings tell us is that living cells are extremely permeable to water.

Now, an unusual advantage offered by these studies is that the data offer an internal check on the validity of the conclusion that the diffusion is truly bulk-phase limited. Being bulk-phase limited, the time-course of labeled water entry into the cell is determined by the diffusion coefficient of labeled water and the diffusion coefficient is thus one of the main harvest of the study. A comparison of the diffusion coefficient thus obtained with the diffusion coefficient of water in the same kind of cell but obtained by other laboratories using entirely different methods could either affirm or refute the conclusion we reached.

Here, the barnacle-muscle study offered a distinct advantage over the ovarian egg study. Four other sets of the diffusion coefficient of water in (intact) giant barnacle muscle cells were already on hand when our work was completed. In units of 10^{-5} cm/sec, they are respectively 1.34 from Caillé and Hinke,(1974), 1.56 from Abetsedarskaya *et al* (1968), 1.20 from Finch *et al* (1971), 1.35 from Walter and Hope (1971.) The average of their values is 1.36 ± 0.13 (s.d.), which compares favorably with the average of our eight sets of data giving a diffusion coefficient of tritiated water inside giant barnacle muscle cells of 1.35 ± 0.125 (s.d.). (A fifth set of data in the literature was rejected because its authors

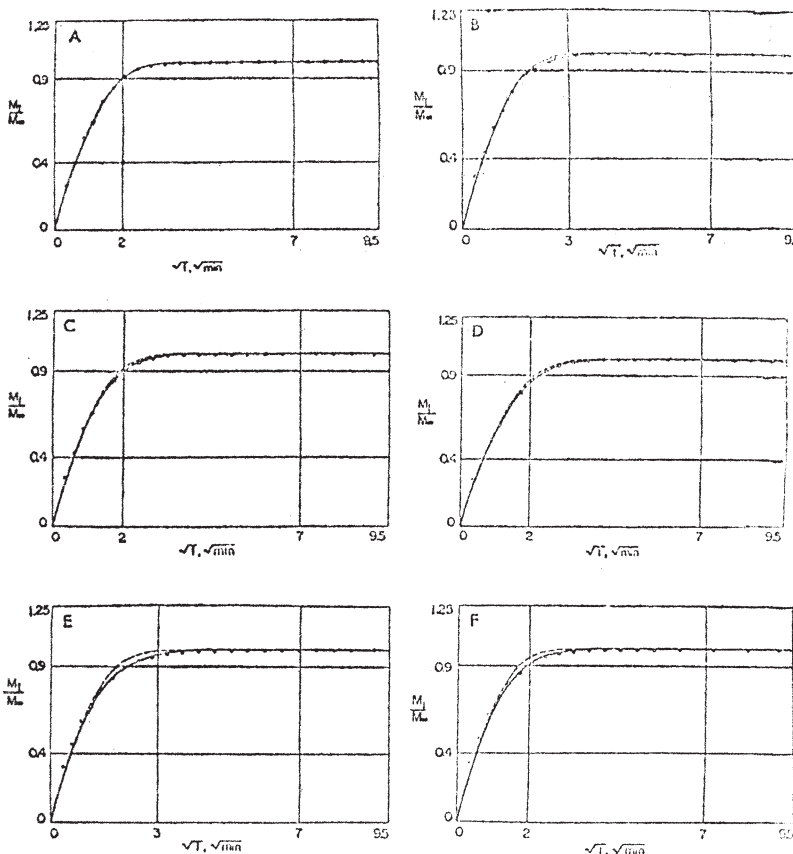


FIGURE 48. Influx profiles of tritiated water into single frog ovarian eggs (D, E and F) and into small clusters of a few single eggs (A, B and C) at 25°C. In all our data collected, represented here or not, the diffusion is bulk-phase limited. In some like A, it is a simple-bulk-phase limited diffusion. In others, it represents bulk-phase limited diffusion followed by adsorption of entry into sub-cellular particles. Points are experimental; lines are theoretical. In units of $10^{-5}\text{cm}^2/\text{sec.}$, the eight sets of data yielded an average of 1.00 ± 0.10 (S.E.) In contrast, the diffusion coefficient of THO into normal liquid water at the same temperature is 2.44 in the same unit. (Ling *et al* 1967, by permission of the Journal of General Physiology)

used muscle fibers with both ends cut. Spreading injury from the cut ends made the data obtained not from normal protoplasm but from that of injured protoplasm, for details, see Ling 2001, p. 126.)

This full confirmation leaves no doubt that in at least two kinds of widely different living cells the diffusion of water in and out of the cells is bulk-phase limited. Since in multi-cellular organisms like us humans, all types of cells originate from one fertilized egg cell, the chance that non-egg, non-muscle cells show entirely different rate-limiting steps for water seems unlikely.

Even more important, this finding strongly refutes the widely-accepted concept that the cell membrane is primarily a phospholipid bilayer — because an *authentic* phospholipid



R. C. Murphy, Z. Zhang, J. F. Brogan, J. T. Greenplate, M. M. Ochsenfeld, W. Negendank, G. Karreman, C. F. Hazlewood, and G. N. Ling

Group picture taken in 1983

bilayer is known to be virtually impermeable to ions, non-electrolytes and water (Miyamoto and Thompson 1967; Miyamoto 1966; Wood *et al.* 1968.) Just as important, the present finding also strongly refutes the idea that the cell interior is connected to the outside medium by narrow water-filled channels. For the data show that most of the surface of frog ovarian eggs and giant barnacles muscle fibers are in the form of (polarized-oriented) water.

And, by the same token, the data confirms the concept of nano-protoplasm containing as an integral part a large amount of water and that similar nano-protoplasm with large water content makes up the cell membrane, the cell cytoplasm as well as other organelles of one kind or another.

3.2.2.2 Results of experimental study of the control of ionic permeability

a. Control by ouabain

Twenty years later, Ling and Fu published their study of the influence of ouabain on the relative effectiveness of different alkali metal ions in competing against and thus suppressing the rate of permeation of radioactively-labeled Cs⁺ into frog ovarian eggs.

The data presented in Figure 49 show that ouabain consistently enhances the effectiveness of Li⁺ in competing against and thus suppressing the rate of entry of Cs⁺ while it also consistently reduces the effectiveness of Rb⁺ in suppressing the rate of entry of Cs⁺. With some deviation, ouabain also increases the effectiveness of both Na⁺ and K⁺ in suppressing the rate of entry of Cs⁺. Ling and Fu then showed how these results could be anticipated on the basis of alterations of the c-value of the egg-surface β-, and γ-carboxyl groups and hence their relative ionic preferences brought about by ouabain acting as an EDC.

b. Control by valinomycin

Andreoli, Tiffenberg and Tosteson showed the “black lipid membranes” (Jain 1972 p. 85) prepared from phospholipids extracted from sheep erythrocytes has high electrical resistance ($1\text{-}3 \times 10^8 \text{ ohm/cm}^2$) that is indifferent to the concentration of KCl solutions that the membrane separates. However, the introduction of 10^{-7} M of valinomycin — a “failed” antibiotic isolated from the bacteria (not fungus) *Streptomyces* strains — or a mixture of monactin and dinactin to the bathing solution drastically reduced that electrical resistance

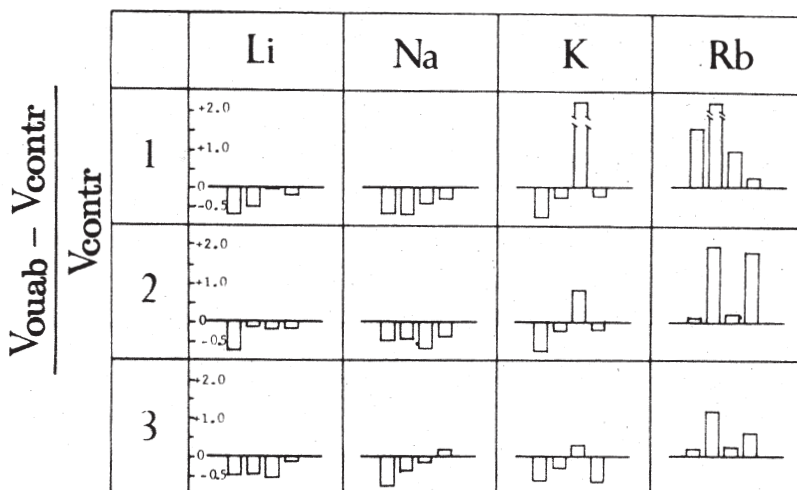


FIGURE 49. The effect of ouabain (10^{-6} M) on the rate of entry of labeled Cs^+ into frog ovarian eggs in the presence of 20 mM of competing Li^+ , Na^+ , K^+ or Rb^+ . The influx rate during a 13 minute incubation of the egg clusters was determined from the zero time intercepts of the efflux curves which were resolved into three fractions 1, 2 and 3. V_{contr} and V_{ouab} represent the rate of labeled Cs^+ entry in the absence and presence of ouabain respectively. The fractional change of influx rate is represented by $\{(V_{\text{ouab}} - V_{\text{contr}})/V_{\text{contr}}\}$. In all four complete sets of experiments performed, exposure to ouabain consistently increased the effectiveness of Na^+ and Li^+ in reducing the rate of Cs^+ influx. In all four cases, exposure to ouabain did just the opposite in consistently decreasing the influence of Rb^+ in reducing Cs^+ influx. The influence of ouabain on the influence of K^+ shows some variation, but by and large, ouabain also reduced the inhibitory effect of K^+ on Cs^+ entry. (from Ling and Fu 1988)

— by as much as 3 to 4 orders of magnitude, if and only if the bathing solution contained a high concentration of KCl (10^{-1} M for valinomycin and 10^{-2} M for monactin-dinactin) (Andreoli *et al* 1967.)

Before long, we learnt about this finding and realized that it had created an opportunity to test the various models of cell membranes. They include the pure phospholipid membrane model labeled Model I in Figure 50, a pure fixed charge-polarized-oriented water model labeled Model III and a mixed phospholipid-fixed charge-normal water membrane labeled Model II. The length of the vertical arrows indicates the specific rate of K^+ permeability of a specific membrane model.

Thus, the pure phospholipid membrane would have zero or near zero inward K^+ permeability in the absence of “ionophores” like valinomycin or monactin/dinactin but showed marked K^+ permeability after the introduction of the ionophore (and KCl.) In contrast, in the Type III pure fixed anionic site-polarized-oriented water model, there is substantial K^+ permeation without ionophores and addition of an ionophore does not change it. Between these two extremes is the mixed model II, which has low K^+ permeability in the absence of ionophores, but the K^+ permeability could increase on exposure to the ionophore.

With these theoretical insight in mind, Ling and Ochsenfeld (1986) carried out a study of three K^+ -specific ionophores (valinomycin, monactin and nonactin) on three varieties

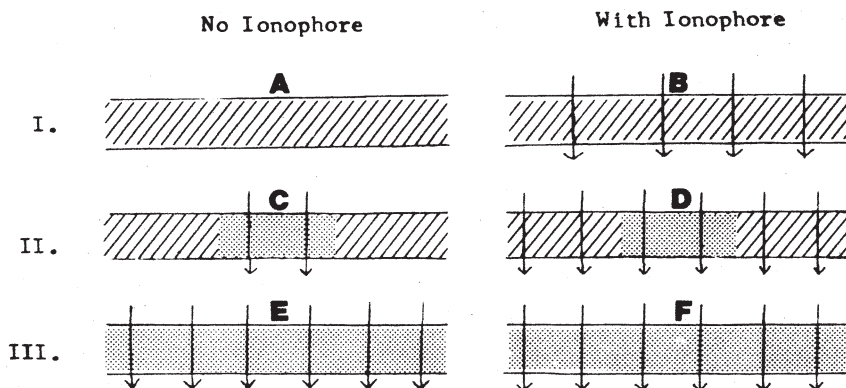


FIGURE 50. Three types of idealized cell membrane models and the anticipated influence of the addition of K^+ ionophores upon the rate of K^+ entry into the cell. Type I, pure phospholipid membrane; Type II, mixed (lipid, fixed charge-polarized-oriented water); Type III, pure or effectively pure (fixed charge-polarized-oriented water) membrane. Downward arrows indicate K^+ permeation. (from Ling and Ochsenfeld 1986)

of living cells: frog ovarian eggs, frog voluntary muscles and human red blood cells. The results are summarized in Figure 51. Valinomycin, monactin and nonactin have no detectable influence whatsoever on the K^+ permeability of frog ovarian eggs, nor on frog voluntary muscle. In contrast, the human red blood cells showed a consistent but moderate (80%) increase of its K^+ permeability to all three ionophores investigated.

The indifference of frog ovarian eggs and frog voluntary muscle to the ionophores adds two more types of physiological active cell types to prior reports of similar indifference of squid axon membrane to valinomycin (Stillmann *et al* 1970) and of the inner membrane of rat liver mitochondria (Maloff *et al* 1978) to be followed by a still later report of similar indifference to valinomycin of the human lymphocytes (Negendank and Shaller 1982.)

But even the only cell type that does show (some) response, the human red blood cell, did so in a way that suggests other reasons than these monocyclic compounds acting as K^+ -carriers. For if it were so, the increased K^+ permeability should be intimately related to the concentration of K^+ in the bathing medium as the original work of Andreoli *et al* had demonstrated in authentic phospholipid membranes. In fact, an increase of K^+ concentration from 10^{-3} M to 10^{-2} M that should have produced a 40-fold increase of K^+ permeability, produced no increase of K^+ permeability at all.

Whatever the true mechanism for the moderate increase of K^+ permeability in red blood cells, it should not obscure the main finding of this series of studies. They conclusively support the idea that in all these highly physiologically active cells, the cell membrane is mostly polarized-oriented water — as the bulk-phase limited diffusion of water in and out of frog egg and barncale muscle fibers have already demonstrated in the preceding section. That, of course, offers yet another confirmation of the contention that nano-protoplasmic units essentially as described in Equation 1 provide the building blocks not only of the bulk phase cytoplasm but also of what is conventionally called the cell membranes of all living cells as well.

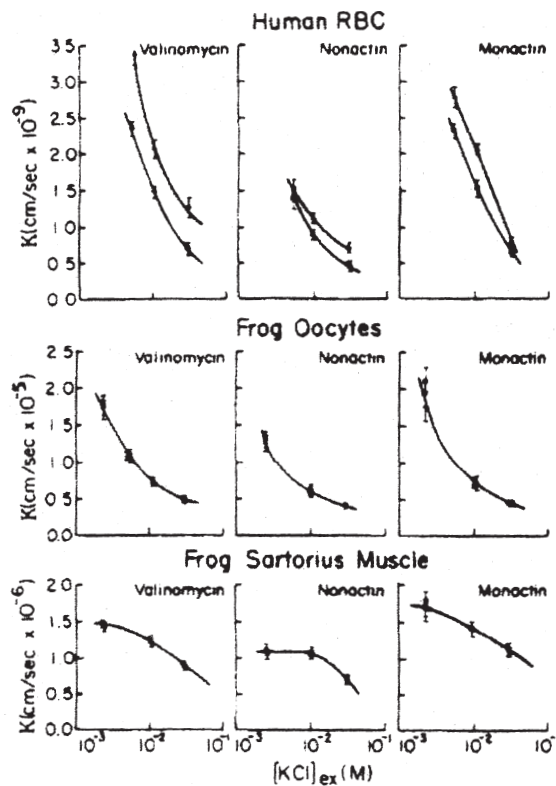


FIGURE 51. Effects of three K⁺-specific ionophores — valinomycin, nonactin and monactin all at the concentration of 10⁻⁷M — upon the rate of labeled K⁺ entry into human red blood cells, frog ovarian eggs and frog sartorius muscles. △, ionophore treated; ○, control. (from Ling and Ochsenfeld 1986)

In the section immediately following, we will have another chance of visiting the cell surface of frog muscle cells but from a different perspective, the electric potentials.

3.2.3 Cellular electric potentials and its control

Reviews: Ling 1962 Chapt.10; 1984 Chapt.14; 1992 Chapt.11; 2001 Sect.15.5; 15.6; Ling 1982

3.2.3.1 The resting potential

3.2.3.1.1 Theory

My career as a cell physiologist began with improving the Gerard-Graham-Ling (alias Ling-Gerard) microelectrode to make it a useful tool to measure the electric potential difference across the surface of living cells, big or small (Ling and Gerard 1949.) That done, I then went on to study the electric potential across the surface of single frog muscle cells with the microelectrode. In time, I completed my Ph.D. thesis with the title: "Membrane Potential and Metabolism of Muscle." More detailed presentation of my research findings came later in the form of four full-length papers published in 1949, three co-authored with my professor and sponsor, Prof. R. W. Gerard (Ling and Gerard 1949, 1949a, 1949b) and one with a visitor from the west coast, Dr. W. Woodbury (Ling and Woodbury 1949.) The

title of each paper also includes explicitly the term, membrane potential — a name introduced by Julius Bernstein (1912.) Much of what I found appeared to be in harmony with the Bernstein's membrane theory of what used to be called the resting potential (ψ), as described by the following Equation:

$$\psi = \{RT/F\} \ln \{[K^+]_{in} / [K^+]_{ex}\}. \quad (25)$$

Then, as I began to spend more time in the library and my knowledge of the literature improved, I discovered that Bernstein's equation as such was no longer tenable. A great collection of reports on radioactive tracer studies showed without a doubt that the cell membrane is not impermeable to Na^+ as Bernstein assumed, but quite permeable to this ion (See Ling 2006a, p. 55; 2007, pp. 43–45.) That being the case, one can no longer ignore Na^+ in constructing an equation for the resting potential. Rather, Equation 25 would have to be rewritten into the following new form:

$$\psi = \{RT/F\} \ln \{([K^+]_{in} + [Na^+]_{in}) / ([K^+]_{ex} + [Na^+]_{ex})\}. \quad (26)$$

However, $([K^+]_{in} + [Na^+]_{in}) / ([K^+]_{ex} + [Na^+]_{ex})$ equals 1, ψ would become zero, contrary to facts.

In time, two alternative new models emerged. In 1949, Hodgkin and Katz introduced what was to be known as the Hodgkin-Katz-Goldman equation shown next (but minus the encircling dashed line):

$$\boxed{\psi^+ = \frac{RT}{F} \ln \left[\frac{P_K[K^+]_{in} + P_{Na}[Na^+]_{in} + P_{Cl}[Cl^-]_{ex}}{P_K[K^+]_{ex} + P_{Na}[Na^+]_{ex} + P_{Cl}[Cl^-]_{in}} \right].} \quad (27)$$

Though by far the great majority of workers in this field followed the lead of Hodgkin, Huxley and Katz, only a part of the equation enclosed in the dotted line of the Hodgkin-Katz-Goldman (HKG) equation was verified; the other predicted relationships were not.

In 1955, I suggested in a short note a third alternative theory of the cellular electric potential (Ling 1955.) That is, what I and all my peers used to call the membrane potential is not a membrane potential at all, but a surface adsorption potential like that of a glass electrode (Ling 1955.) As such, it also originates from the β -, and γ -carboxyl groups carried on the cell surface proteins. Interestingly enough, the verified part of the Hodgkin-Katz-Goldman equation matches *in form* the entire intact equation I introduced in 1959 for the surface adsorption model (Ling 1959; 1960 Equation 16), which can be simplified to read

$$\psi = \text{constant} - (RT/F) \ln \{K_K [K^+]_{ex} + K_{Na} [Na^+]_{ex}\}. \quad (28)$$

However, the similarity between the verified part of the (fragmented) Hodgkin-Katz-Goldman (HKG) equation and Equation 28 are, of course only in form. The differences lie in the meaning of the two sets of coefficients. In the HKG equation, they represent *permeability constants*; in the surface adsorption theory (to be renamed later *close-contact surface adsorption theory* in 2001), (Ling 2001, pp. 216–217) they represent *adsorption constants*.

In 1971, Edelmann and Baldauf studied the resting potential of guinea pig heart (papillary) muscle cells, from which they were able to extract both the *permeability constants* and the *adsorption constants* for three alkali-metal ions, Rb^+ , K^+ and Cs^+ (Edelmann and Baldauf 1971.) In their respective permeability, the three ions follow the rank order: $\text{K}^+ > \text{Rb}^+ > \text{Cs}^+$. In contrast, their respective adsorption follow the rank order: $\text{Rb}^+ > \text{K}^+ > \text{Cs}^+$. As shown in Edelmann's figure reproduced here as Figure 52, full accord was found between experimentally determined ψ and theoretical values constructed from the (measured) adsorption constants. The experimental data do not match at all the values of ψ predicted on the basis of the (measured) permeability constants (Edelmann 1973.)

Now, if the new concept of nano-protoplasm presented on earlier pages is correct, these β - and γ -carboxyl groups that give rise of the cellular electric potential should also exhibit basic properties fundamentally similar to those β - and γ -carboxyl groups in the bulk phase cytoplasm that selectively accumulate K^+ over Na^+ . In that case, the underlying adsorption should also follow the Yang-Ling adsorption isotherm given as Equation 5. Following this line of thinking, I introduced in 1979 a new equation for the cellular resting potential, in which auto-cooperative interaction among these surface β - and γ -carboxyl groups was taken into account and the new equation takes on the following form (Ling 1979):

$$\psi = \frac{RT}{F} \ln[f^-] + \frac{RT}{F} \ln \frac{1}{2[\text{K}^+]_{\text{ex}}} \left[1 + \frac{\xi - 1}{\sqrt{(\xi - 1)^2 + 4\xi \exp(\gamma / RT)}} \right], \quad (29)$$

where the *i*th and *j*th adsorbent of Equation 6 (on p. 142) that defines the symbol, ξ , refer to Na^+ and K^+ respectively.

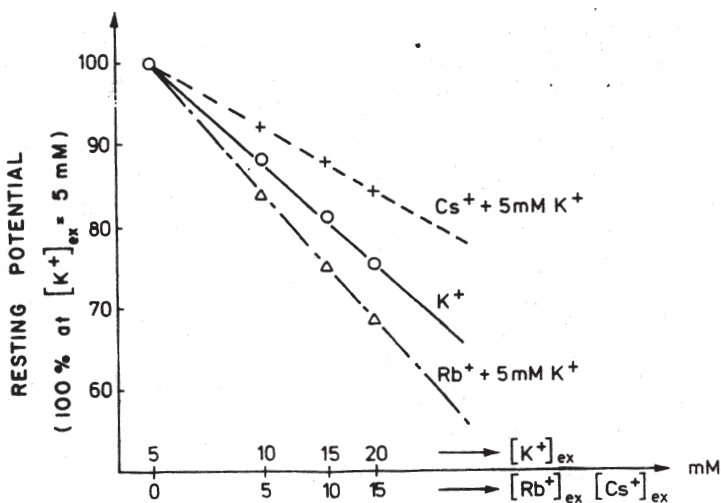


FIGURE 52. Influence of external K^+ , Rb^+ and Cs^+ on the resting potential of guinea pig papillary heart muscle cells. (after Edelmann 1973, by permission of New York Academy of Sciences)

Equation 29, of course, can also be put in the simplified form as follows:

$$\psi = \text{constant} + \{\Omega / [K^+]_{\text{ex}}\}. \quad (30)$$

3.2.3.1.2 Results of experimental study of two new models

Before examining how well these equations can predict the resting potentials measured in my own and in other's laboratories, I want to describe an exciting experience. It is the story how my associate, Leo Kushnir and I created a truly wonderful inanimate model for the steady electrical potential difference measured across the surface of resting muscle, nerve or other excitable cells. As mentioned above, it is called the resting potential now. Before that, it had been wrongly called a membrane potential. But before all that, a member of the great *Reductionist Four*, Emil DuBois Reymond first described and called it an *injury potential* (DuBois Reymond 1849.)

The story began with a glass electrode, the kind we used daily to measure pH. Made from Corning 015 glass, these electrodes are highly specific for H^+ and showed virtually no sensitivity to other mono-valent cations like K^+ — or silver ion, Ag^+ . Yet a German scientist by the name of K. Horovitz (*alias* K. Lark-Horovitz) had made the astonishing discovery that an ordinary glass electrode like that can be turned into a silver (Ag^+) electrode by merely soaking the glass electrode overnight in a solution of silver nitrate (Horovitz 1923.)

Horovitz's finding was one of the reasons that led me to believe that the underlying mechanism of the cellular electrical potential is not a membrane phenomenon as I once sincerely believed for quite some time. Instead, I began to think that the cellular electrical potential is a surface phenomenon. In both the glass electrode and the living cell, it is the electrically charged sites on a microscopically thin surface layer and its adsorbed ions that determines the polarity and magnitude of the measured electric potential (Ling 1955, 1959.)

With this concept in mind, I and my associate, Leo Kushnir first made a Corning 015 glass electrode and showed that it had no sensitivity to external K^+ concentration. We then coated the electrode with a very thin layers of (oxidized) collodion (nitrocellulose.) We expected that the collodion-coated electrode would now behave exactly like a simple collodion thimble electrode (Lewis and Saroff 1957.) And, as such it would show sensitivity to the concentration of external K^+ .

To our great delight, that was precisely what we observed. Indeed, we went a step further and tested on the collodion-coated glass electrode (for short, CCG electrode) the effects of all the other alkali-metal cations, H^+ as well as the divalent cations, Mg^{2+} , Ca^{2+} , Ba^{2+} and Sr^{2+} . The results are shown in Figure 53 and Figure 54. Taken as a whole, three outstanding features have thus been demonstrated on the CCG electrode:

1. The rank order of selectivity among the alkali metal ions is $Rb > K^+, Cs^+ > Na^+ > Li^+$. This rank order suggests that the carboxyl groups introduced into the nitrocellulose are in a low-c-value state. As such, it is entirely in keeping with the rank order seen in the ion accumulation in healthy frog muscle cells, as well as in the surface sites of guinea pig heart (papillary) muscle studied by Edelmann and Baldauf

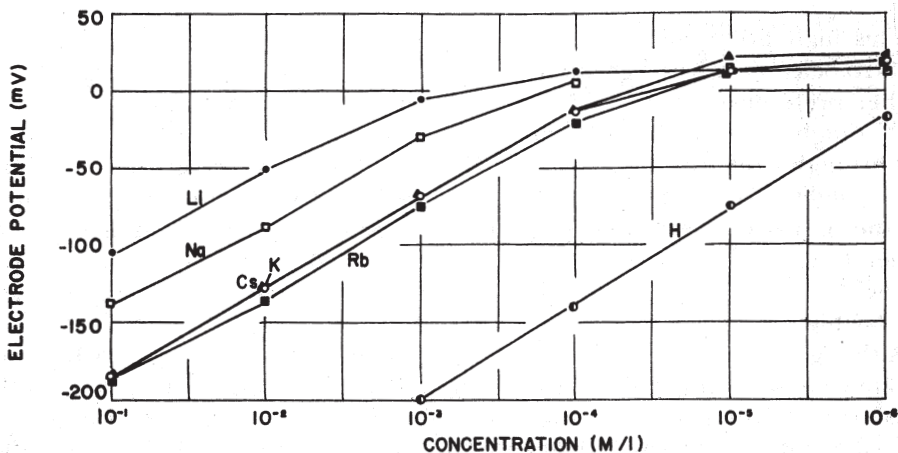


FIGURE 53. Monovalent cation sensitivity of collodion-coated glass electrode. The potential is considered positive if the outside phase of the electrode is positive to the inside phase. (Ling 1967, by permission of Marcel Dekker)

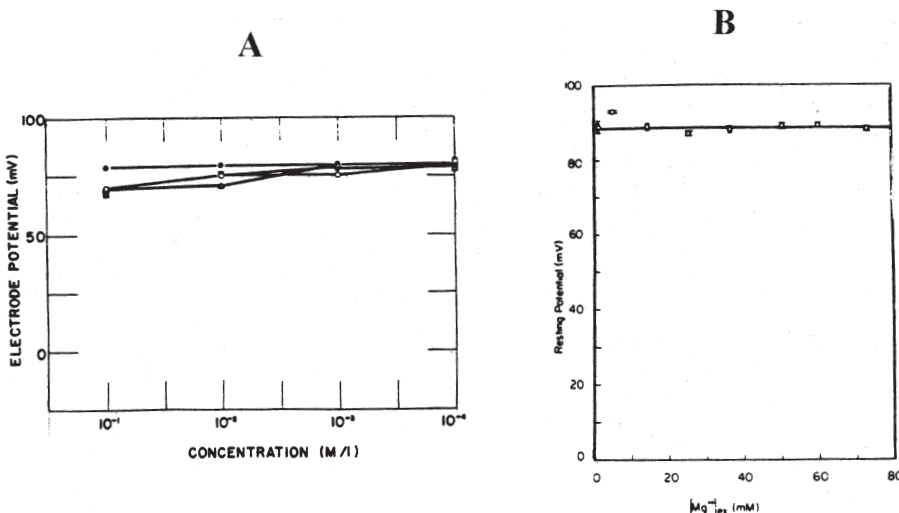


FIGURE 54. Low sensitivity of both the resting potential of frog muscle (B) and collodion-coated glass electrode (A) to one or more alkali-earth ions. In B, only Mg²⁺ was studied and it has no detectable influence on the resting potential. In A, insensitivity extends to all four alkali-earth ions studied: Mg²⁺ (●), Ba²⁺ (○), Ca²⁺ (△) and Sr²⁺ (■). (A from Ling 1967 by permission of Marcel Dekker; B from Ling *et al* 1983.)

(Figure 52.) Since the nitro group is a well-known strong electron-withdrawing group (Ling 2001, Figure 45 on p. 159), that its attachment on the cellulose molecule should have lowered the c-value of the carboxyl groups is understandable.

- (2) The H⁺ was found to be by far the most preferred ion on the low c-value carboxyl groups and it is preferred over K⁺ by about two order of magnitude. Virtually the

same two-order magnitude preference of H^+ over K^+ preference has also been observed in the resting potential of frog muscle cells.

- (3) The CCG electrode shows no sensitivity at all to all four alkaline-earth ions: Mg^{2+} , Ca^{2+} , Ba^{2+} and Sr^{2+} . In agreement, the resting potential of frog muscle cells also shows no sensitivity to Mg^{2+} (Figure 54B.) This is so even though the frog muscle cell is quite permeable to this divalent ion. (See Ling 2007, Table 11 on p. 59.)

All told, we have found in the CCG electrode a nearly perfect model of the electric potential generating cell surface, adding strong evidence once more that similar low-c-value β -, and γ -carboxyl groups are the seats of the cellular resting potential. At this juncture, we should not forget that the close behavioral parallelism seen between the surface of nerve and muscle cells and the oxidized collodion layer of a CCG electrode has an earlier precedent: the close behavioral parallelism between frog skin and cellulose acetate membrane. After all, collodion is a derivative of cellulose just as cellulose acetate is a derivative of cellulose. And, we have pointed out how water molecules dominated by fixed bipolar (CO, OH) groups on cellulose acetate bears close relationship to water under the influence of similar bipolar (CONH) groups in frog skin nano-protoplasm. Now, it is the carboxyl groups inadvertently or deliberately introduced into the cellulose molecules and their interaction with alkali metal ions that give rise to the electrical potential difference (Sollner *et al* 1941; Ling 1984 pp. 108-109; Ling 1992 p. 283) that matches the resting potential produced by the cell surface nano-protoplasmic β -, and γ -carboxyl groups and their associated alkali-metal ions.

As a corollary to this exciting page, I want to add that Leo Kushnir and I took yet another step further. We converted such a cation-sensitive CCG electrode into an anion-electrode by exposing a CCG electrode to a solution containing poly-lysine, which carries on its side chain fixed cationic ϵ -amino groups. In a moderately acidic medium ($pH = 5$), the cation-sensitive CCG electrode now metamorphosed into a perfect anion electrode. Once more, the fact clearly shows that it is only the charged sites on the surface of the cell or suitable model system that determines the magnitude and polarity of the surface potential (Figure 55.).

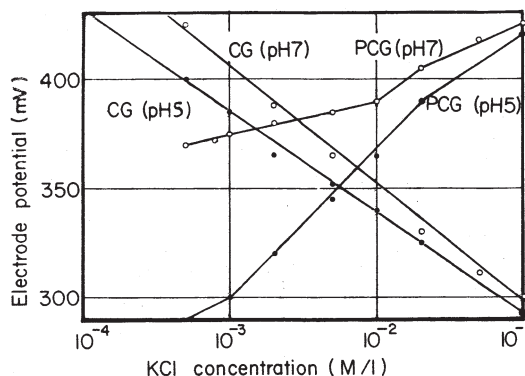


FIGURE 55. Anion and cation sensitivity of a collodion-coated glass electrode (CG electrode) and of a polylysine-treated CG electrode (PCG electrode) at two different pH's: 5 and 7. (from Ling 1967 by permission of Marcel Dekker)

3.2.3.1.3 Results of experimental study of the resting potential and its control

In the remaining part of this section I shall demonstrate that the nano-protoplasm making up the surface of frog muscle and other cell types, also shows auto-cooperative interaction. And that it too can be controlled by cardinal adsorbents that have been shown to control the β -, and γ -carboxyl groups of the nano-protoplasm making up the bulk of cell interior, as well as cell surface β -, and γ -carboxyl groups that mediate cation entry into frog ovarian eggs.

In all the figures to follow, the cell resting potential were as a rule measured with a Gerard-Graham-Ling microelectrode either by ourselves or by others. And, regardless of where the data points came from, the curves going through or near most of the experimental data points are theoretical according to Equation 29.

a. Control by ouabain

The top curve labeled “control” in Figure 56A shows a plot of the resting potential (Ψ) of a normal frog muscle cell against the logarithm of external K^+ concentration. The solid line going through or near all the data points are theoretical according to Equation 29 with the intrinsic equilibrium constant $K_{Na \rightarrow K}^{oo}$ set at 96 — compared to its counterpart in the K^+/Na^+ adsorption on bulk-phase cytoplasm, set at 100. The $-(\gamma/2)$ is 0.73 kcal/mole compared to its bulk-phase counterpart of 0.67 kcal/mole.

The data points of the top curve of Figure 56B are from Akaike (1975.) They are the resting potentials of soleus muscles in which most of the cell K^+ has been replaced by Na^+ — after the host rats had been fed a low K^+ diet for 40 to 49 days. Nonetheless, the $K_{Na \rightarrow K}^{oo}$ of the theoretical curve that fits the data is equal to 96.3 and the $-(\gamma/2)$ is equal to 0.67 kcal/mole — virtually identical to what was collected from resting potential studies on (normal K^+ -loaded) frog muscle resting potential as shown in Figure 56A.

It bears mentioning that the perfectly normal resting potential of Akaike’s Na^+ -loaded muscle cells is the converse of Ling and Kushnir’s collodion-coated glass electrode — both provide evidence that the standing electrical potential difference measured across the surface of either a resting cell or a (collodion-coated) glass electrode is a close-contact surface adsorption potential and as such, independent of the ionic content of the bulk-phase cytoplasm or that of the glass (electrode) beneath the thin layer of collodion painted on top of it. Having examined in some detail the two top curves of Figure 56A and B, we now go to the two bottom curves in Figure 56 A and B.

The data points on or near the lower curve in Figure 56 A are the resting potential values of frog sartorius muscle treated with ouabain at a concentration of 3.26×10^{-7} M. The intrinsic equilibrium constant, $K_{Na \rightarrow K}^{oo}$ of the data-fitting theoretical curve has fallen to 12.5 compared to its counterpart in the bulk-phase protoplasm exposed to the same concentration of ouabain, 21.7. However, the nearest neighbor interaction energy, $-(\gamma/2)$, of 0.56 kcal./mole is close to the value of 0.67 kcal/mole in the ouabain-treated bulk phase β -, and γ -carboxyl groups.

In comparison, the data points on or near the lower theoretical curve in Figure 56B are from Akaike’s Na^+ -loaded rat soleus muscle treated with a much higher concentration of ouabain (i.e., 10^{-4} M.) The $K_{Na \rightarrow K}^{oo}$ has dropped down only to 35; $-(\gamma/2)$, on the other hand, has fallen to zero. The much higher concentration of ouabain used by Akaike most likely played an important role in producing the differences observed.

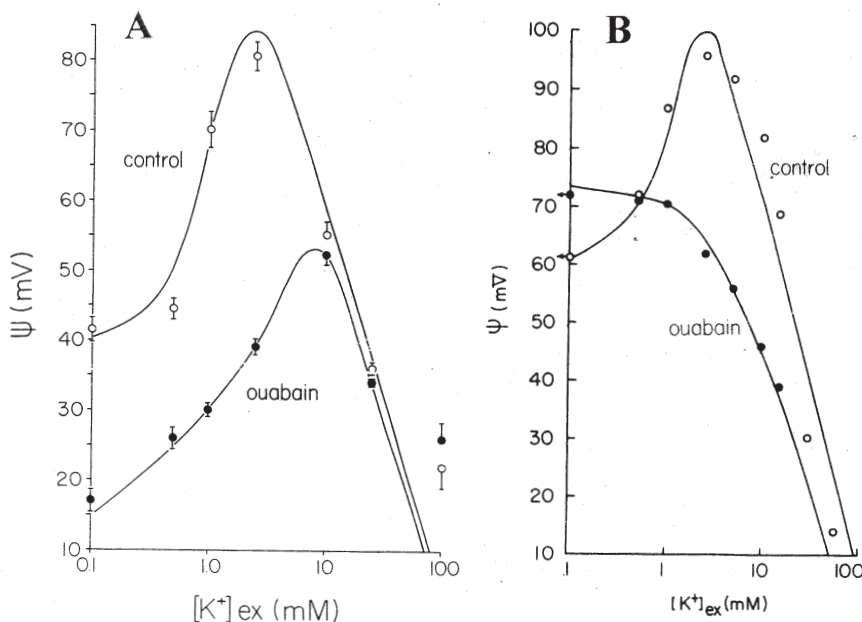


FIGURE 56. Effect of ouabain on the resting potential of frog sartorius muscle cells (A) and that of Na^+ -loaded rat soleus muscle cells (B). Electric potentials were all recorded with a GGL (alias Ling-Gerard) microelectrode. The control frog sartorius muscle is freshly isolated from normal North American leopard frogs. The control rat soleus muscles were not from normal rats. Instead, their normal intracellular K^+ had been largely replaced by Na^+ as a result of feeding the host animals for 40 to 49 days on a low K^+ diet. Notwithstanding, the two control curves are highly similar. The experimental frog sartorius muscles were incubated for 72 hours at 25°C in a Ringer-GIB medium containing 3.27×10^{-7} M of ouabain. Data presented in Figures 34 and 37 show that virtually all its intracellular K^+ has been replaced by Na^+ . The experimental rat soleus muscle was exposed to a much higher concentration of ouabain (10^{-4} M) but only for a short time. All four solid lines going through or near the experimental points are theoretical according to Equation 29 (with ξ as defined in Equation 6.) For the frog muscle cell, ouabain reduced $K_{\text{Na} \rightarrow \text{K}}^{oo}$ from 90 to 12.5 and increased $-(\gamma/2)$ from 0.56 to 0.73 kcal/mole. For the rat muscle cell, ouabain reduced $K_{\text{Na} \rightarrow \text{K}}^{oo}$ from 96.3 to 35 and $-(\gamma/2)$ from 0.67 to 0 kcal/mole. (experimental data on rat soleus muscles from Akaike 1975; all figures reproduced from Ling, Baxter and Leitman 1984)

b. Control by valinomycin

Earlier we have shown that valinomycin does not influence the rate of K^+ permeation into most living cells studied. That is not to say that valinomycin has no physiological impact on living protoplasm. On the contrary, Maloff and his coworkers demonstrated pronounced effect of valinomycin on the resting potential of isolated giant liver mitochondria (Maloff *et al* 1978.) This is shown in Figure 57, which replots their data according to Equation 29. The data-fitting apparent intrinsic equilibrium constant or K_K^{oo} equals 50 M^{-1} in control mitochondria; it falls to 16.6 M^{-1} in mitochondria treated with 10^{-7} M valinomycin. This action suggests that valinomycin acts like an EWC. As such, it lowers the c-value of the surface β - and γ -carboxyl groups of the mitochondria, increases their preference for K^+ and raises the surface potential.

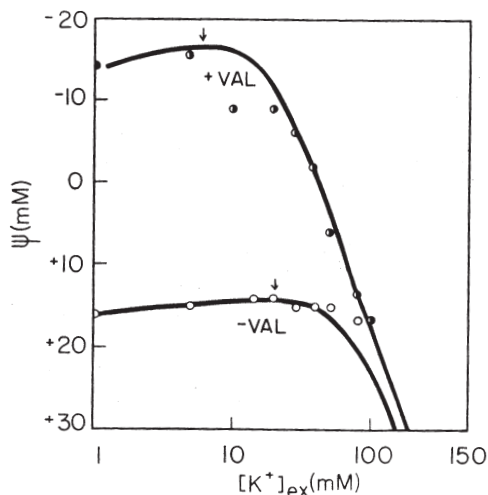


FIGURE 57. Effect of valinomycin on the resting potential of isolated giant liver mitochondria from cuprizone-fed mice. Data from Maloff *et al* (1978.) Points are experimental. Lines going through or near the experimental points are theoretical according to Equation 29. Valinomycin treatment reduced the apparent intrinsic equilibrium constant, K_K^{eq} from 50 to 16.6 M^{-1} . $-(\gamma/2)$ remains unchanged at 0.2 kcal/mole. (from Ling 1982)

3.2.3.2 The action potential

To survive and prosper, a living organism must be able to detect what is going on in its environment and to respond in one way or another. To achieve these goals, sensory organs like the eye and ear are installed to see or hear and to send what they detect in coded messages to the brain. In turn, the brain may send messages to the locomotive organs in order to flee or fight. For multi-cellular organisms, these messages are sent along nerve fibers in the form of *action potentials*, which are self-propagating, all-or-none electric perturbations of the resting potential.

Figure 58A shows a recording of a train of action potentials along a single nerve fiber connected to the eye (or ommatidium) of a horseshoe crab when short flashes of bright light were turned on and off. Traveling along the nerve fiber at the speed between a fraction of a meter per second to as high as 100 meters per second, each action potential lasts only 1/1000 of a second.

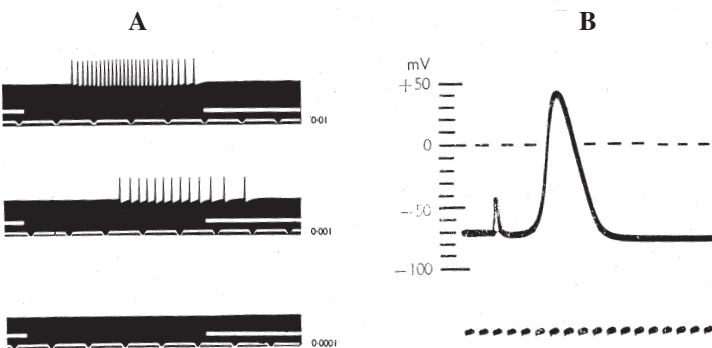


FIGURE 58. The nerve impulse (or action potential) seen at two different speeds of recording. A. Impulses along Limulus nerve fiber elicited by one-second long light flash. Lower interrupted white line marked 0.2 second intervals. B. An action potential recorded from an intact squid axon with a GGL microelectrode. Time marks are 0.4 msec. apart. (A from Hartline 1934 by permission of J. Cell and Comp. Physiology; B from Hodgkin 1958, by permission of the Royal Society of London)

In the preceding section, we have discussed how the Gerard-Graham-Ling (GGL aka Ling-Gerard) microelectrode with a tip half of a micron wide made it possible to record the resting and action potential of big and small single cells as well as even smaller sub-cellular organelles. (For history and fine examples of recordings respectively, see *The Microelectrode and the Heart 1950-1970* by S. Weidemann 1971 and *Electrical Activity of Single Cells* edited by Y. Katsuki 1960.) However, this should not obscure the fact that years before the GGL electrode became a usable tool, accurate intracellular recording of the resting and action potential had been successfully made with much wider glass capillary electrodes on the giant nerve fibers of squids and cuttlefish.

Note that when a GGL microelectrode is inserted into a resting nerve axon, it registers an inside-negative resting potential some 70 mV below that of the outside ground level marked 0 mV. If the nerve is then stimulated with an electric pulse upstream, an action potential would be launched and travel down the nerve. Recorded on a more expanded time scale, the action potential reveals a profile like that shown in Figure 58B. Note that the action potential does not represent a mere cancellation of the inside-negative resting potential, it actually becomes inside-positive by some 40 mV. The part of the action potential that goes beyond the zero-potential dashed line is known as the “Overshoot.”

3.2.3.2.1 Theories of the action potential

In 1952 British cell physiologists, Alan Hodgkin and Andrew Huxley discovered that the action potential is primarily an expression of the transient activity at the (muscle or) nerve surface associated with a local and transient movement of the Na^+ ion (Hodgkin and Huxley 1952a,b,c,d; Hodgkin, Huxley and Katz 1952.) A sketch of their theory of the action potential follows.

To begin, they accepted Bernstein's membrane theory of the resting and action potential. But by the end of the 1940's, Bernstein's postulated impermeability of the cell membrane to Na^+ and Cl^- had already been completely and unequivocally disproved (Ling 2006a, 2007.) To overcome the difficulty these new findings posed, Hodgkin and Katz reactivated the pump idea, which Theodor Schwann first introduced in 1839 (p. 112.) That is, the steady activity of a battery of postulated Na pumps in the cell membrane keeps the intracellular Na^+ at the low level as found in most living cells. In addition, they introduced what has been known as the Hodgkin-Katz-Goldman equation shown earlier on p. 196 above as Equation 27.

By postulating a much higher membrane permeability for K^+ (P_K) than for Na^+ (P_{Na}) in a resting muscle or nerve cell membrane and a reversal of this preference during activity, quantitative agreement between theory and observed values was achieved. However, many difficulties beset this model. Not the least was the disproof of the membrane-pump concept already mentioned on p. 115. Another concept introduced by Hodgkin and Katz was that the cell membrane has two kinds of pores or channels, one specific for K^+ and another kind for Na^+ . This concept too encountered difficulty because K^+ was shown to travel the alleged Na^+ channel etc., etc. The details of these contradictory findings will not be reiterated here since more than one review on the subject are already available (Ling 1984, pp. 463-470; Ling 1992, pp.276-280; Ling 2001, pp.209-226.)

In the preceding section, I have shown why the resting potential is not a membrane potential — as I myself once believed and wrote my Ph.D. thesis upon. Indeed, there is now

grave doubt that the membrane potential exists anywhere in the real world, living or dead. (See Ling 1992, pp. 282-285, Ling 2001, pp. 253.)

Rather, the resting potential is a *close-contact surface adsorption potential* like that of a glass electrode or a collodion-coated glass electrode described earlier.

Cell permeability studies presented on pp. 191 to 195 also left no doubt that living cells are not enclosed in a continuous phospholipid bilayer. On the contrary, the demonstrated bulk-phase-limited diffusion of labeled water into frog eggs and into barnacle muscle fibers (p. 191) shows that the living cells like the frog egg and giant barnacle muscle fibers at least are covered with (polarized-oriented) water at percentages not far from that of the entire cell, which is 49% in frog ovarian eggs and 76% in giant barnacle muscle fibers. (See Ling 2004, p. 5; Hinke 1970.)

One adds that this is exactly what one would expect if, as we maintain, that all active parts of the living cell are made of basic units of nano-protoplasm as described in Equation 1 on p. 124 or diagrammatically as in Figure 5 and 15.

However, there are reasons to believe that significant differences exist between nano-protoplasm at the cell surface like that of muscle and nerve cell and nano-protoplasm in the interior of these and other cell types — just as there is difference in the nano-protoplasm making up the surface of interior body cells like frog muscle and that making up the surface of frog skin as pointed out earlier in section 3.2.2.2b. The surface of these excitable nerve and muscle cells appears to be occupied by β -, and γ -carboxyl groups uncontaminated by fixed cations. Indeed, this is what is known as the Faraday cage effect. That is, in a conductor, electric charges congregate at the surface. The Law of Macroscopic Electro-neutrality also forbids the existence of a measurable amount of net electric charges inside a conductor.

Other persuasive evidence to the same effect is experimental. In most excitable cells, a plot of the resting potential against the logarithm of external KCl concentration is as a rule very close to theory, (e.g., a 58 mV drop of the resting potential per 10-fold increase of external KCl concentration. See Ling 1962, Figure 10-1, on p. 259.) In addition, the resting potential of frog muscle is constant between pH 5 and 10 (Ling and Gerard 1949, p. 389.) If there were “contaminating fixed cations”, the slope of the plot would be pH-dependent as shown for the PCG electrode in Figure 55.

This demonstrated absence of intermingling fixed cations at the surface of excitable cells has other important implications, which can be understood by going back to Figure 5. There, an across-the-board c-value rise of the β -, and γ -carboxyl group in consequence of (EWC) ATP depletion, changes the β -, and γ -carboxyl groups from adsorbing K^+ to forming salt-linkages with close-by fixed cations. (This postulation is backed by the experiment observations presented in Figure 33 on p. 172.)

However, when there are no fixed cations around to form salt-linkages, an across-the-board increase of the c-value of the β -, and γ -carboxyl groups at the cell surface would lead instead to a shift from adsorbing K^+ to adsorbing Na^+ . That, of course, is according to the AI Hypothesis an important activity underlying the creation of an action potential. Having made clear this basic issue involved, we are now ready to outline what an action potential is and does in terms of the AI Hypothesis:

In brief, the action potential is the manifestation of a specific case of controlled auto-cooperative AI-cascade transition of the nano-protoplasm at the surface of nerve, muscle and other excitable cells. This transition embodies a transient c-value rise of the cell

surface β -, and γ -carboxyl groups, *pari passu* with a transient c-value analogue rise of the cell surface backbone CONH groups. The c-value rise of the β -, and γ -carboxyl groups momentarily changes what is like a close-contact K^+ -selective surface potential to a Na^+ -selective potential. The c-value analogue rise of the backbone CO groups creates momentarily a depolarization-disorientatn of the cell surface water, which in turn brings about a q-value rise for Na^+ in the cell surface water. An inward Na^+ diffusion potential is created momentarily, giving rise to the “overshoot.”

Quantitatively, the polarity and magnitude of the action potential at its peak height is described by the following equation (For derivation, see Endnote 2 at the end of the article.):

$$\psi = \text{constant} + \{\text{RT/F}\} \ln \{\Omega / [K^+]_{\text{ex}}\} + \{\text{RT/F}\} \ln q_{Na^+}. \quad (31)$$

Counting from the right, the first term is the Na^+ diffusion potential responsible for the overshoot. The second term is the close-contact, surface adsorption potential of high c-value surface β -, and γ -carboxyl groups.

Now, we pose a key rhetoric question, What triggers the muscle or nerve surface protoplasm into the active state that reveals itself as the action potential? On this specific point, I have adopted an idea first introduced by Gordon and Welsh (1948.) That is, the stimulating electric current excites the cell by removing Ca^{++} from a chelating negatively charged site at the cell surface. But how does that removal of Ca^{2+} from the chelating site create an action potential is a question that to the best of my knowledge, only the AI Hypothesis had provided a molecular and electronic answer.

The answer is based on the (unsurprising) suggestion that Ca^{++} , being positively-charged, tends to draw negatively charged electrons toward itself and thus acts as an electron-withdrawing cardinal adsorbent or EWC — a postulation that Gulati has already affirmed in his experimental study on Ca^{++} activity reproduced in Figure 39 on p. 178.

As an EWC, Ca^{++} normally occupies an *auxillary cardinal site* (Figure 5.) and its electron-withdrawing impact synergistically compliments the influence of the principle EWC, ATP in maintaining the low c-value and low c-value analogue profile of a resting cell surface. The sudden removal of Ca^{++} then triggers an AI cascade mechanism leading to the across-the-board c-value and c-value analogue rises outlined above.

Figure 59 diagrammatically depicts what are described in words above. It shows the surface of a nerve or muscle fiber at rest (top) and during activity (bottom). In the resting nano-protoplasmic units, the EWC Ca^{++} represented by the circle with two + signs is enthroned on the (auxillary) cardinal site. Most of its β -, and γ -carboxyl groups are associated with K^+ . All the cell water molecules assume the dynamic structure of polarized-oriented multilayers, in which only a few Na^+ are found.

With the detachment of the EWC, Ca^{++} by either a stimulating cathode or the (negative) front end of an arriving action potential, an all-or-none shift takes place. And this shift is diagrammatically represented by the sequence of events starting at the top illustration of Figure 59 and ending on the bottom illustration of the same figure. A recording GGL electrode would see both the annulment of the 70 mV inside negative resting potential and superimposed on it an inward diffusion potential of (unaccompanied) positively-charged Na^+ , giving rise to the “overshoot.”

No longer under a disengaging local negative electric field of a stimulating cathode or the advancing front end of an approaching action potential, Ca^{++} returns to its cardinal

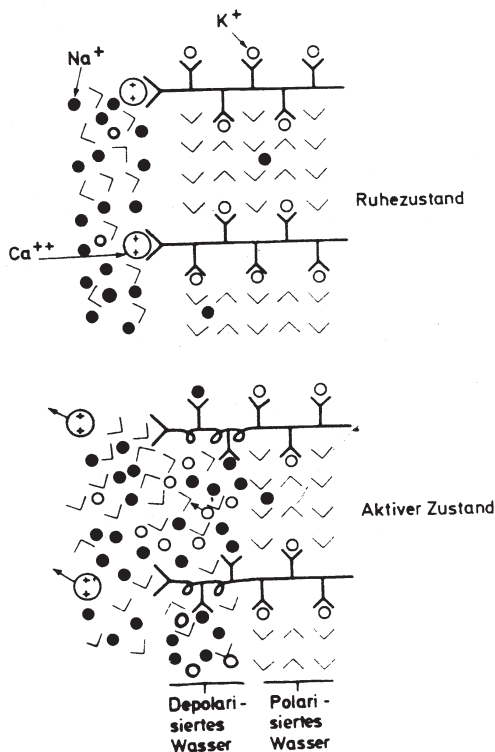


FIGURE 59. Diagram of a microscopic region of nano-protoplasm at the surface of an excitable cell in the resting state ("Ruhezustand") and at an activated state ("Aktiver Zustand"). Detachment of the cardinal adsorbent, Ca⁺⁺, triggers (i) the desorption of adsorbed K⁺ and its displacement by Na⁺ and (ii) a concomitant depolarization-disorientation of the nano-protoplasmic water, increasing its q-value for Na⁺, which in turn leads to an inrush of Na⁺ from the external medium, producing the "overshoot." K⁺ ●, Na⁺ ○, water molecules △. (from Ling 1981a, by permission of Wissenschaftliche Verlag)

site. That in turn reverses every move involved in the top to bottom figure transition to its initial resting living state. Electrically, the falling phase of the action potential fully returns to its pre-excitation status after a short burst of outward loss and regain of K⁺.

3.2.3.2.2 Results of experimental studies on the action potential

a. On intact living cells

In support of this theory, it is known that decreasing external Ca⁺⁺ concentration lowers the threshold for stimulation. Decreasing external Ca⁺⁺ concentration also causes spontaneous firing of nerve and muscle cells (Adrian and Gelfan 1933.) In contrast, increasing external Ca⁺⁺ concentration increases the threshold for electric stimulation (Cole 1949.)

From permeability studies, Ling and Ochsenfeld showed that the β-, and γ-carboxyl groups of resting frog muscle cell surface adsorb the alkali metal ions in the rank order Rb⁺ > Cs⁺ > K⁺ > Na⁺, while the β-, and γ-carboxyl groups of guinea pig heart muscle show a rank order of Rb⁺ > K⁺ > Cs⁺. Both correspond to a low c-value of about -4.0 Å.

In sharp contrast, the anionic groups of giant squid axon mediating Na⁺ entry during an action potential follow the rank order Li⁺ = Na⁺ > K⁺ > Rb⁺ > Cs⁺ as reported by Hille (1975.) That rank order corresponds to a much lower c-value of about -3.0 Å. The data from Chandler and Meves (1965) can be interpreted as indicating an even lower c-value of -2.65 Å (For details, see Ling 1992, p.311; 2001, p.230.)

Villegas, Blei and Villegas (1965) then showed that during activation, there is also a travelling wave of increased non-specific permeability to non-electrolytes (Table 6.) This finding is in harmony with the theoretical prediction that there is a wave of reversible increases of c-value analogue of the backbone carbonyl groups. This harmony is further enhanced by their demonstration that this increase of membrane permeability to non-electrolytes depends on the presence of a high concentration of Na^+ in the bathing medium. A high concentration of external Na^+ makes the K^+ to Na^+ adsorption exchange on the β -, and γ -carboxyl groups feasible as part and parcel of the auto-cooperative transition at the cell surface.

b. on isolated protoplasmic droplets

In 1956, Kamiya and Kuroda succeeded in keeping alive droplets of isolated Nitella protoplasm for as long as 50 hours in an artificial salt solution. In 1971, Inoue *et al* (1971) discovered how such an isolated protoplasmic droplet could be excited by an electrical stimulus. With the aid of a GGL electrode, a record of an action potential like that shown in Figure 60A was obtained. Obviously this recording bears strong resemblance to the action potentials recorded with a similar GGL electrode in squid axon, frog muscle and other intact excitable cells and shown in Figure 58B.

The top curve of Figure 60B shows that an inside-negative resting potential of 90 mV is recorded when the microelectrode enters the Nitella protoplasmic droplet. The magnitude and polarity are exactly like that recorded in a single frog muscle cell. Inoue *et al* called such an impaled protoplasmic droplet in A state. It is while the droplet is in this A state, that an electric pulse would elicit an action potential like that shown in Figure 60A. The transition is *all-or-none* and hence an example of what we call a controlled auto-cooperative transition shown in Figure 13B.

However, if one does not apply the electric stimulus but steadily increases the concentration of Na^+ in the bathing medium, a point will be reached when another all-or-none

TABLE 6. Permeability of resting and stimulated squid axons to ^{14}C -labeled erythritol, mannitol and sucrose. Calculated permeability change made on the assumption that the permeability change during excitation lasts 1 msec. (from Villegas *et al.* 1965, by permission of the Journal of General Physiology)

Molecule	Permeability in 10^{-2} cm/sec ^a			
	Resting axon (axon a)	Stimulated at 25/sec (axon b)	Net increase 25 stimulations/sec (paired data) (b - a)	Calculated permeability during activity ^b
Erythritol	3.6 ± 0.4	6.1 ± 1.0	2.5 ± 0.8	110
Mannitol	2.3 ± 0.4	4.0 ± 0.5	1.7 ± 0.3	75
Sucrose	0.9 ± 0.1	1.8 ± 0.3	0.9 ± 0.3	40

^aThe values are mean \pm SE of ten nerve fiber pairs.

^bCalculated permeability during activity obtained by considering that the permeability change per impulse lasts 1 msec.

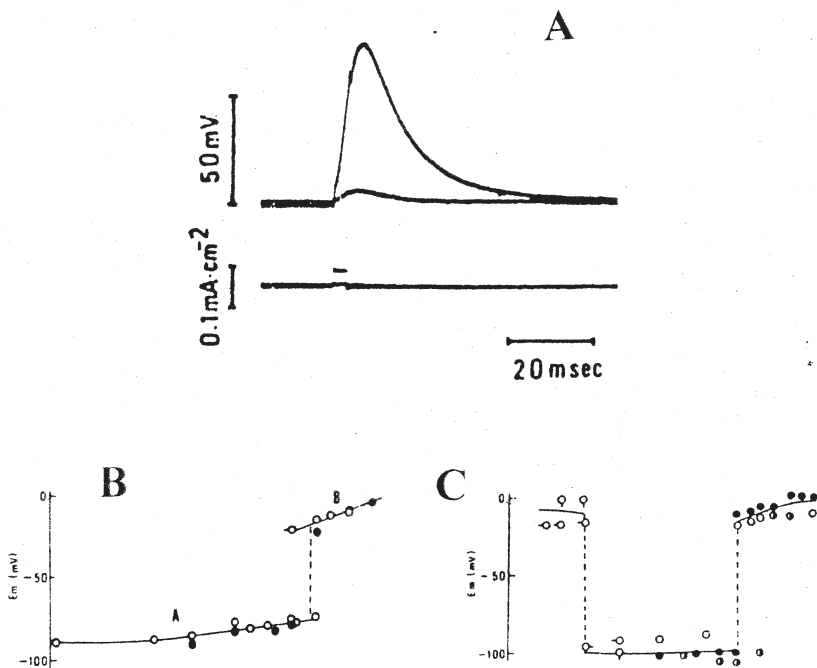


FIGURE 60. Electrical recordings with a GGL electrode from isolated Nitella protoplasmic droplets in a life-sustaining "test solution" containing 0.5 mM NaNO₃, 0.5 mM KNO₃, 1 mM Ca(NO₃)₂ and 2 mM Mg (NO₃)₂. (A) Action potential induced by an outwardly directed current pulse when the droplet was in State A (see legend for B.) (B) Dependence of resting potential on external Na⁺ concentration as given on abscissa in a solution with ionic composition same as in "test solution" except Na⁺. A, B in graph denote resting A state, and depolarized B state respectively. (C) Dependence of resting potential on external Ca⁺⁺ concentration as shown on abscissa. Except for Ca⁺⁺, all other ionic concentrations are the same as in "test solution." (from Inoue *et al* 1973 by permission of Biochimica Biophysica Acta)

change will take place, dramatically reducing the resting potential from -90 mV to some -20 mV. In fact, this constitutes another example of what I call spontaneous auto-cooperative transition and illustrated in Figure 59A.

Let us now return to the controlled auto-cooperative transition shown in Figure 59A. As mentioned above, and in accordance with our working hypothesis, it is the detachment of the EWC, Ca⁺⁺ that triggers off the action potential in muscle and nerve fibers. There is evidence provided by Figure 60C that here too it is the detachment of Ca⁺⁺ that triggered the transition.

Thus, the -90 mV resting potential is maintained as long as the bathing medium contains Ca⁺⁺ within the concentration range 0.1 to 10 mM. However, once the Ca⁺⁺ concentration falls to 0.1 mM or beyond, the resting potential undergoes an all-or-none transition to -10 mV.

In summary, the isolated protoplasmic droplet from Nitella internodal cells shows a resting potential of the same size and same polarity as a typical excitable intact living cell.

It can also be stimulated to produce an action potential resembling in overall profile the action potential recorded from a squid axon or frog muscle cell.

3.2.4 Cellular swelling and shrinkage

Reviews: Ling 1962 Sect. 9.4; 1984 Chapt. 13; 1992 Chapt. 10; 2001 Sect. 15.3

3.2.4.1 Theory of cell swelling and shrinkage

In 1962 as part of the original AI Hypothesis, I suggested that the profound impact of high concentration of KCl in causing extensive cell swelling while an equal concentration of NaCl has no or little impact can be explained by the difference in their respective power in breaking up salt linkages (Ling 1962 pp. 246–250.) An underlying assumption of this interpretation is that cell protoplasm has the power of drawing into the cell more water if part or all of the restraining salt linkages are broken by KCl. This idea gained strength with the subsequent introduction in 1965 of the polarized-oriented multilayer (POM or PM) theory of cell water, according to which, all or virtually all water already in living cells (and yet to enter) exists in the form of polarized-oriented multilayers on the fully-extended polypeptide chains of cell proteins (Ling 1965.)

In 1970 Ling and Negendank confirmed the POM theory of cell water by demonstrating that 95% of the water in healthy strips of frog muscle cells follow the Bradley adsorption isotherm at relative vapor pressure ranging from 4.3% to 99.6% saturation (Ling and Negendank 1970) (see Figure 26.)

Following up on Ling and Negendank's finding, Cope went on to show that if the NaCl concentration providing the right relative vapor pressure is designated C, then the Bradley adsorption isotherm just mentioned can be rewritten in a form that describes the relationship between the volume of the cell, V, in equilibrium with the NaCl solution at concentration, C such that

$$V = B - A \log_{10} C, \quad (32)$$

(Cope 1967.) Cope's equation was later incorporated into a more comprehensive equation by Ling and Peterson (1977) (to be quoted here below as Equation 34) that describes the changing volume of living cells in solutions containing increasing concentrations of NaCl and other salts.

A fundamental assumption of this theory of cell swelling (and shrinkage) is that each living cell is seen as an aggregate of n types of *microcells*. Every microcell contains just one salt linkage, which can be either in the (associated) salt linkage form or in the fully dissociated form of fixed cation-fixed anion pair. Representing the salt linkage in the associated form as $F^+ F^-$, where F^+ represents a fixed cation usually an ϵ -amino group or a guanidyl group. F^- represents a fixed anion usually a β -, or γ -carboxyl group, we then have



where X^+ and Y^- are respectively the cationic and the anionic component of the salt added which causes the dissociation of the salt linkages. It is assumed that the F^+ and F^- are in

the fully (associated) salt linkage form when there is no salt in the environment. When there is salt in the surrounding medium, the reaction described by Equation 33 proceeds in an all-or-none, auto-cooperative manner according to the Yang-Ling cooperative adsorption isotherm (Equation 5 or Equation 8.) Putting all these concepts together, we have the equation for the ratio of the final cell volume (W_f) over the initial cell volume (W_i) as follows:

$$\frac{W_f}{W_i} = \sum_{l=1}^n \phi_l [(b_l^1 - a_l^1 \log C) \Omega_{diss}^l + b_l^2 (1 - \Omega_{diss}^l)], \quad (34)$$

where ϕ_l is the molar concentration of the l th type of microcells divided by a constant W_i , equal to the original or initial total volume of the cell. C is the concentration of the salt in the bathing medium, b_l^1 , a_l^1 and b_l^2 are all constants. Ω_{diss}^l is, as usual, the abbreviation of the Yang-Ling cooperative adsorption isotherm describing the autocooperative adsorption exchange taking place inside the l th type of microcells.

3.2.4.2 Results of experimental studies on swelling and shrinkage of living cells in solutions containing an increasing concentrations of chloride salts.

Figure 61A represents plots of the relative cell weight ($W_{final}/W_{initial}$ or W_f/W_i) as ordinate against the concentrations of the chloride salts of Rb^+ , Cs^+ , K^+ , Na^+ , Li^+ and choline in the bathing medium after 7 days of incubation at 4°C. Focussing attention on the lower salt concentration range up to 150 mM, the relative power in producing the most swelling follows the rank order: $Rb^+ > K^+ > Cs^+ = Li^+ > Na^+$ — suggesting that the anionic β -, and γ -carboxyl groups of the salt linkage being dissociated have a low c -value. And in this way, they resemble, first, the (free) β -, and γ -carboxyl groups that selectively adsorb the alkali-metal ions in the bulk phase cytoplasm of similar frog muscle cells as described in Figure 37A and Figure 38. and, second, they resemble the surface β -, and γ -carboxyl groups mediating cation entry into guinea pig papillary muscle and also give rise to its resting potential (Figure 52).

In general pattern, the swelling effect of the six salts on frog sartorius muscles falls into three groups: the $RbCl$ and KCl group; the $NaCl$ and $LiCl$ group and the $CsCl$ and choline chloride group. In contrast, Figure 62A shows similar KCl -induced weight change profiles of four different types of small frog muscles. Their respective names are given at the lower right corner of the graph. As the data clearly indicate, there is a high degree of reproducibility among all these muscle types.

The $NaCl$ - $LiCl$ group did not show swelling until a much higher concentration range of 150 to 250 mM was reached. The $CsCl$ -choline chloride groups did not show swelling until an even higher concentration beyond 300 mM. In the end, the final weights of all three groups converged to more or less the same value, when the salt concentration reached 1500 mM or 1.5 M.

Ling and Peterson then showed that Equation 34 can generate theoretical curves that match each one of the different types of observed volume changes. Only one of these theoretically calculated curves will be presented here as Figure 61B.

The data points of the top figure of Figure 61B are experimentally observed. The solid line that goes through or near most of the data points are theoretically computed according to Equation 34 and is itself a composite of three theoretical curves each corresponding to a different type of fixed β -, and γ -carboxyl groups, each with a different c -value.

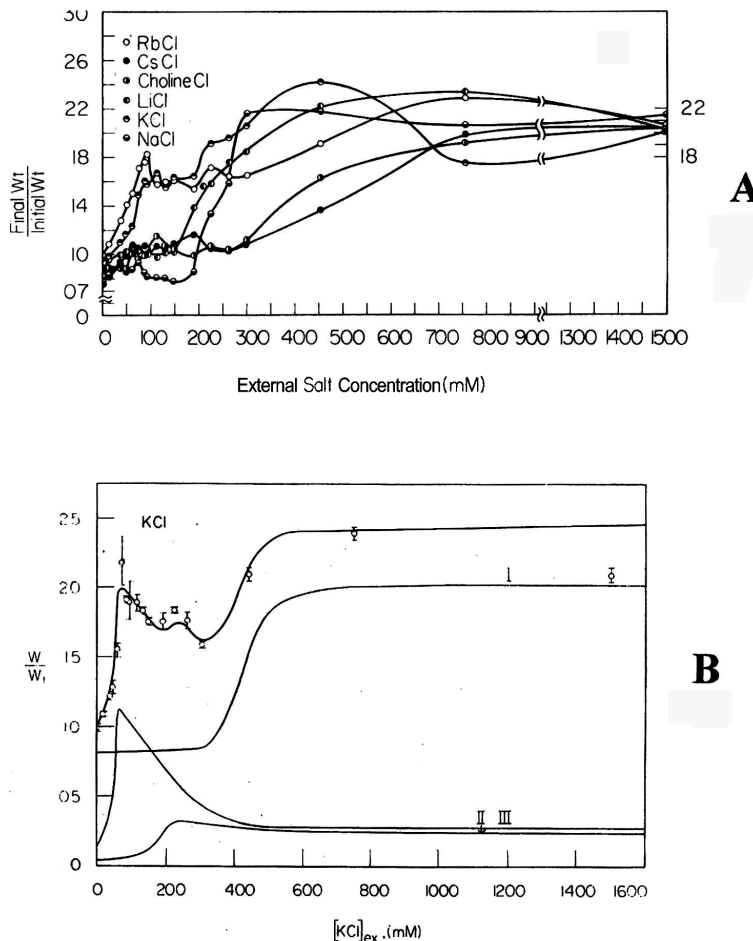


FIGURE 61. Swelling and shrinkage of frog voluntary muscles in increasing concentrations of the chloride salts of Li^+ , Na^+ , K^+ , Rb^+ , Cs^+ and choline. (A) Experimental observations. Incubation at 0°C lasted 7 days in modified Ringer-GIB media (see Ling and Bohr 1969) before the final weight was determined and expressed as a ratio over the initial weight as the ordinate (Final wt/Initial wt). (B) Theoretical interpretation. Points are experimental. Line going through or near most of the experimental points are composites of three (I,II,III) theoretical curves involving the dissociation of different types of salt-linkages and all describable by the Yang-Ling cooperative adsorption isotherm. In all three fractions (I, II, III) the rising phase is the consequence of the strong auto-cooperativity with nearest neighbor interaction energy ($-\gamma/2$) of 0.50 kcal/mole or higher. The following phase of each of these curves could be a sharp fall or a flat plateau or something in between. The interpretation Ling and Peterson offered for the sharply falling curve as shown in fraction III is simply due to further decline of the activity of water with the continually rising salt concentration bathing the cells. This interpretation is based on the assumption that cell water stays largely polarized-oriented as in normal cells. By exclusion, the flat plateau type seen in fraction I would then indicate a depolarization-disorientation of cell water. (from Ling and Peterson 1977, by permission of the Bull. Math. Biology)

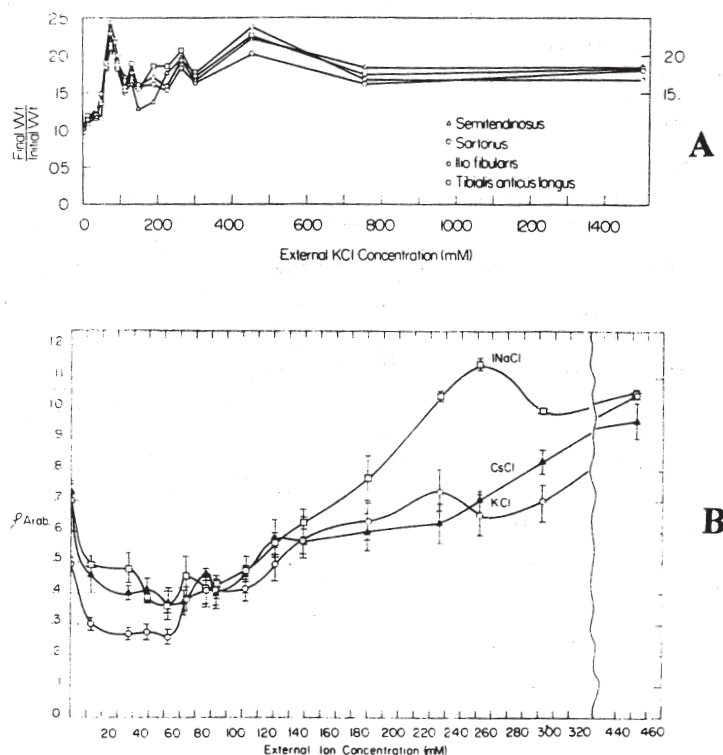


FIGURE 62. Swelling or shrinkage of isolated frog muscles in increasing concentrations of KCl (A) or of KCl, CsCl and NaCl (B). (A) Swelling-shrinkage curves of four different types of small intact frog muscles in increasing concentration of KCl solution. Names of the four types of muscles are listed in the lower right corner of the graph. While some minor differences exist, by and large, there is agreement, giving one indication of the validity and accuracy of this type of observation. (B) The apparent equilibrium distribution coefficients of D-arabinose (p_{Arab}) of muscle cell water in muscles that have been exposed for 7 days at 4°C in solutions of KCl, CsCl and NaCl of increasing concentrations. Shown as the ordinate, p_{Arab} is equal to the concentration of radioactively labeled D-arabinose in the muscle cell water in each muscle divided by the final concentration of D-arabinose in the bathing solution of that experiment. p_{Arab} in the range of 0.2 to 0.3 indicates a normal polarized-oriented state of the cell water. Rising p_{Arab} indicates deterioration. (from Ling and Peterson 1977, by permission of the Bull. Math. Biology)

The first curve giving rise to the first sharp peak has β -, and γ -carboxyl groups with the strongest affinity for K^+ and in all probability, the lowest c-value. The other two curves have decreasing affinity for K^+ as judged by the much higher KCl concentration required to bring about the swelling. However, besides the location and shape of the rising phase of each curve, there is another question to answer. It is what happens after the top of the peak has been reached. In the first curve, the swelling peak is followed by an immediate and sharp shrinkage. In the second and third curve, they are both more or less flat plateaus. The explanation for this difference was given by Ling and Peterson as follows.

The shrinkage phase of the first sharp peak is created by the increasing KCl concentration to the right of the peak. For that to happen, the bulk phase water must be in the normal polarized-oriented state. On the other hand, the appearance of a flat plateau after the peak bespeaks of a weakening or disintegration of the dynamic structure of polarized-oriented water. Thus underlying the three theoretical curves, which together reproduce what was experimentally observed, is that the cell water remains more or less normal until the NaCl concentration has reached about 400 mM. Further beyond, the dynamic water structure appeared all destroyed. Fortunately, by that time, we already had a well-developed method for monitoring the state of health of the bulk phase water. It is the D-arabinose probe method based on the fact that this pentose is not metabolized at a significant rate by frog muscle at low temperature (Ling and Ochsenfeld 1988.)

To monitor the state of health of the cell water, Ling and Peterson studied the apparent equilibrium distribution coefficient or ρ -value of (radioactively-labeled) D-arabinose in muscles similarly treated with salts of different concentration. Figure 62B shows the state of water as monitored by the D-arabinose distribution pattern in frog muscles exposed to increasing concentrations of KCl, NaCl and CsCl.

Within the range of salt concentration of 10 to 100 mM, the D-arabinose ρ -value is low pointing out that by and large the normal dynamic water structure is preserved. At very high salt concentration (440 to 460 mM), $\rho_{D\text{-arabinose}}$ approaches unity, suggesting that the water has, to all intent and purposes, turned into normal liquid water. This finding then completes the evidence showing concordance between theory and experiments on the effect of increasing KCl concentration on the swelling and shrinkage of isolated frog muscle.

As mentioned, other similar theoretical confirmations were also achieved for all the swelling and shrinkage curves produced by all six kinds of chloride salts. In concluding this section, we turn our attention to the control of cell volume by cardinal adsorbents, beginning with the queen of all cardinal adsorbents, ATP.

3.2.4.3 Results of experimental studies on the control of swelling and shrinkage.

a. Control by ATP

ATP, is the ultimate end product of energy metabolism in all living organisms. It is also what we sometimes call the Queen of cardinal adsorbents. As a powerful EWC, ATP keeps the β -, and γ -carboxyl groups at a low c-value state, in which Rb^+ and K^+ are highly preferred over Na^+ . The fact that ATP is a strong EWC also suggests that ATP depletion could offer a possible explanation of what we know too well while a child. A collision with a hard object may produce a swelling of some part of our body. Other collisions with heavier objects may cause life-threatening brain swelling.

More specifically, the underlying mechanism of traumatic edema is not unlike that of healthy tissues brought about by high concentration of KCl. Yet the agent that brings about the swelling of injured tissues is not an abnormally high KCl concentration in the plasma or tissue fluid. Ironically, it is the high concentration of Na^+ and Cl^- found in all normal blood plasma and its man-made substitute, the Ringer-Locke soluton. Indeed, if we remove that high level of Na^+ (and its counter-anion, Cl^-) from a normal plasma, the animal would soon be paralyzed and perish. That being the case, one asks, What then turns a vitally needed friend into a deadly enemy? The answer is, loss of ATP.

For with ATP gone, the high concentration of Na^+ found in perfectly normal blood plasma now suddenly becomes life-threatening because with ATP reduced, the β -, and γ -carboxyl groups are no longer held at the safe low c-value but rise to a higher c-value at which the preference for Na^+ is sharply increased — so that it begins to act like a high concentration of KCl on normal tissue cells and as such cause extensive swelling or oedema.

Now, if this theory of injury induced tissue swelling is fundamentally sound, it would predict the following:

Prediction 1: Injury induced swelling will only occur in the presence of a high concentration of Na^+ (or Li^+) since both both ions are according to theory, highly preferred only at high c-value (see Figure 7, or Figure 36.)

Prediction 2: The degree of swelling would be inversely related to the concentration of ATP existing in the injured tissue.

Figure 63 shows some of the observations my one-time summer student Chet Kwon and I made confirming both of these predictions. Next I examine these figures in greater detail.

Figure 63 has four panels. In each, the abscissa comes in two parts. The top abscissa shows the increasing concentration of the specific salt used in the modified Ringer's solution with the name of the salt indicated near each experimental curve. The bottom abscissa represents decreasing concentration of sucrose in the modified Ringer's solution to maintain osmotic balance.

Figure 63A shows that with increasing concentration of NaCl (and decreasing sucrose) all three mouse tissues kept for 48 hours in a cold (4°C) and anoxic environment, steadily increased their respective weights. But the extent of swelling varied, being more prominent in the kidney and liver than in the spleen.

Also worth noticing is that all three tissues lost about half their original weight after 48 hours in the cold-anoxic environment in the high sucrose bathing medium with the exception of the brain tissue (Panel C and D.) A possible cause for this shrinkage in kidney, liver and spleen cells is the presence of high-c-value, free β -, and γ -carboxyl groups (in these cells) that are normally associated with Na^+ in the cells. Removal of NaCl from the environment and replacing it with sucrose takes away the adsorbed Na^+ . That in turn would enhance the chance for the now-liberated β -, and γ -carboxyl groups to engage in the formation of new salt-linkages. Formation of new salt linkages could of course causes cell shrinkage as both Figure 19 and Equation 33 show in the right to left direction.

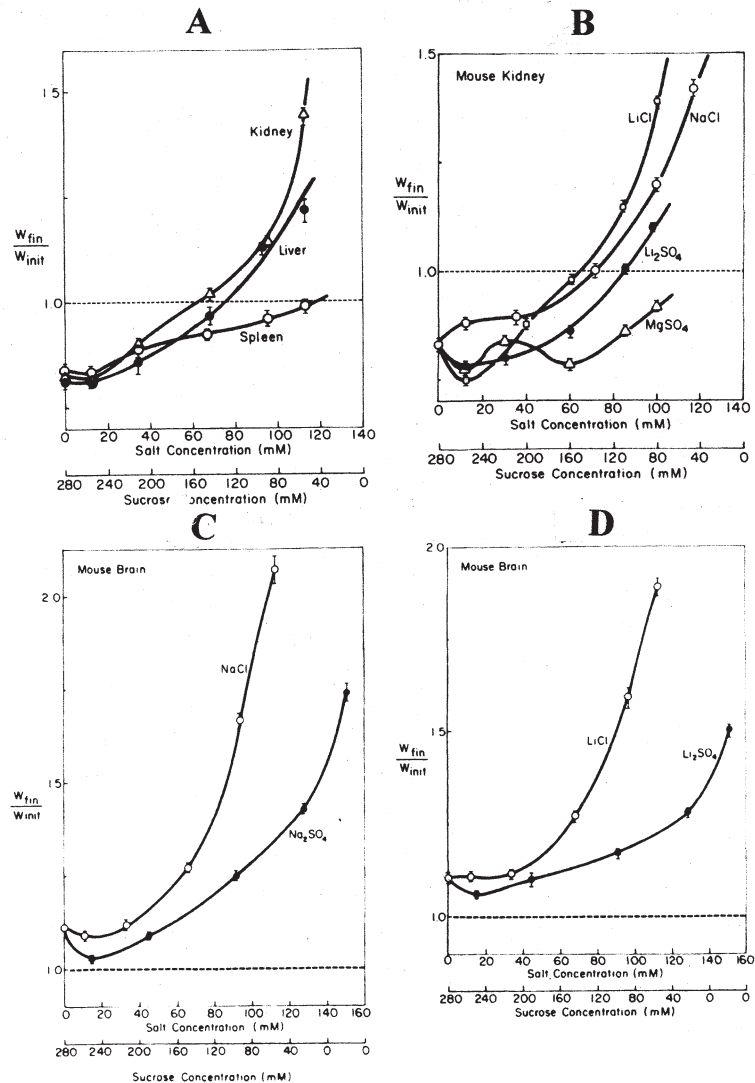


FIGURE 63. Injury induced tissue swelling and its dependence upon the presence of the high concentration of NaCl present in blood plasma or Ringer-Locke solution. Injury was produced by keeping isolated mouse organs in a small volume of unstirred salt solution without a continuing supply of oxygen combined with chilling (4°C.) (A) Data show that mouse kidney, liver and spleen lost half of their normal weight after incubation for 7 days in a modified Ringer-Locke solution in which all the NaCl has been replaced by an isotonic equivalent of sucrose (280 mM). (For exception see Figure 63C.) Substitution of sucrose with an iso-osmotic equivalent of NaCl brings about progressive weight increase until they had swollen to 140% of the original weight. (B) Data show LiCl caused the most swelling, NaCl the next, Li₂SO₄ still less, while MgSO₄ showed virtually no influence. (C, D) Comparable study with isolated mouse brain. Otherwise alike, the brain did not undergo shrinkage when placed in a modified Ringer-Locke solution containing 280 mM sucrose. (from Ling and Kwon 1983)

Figure 63B shows the high level of swelling of injured mouse kidney in solutions containing high concentration of NaCl, and even higher swelling in medium containing high concentrations of LiCl. In contrast, Li₂SO₄ produced much smaller gain in weight; MgSO₄ produced even less. Pretty much the same pattern of response happens in the injured mouse brain as shown in Panel C and D. Only the level of swelling in the brain is by far the highest among all the tissues examined. Once more, it tells us why brain swelling due to injury can be life-threatening and calls for speedy attention in human cases. All in all, these findings affirm the theoretical claim of high c-value of the β -, and γ -carboxyl groups in the salt linkages involved.

While Figure 63 offers insights into the details on how high concentration of NaCl contributes to injury-induced tissue swelling — thereby confirming Prediction I, it is the data presented in Figure 64 that confirms Prediction 2.

For what Figure 64 shows is that in the presence of full concentration of NaCl, the swelling of the cold and anoxia induced swelling is strongly dependent on the state of depletion of ATP. As long as the ATP concentration is normal and high, the water content of the brain tissue is normal (ca. 4 grams of water per gram of dry weight.) With decreasing ATP concentration, NaCl-dependent swelling took off, reaching the highest level of swelling when ATP concentration is near undetectable.

The confirmation of both Predictions led us to pose another question. Now in theory, the depletion of an EWC is equivalent to the addition of an EDC. Since we have repeatedly pointed out above that while ATP is an EWC, ouabain is an EDC, the theory cannot escape making an additional prediction. That is, if we can keep the tissue ATP level from being secondarily reduced, by exposing frog muscle to a concentration of ouabain just high enough, but not too high, that ouabain treatment should also bring about a NaCl-dependent swelling of the tissue cells. Whether or not this prediction can also be answered in the positive will be made clear in the next and last section of this communication.

b. Control by ouabain

Our purpose is to test the hypothesis that exposure to a very low but above-threshold concentration of the EDC, ouabain should bring about a NaCl-dependent swelling of healthy

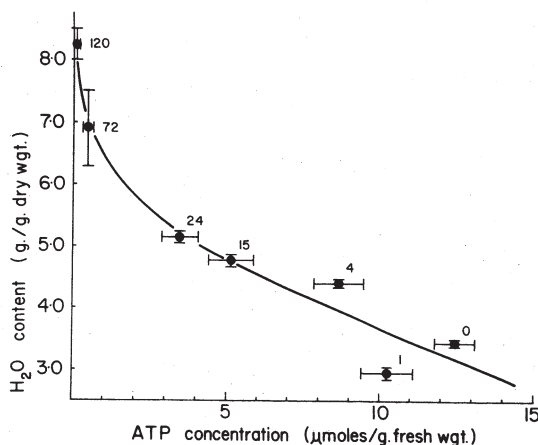


FIGURE 64. The relation between the extent of brain swelling in a Ringer's solution containing 118 mM NaCl and the ATP content of the tissue. Brain injury was produced by incubation in a small volume of unstirred anoxic and cold Ringer-Locke solution for number of hours indicated by the number near each point. Each point represents average of 3 or 4 determinations \pm S.E. (from Ling and Kwan 1983)

normal frog muscle to match that brought about by the injury-induced depletion of the EWC, ATP in mouse tissues (Ling and Bohr, unpublished.)

In the set of experiments shown in the last figure of this communication and labeled Figure 65, we isolated many sartorius muscles of North American leopard frogs and incubated 4 muscles to a flask for between 3 to 4 days at 25°C. At the conclusion of the experiment, the muscles were taken out and blotted dry by a standardized procedure described earlier (Ling and Bohr, 1969) and weighed before and after drying. The final water contents of the muscles were plotted against the increasing NaCl concentration in a way similar to those in Figure 61 and 62.

Now, the normal water content of frog sartorius muscle is 80% (w/w.) The control muscles actually lost some water in the modified Ringer-GIB medium containing the higher NaCl concentrations. In contrast, the water content of the experimental muscle exposed to 3.26×10^{-6} M ouabain rose sharply in two steps to reach the highest value of 88.4%. The $W_{\text{final}} / W_{\text{initial}}$ corresponding to this water content is 1.53, which matches that seen in mouse kidney but lower than that seen in injured mouse brain.

However, since at the concentration of 3.26×10^{-6} M our (later) study showed some decrease of the ATP concentration in frog muscles, the question whether the observed marked swelling shown in Figure 65 is entirely due to the EDC, ouabain or partly due to the EDC, ouabain, and partly due to the decrease of the EWC, ATP, the answer awaits future studies.

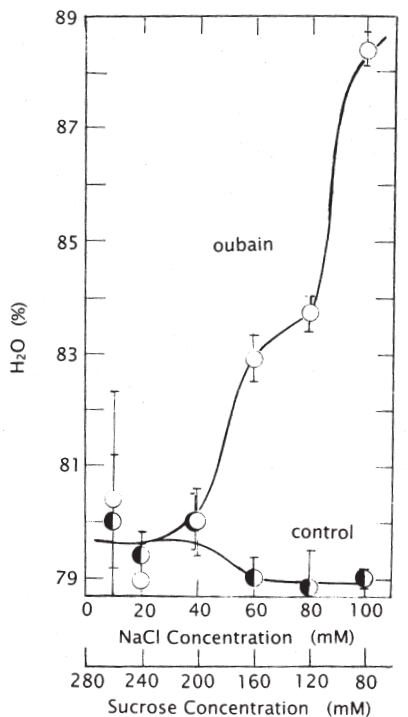


FIGURE 65. Na^+ -dependent swelling of frog sartorius muscles exposed to 3.26×10^{-6} M ouabain. Sterile incubation at 25° C for 72 hours. The composition of the modified Ringer-GIB media are the same as in a normal 731 medium except NaCl, which varied between 0 mM and 100 mM. Iso-osmotic sucrose is added to maintain isotonicity. (from Ling and Bohr, unpublished)



Gilbert Ling

Discussion

A. Uniformity of nano-protoplasm — as revealed by the ubiquitous two-number rule seen both *in vitro* and *in vivo*

It is hard to exaggerate the importance of Lyster's highly accurate data on oxygen binding cited here in Figure 17. With anything less precise, it would not be possible to visualize as we can do now, just how well does the AI theory of nano-protoplasm work. As such, the binding of oxygen over the entire (wide) range of oxygen tension is described to perfection by just *two numbers*: a K_o^{oo} of 5.88×10^{-6} M and a $(-\gamma/2)$ of 0.67 kcal/mole.

Moreover, the whole set of oxygen-binding data came from nothing beyond a mix of *pure* hemoglobin, *pure* water and *pure* salt. As such, it meets the exact definition of an *ultra simple model* of nano-protoplasm in its “active living state” — as diagrammatically illustrated in the left-side picture of Figure 5.

We could not access first hand Lyster's Ph.D. thesis. Nor did Rossi-Fanelli *et al.*, from whose review we obtained Lyster's data, give any information on the hemoglobin or salt concentration used in the data we cited. However, for a comparable set of data on horse hemoglobin, the hemoglobin concentration used was 4.6% and the salt used was given as 0.7 M phosphate. Table 3 shows that a $(-\gamma/2)$ of 0.67 kcal/mole is equivalent to a Hill coefficient of 3.1. Based on this n-value and Enoki and Tyuma's data shown in Figure 18, we come to the conclusion that the salt concentration in Lyster's data we cited must be quite high. In a 36% bovine hemoglobin solution, all the water is weakly but uniformly polarized-oriented (See Figure 31.) Regardless of what was the exact concentration of hemoglobin Lyster used, what he studied qualified as an ultra-simple model of nano-protoplasm in the active living state (as shown in the left-hand side diagram of Figure 5.)

Next, we go to Figure 28. In appearance, this figure resembles Figure 17 — but instead of (oxygen) binding on a single protein, it describes (K^+ and Na^+) adsorption in intact living muscle cells. In these cells, an estimated 67% to 80% of the K^+ / Na^+ - adsorbing β -, and γ -carboxyl groups belong to one protein, myosin; 15% to 30% belong to a set of

several I-band proteins and 3% to 5% belong to a second set of Z-line proteins (Ling and Ochsenfeld 1991, p.150.) Needless to add that each of these proteins occupies a different locations in a given cell. And, thousands of these cells together produced each data point shown in the figure.

Notwithstanding, all these β -, and γ -carboxyl groups from a gamut of different host-proteins found in different locations in different cells behave as if they were one single entity. And, the entire range of adsorption is also neatly described by two numbers, a $K_{\text{Na} \rightarrow K}^{\text{oo}}$ of 100 and a $(-\gamma/2)$ of 0.62 kcal/mole.

Furthermore, this two-number rule is not limited to K^+ / Na^+ adsorption in frog muscle cells. It extends to the K^+ / Na^+ adsorption in all the other types of living cells studied thus far: the canine carotid artery, the guinea-pig *taenia coli* and the human lymphocytes. With no exception, all follow the two-number rule. But even this is only the beginning.

Nor is this two number rule limited to selective *ionic accumulation* in bulk-phase cytoplasm. It extends to *selective ionic permeability* (Ling 1986a) as well as *cellular resting potential*. Once more, each phenomenon is quantitatively described by a set of two numbers, $K_{\text{Na} \rightarrow K}^{\text{oo}}$ and $(-\gamma/2)$. In fact, the two numbers describing respectively the resting potentials of the normal K^+ -loaded frog sartorius muscle and the resting potential of the artificially-induced Na^+ -loaded rat soleus muscle are the same two numbers.

In summary, pairs of closely similar $K_{j \rightarrow i}^{\text{oo}}$ and $(-\gamma/2)$ numbers can describe the relevant quantitative data on a variety of different cell physiological phenomena. Together, they affirm the AI theory of nano-protoplasm, i.e., in the normal physiological environment in which a living cell finds itself, only *one* auto-cooperative state prevails for all the nano-protoplasm units present. And, that auto-cooperative state corresponds to the resting living state as illustrated by the right-hand side figure of Figure 5.

For the same reason, one sees why Equation 12 on p. 163 and Equation 17 on p. 181, each invoking a multitude of different types of adsorption sites, were included only to be excluded. In their place, we are forced to choose the far simpler Equation 13 on p. 163 and Equation 18 on p. 182, each invoking only *a single type of adsorption sites*. This too is of great importance because it too supports the concept of a pervasive nano-protoplasm — found in all places and serving all physiological functions.

That said, we recall that in theory nano-protoplasm does not always stay in one state. It can also assume an alternative state in response to the sustained or transient command of a controlling agent, a cardinal adsorbent.

B. All-or-none control of nano-protoplasm by cardinal adsorbents *in vitro* and *in vivo*

To demonstrate how the (principal) cardinal adsorbent, ATP and its counterparts, 2,3-DPG or IHP work, we had the gift of yet another set of highly accurate data — this time from Benesch and Benesch of the United States. They too studied the *same* ultra-simple model of nano-protoplasm that Lyster studied: a mix of *pure* hemoglobin, *pure* water and *pure* salt. Only they studied it in the presence of varying concentrations of IHP, from zero to 4.5×10^{-4} M.

Once more each full set of data over a broad range of oxygen tension is quantitatively described by a set of two numbers, $K_{j \rightarrow i}^{\text{oo}}$ and $(-\gamma/2)$ as shown in Figure 25. In terms of the AI theory of nano-protoplasm, the two sets of parameters define the ultra-simple model of nano-protoplasm. It exists in its resting living state with IHP, or 2,3-DPG or ATP adsorbed on its cardinal site; it exists in its active living state with IHP, or 2,3-DPG or ATP off its cardinal site.

Of course, ATP is far better known for its ability to sustain selective K^+ adsorption in living cells — as part of the resting living state — by keeping the β -, and γ -carboxyl groups at a low c-value (and the backbone carbonyl groups at a low c-value analogue status.) (See Figures 32 and also Ling 2005.) Figure 33 shows that the c-value rise of the β -, and γ -carboxyl groups following a depletion of (the EWC,) ATP, did not lead to a displacement of adsorbed K^+ by (adsorbed) Na^+ . Rather, the β -, and γ -carboxyl groups with their own specific elevated c-value preferred to form salt-linkages with fixed cations.

(1) The role of different categories of auxillary cardinal adsorbents in the control of all-or-none transitions of nano-protoplasm

Figure 5 diagrammatically illustrates the nano-protoplasm with its ATP-binding cardinal site. In addition, it also displays another cardinal site occupied by an entity represented by the letter **Z**. As a symbol for what we call *auxiliary cardinal adsorbents*, **Z** may stand for a physiological active cardinal adsorbent like Ca^{++} , a hormone like insulin, a drug like ouabain or just a simple proton, H^+ (See below.)

In greater detail, I have shown in Figure 40, how insulin can cause the “creation” of D-glucose adsorbing sites in frog muscle cells. And, how lowering the Ca^{++} concentration has a similar impact on K^+ adsorption in canine carotid arteries as ATP depletion. But the most extensively studied auxillary cardinal adsorbent is the cardiac drug, ouabain.

At the pharmacologically low concentration ($3.26 \times 10^{-7} M$), ouabain does not alter the ATP concentrations of the frog muscle. Thus, whatever effect ouabain produces on this tissue, it does so on top of the action of a normal amount of (adsorbed) ATP. That said, I must point out that ouabain acts as a strong electron-donating cardinal adsorbent or EDC — a fact made persuasive by the altered distribution pattern of five alkali-metal ions in response to a minute amount of this drug (Figures 37 and Figure 38.)

On the other hand, Figure 34 and Figure 35 show that in an environment containing only two alkali-metal ions, K^+ and Na^+ , (EWC) ATP depletion causes the loss of adsorbed K^+ period. In contrast, ouabain (on top of normal amount of adsorbed ATP) causes a one-on-one displacement of all the adsorbed K^+ by adsorbed Na^+ . A different set of the same two numbers ($K_{Na \rightarrow K}^{oo}$ and $-\gamma/2$) emerged in consequence of interaction with the cardinal adsorbent and, with that, an all-or-none transition of state in bulk-phase ion adsorption follows.

A parallel effect is also produced by ouabain on how a second mono-valent action affects the rate of Cs^+ permeation into frog ovarain eggs (Figure 49), and in reducing the magnitude of the resting potential of frog sartorius muscle as well as that of rat soleus muscle as shown in Figure 56 and in bringing about the Na^+ -dependent swelling of frog sartorius muscles as shown in Figure 65.

Taken together, these data indicate that the auxillary cardinal adsorbent —no less than the principle cardinal adsorbent (ATP) — is capable of bringing about an across-the-board uniform change in the vast number of nano-protoplasm units throughout a living cell.

(2) The unique living chemical structure that mediates long-distance information and energy transfer, hence the pervasive coherence that distinguishes life

By now, it is obvious that the *nearest* neighbor interaction energy or ($-\gamma/2$) in cell and sub-cellular physiology is a parameter of central importance. However, it is, as a rule, not near.

A simple calculation shows how far apart are the average nearest-neighboring pair of β -, and γ -carboxyl groups in say, a hemoglobin molecule. The total number of amino-acid residue in a bovine hemoglobin molecule is 572. The total number of β -, and γ -carboxyl groups in the same hemoglobin molecule is 64. Thus, on the average, each β -, and γ -carboxyl groups is separated from its two nearest neighboring β -, or γ -carboxyl groups by $572/64$ or 8.9 peptide linkages. In truth, the number of peptide linkages between any nearest neighboring pair of β -, and γ -carboxyl groups is as a rule quite different from the average and highly variable. Notwithstanding, all the data we have collected and shown above can be described by more or less the same ($-\gamma/2$) value of around 0.67 kcal/mole equivalent to a Hill coefficient of about 3.1. But how can this uniformity comes from the great diversity?

A moment of thought would convince the reader that this can happen if the system works like a falling-domino chain. No matter how many dominoes separate the starter domino and the terminal domino, the energy involved in knocking down the next one is always the same. The AI cascade mechanism can do exactly the same like a falling domino chain. Only the falling domino chain goes only one way. The AI cascade mechanism, on the other hand, can go both ways — but only because it is aided by a cardinal adsorbent, like ATP. Speedily removable by the enzyme , ATPase, it is just as promptly regenerated from the store of creatine phosphate and *via* other energy metabolism of the living cell.

Thus far, we have reviewed results of studies on the control by cardinal adsorbents on two kinds of functional groups on short side chains: heme and β -, or γ -carboxyl groups as the eyes and hands on the polypeptide chains. In the next section, we turn out attention to the most abundant and closest functional groups, the backbone NHCO groups.

(3) Control of dynamic water structure by cardinal adsorbent

So far, I have had the pleasure of describing to you two highly accurate studies of the same ultra-simple models of nano-protoplasm in the form of a mix of *pure* hemoglobin, *pure* water and *pure* salt. One came from Lyster of England; the other from Benesch and Benesch of the US. Now I offer a third study of the *same* ultra-simple model of nano-protoplasm of *pure* hemoglobin, *pure* water and *pure* salt. Only this study came from my own laboratory. However, as of this day, this work, though completed, is still not published. For this reason, I can only offer a very short bird's-eye view.

We put the mixture of *pure* hemoglobin, *pure* water and *pure* salt (NaCl) into dialysis sacs and sort them out into two groups. In the control group, the sacs were equilibrated in a simple 10 mM NaCl solution. In the experimental group we added also an electron-withdrawing cardinal adsorbent (EWC), the proton, H⁺. When diffusion equilibrium was reached, we analyzed the (labeled) Na⁺ concentration inside and outside the dialysis sacs. What we found could not have been more gratifying. For it showed that if the H⁺ added is of the right amount, the equilibrium distribution coefficient or q-value of NaCl in the water within the sacs is not unity. Instead, it is only 0.2 and thus the same as the q-value of NaCl in the water of healthy mature human red blood cells.

Or put in a different language, each time a proton is taken up by another β -, or γ -carboxyl group of the hemoglobin molecule, 1000 or more water molecules in the surrounding medium are converted to a different kind of water molecule that apparently has lost its normal solubility for Na⁺ (as Cl⁻.)

More rigorously, each time a proton is adsorbed on another β -, or γ -carboxyl group of the hemoglobin molecule, the c-value analogue of many backbone carbonyl groups would take on a lower value. And according to the relationship shown between c-value analogue and the preferred partners illustrated in Figure 11 on p. 139, all the water molecules in the sac are changed from near-normal liquid state with unity q-value for Na^+ (as Cl^-) to the state of polarized-oriented multilayer with a q-value for Na^+ (as Cl^-) numerically close to, if not equal to that seen in mature mammalian red blood cells.

Of course, a low q-value of around 0.2 for Na^+ (as Cl^-) is not found only in mature mammalian red blood cells. It is a virtually universal physiological trait shared by virtually all living cells. Thus, this ultra-simple model demonstration provides yet another set of decisive evidence for the AI model of nano-protoplasm.

(3.1) Lasting control of intensity of water-to-water interaction controls the diversity of permeability barriers.

The demonstrated bulk-phase limited diffusion of water molecules in a barnacle muscle cell (and frog ovarian egg) tells us something far-removed from conventional beliefs. It shows that the percentage of space occupied by water in the cell surface is the same as that in the surface of any imaginary concentric cylinder drawn inside the muscle cell. Since the overall percentage of water in all living cells is as a rule very high, the overall permeability of the muscle fiber must be quite high — a deduction clearly affirmed by the data given in Figure 46 from frog muscle cells. This is highly reasonable because muscle cells need D-glucose, free amino acids and a host of other essential chemicals to function properly.

However, we have also shown in Figure 47 how the epithelial cells making up the outer covering or skin of the frog have an altogether different rate of solute permeation. In the AI Hypothesis, it is the intensity of polarization-orientation of the polarized-oriented water in the nano-protoplasm. that plays the decisive role of high or low permeability.

Yet, because of the exponential relation between \mathcal{U}_{vp} and q (Equation 4), all one needs is a minor adjustment in the numerical value of \mathcal{U}_{vp} that would solve the problem of the needed diversity illustrated by the frog skin. This then winds up our summary of the experimental verification of the new concept of nano-protoplasm, at once similar and dissimilar to meet the shared need and unshared unusual demands.

(3.2) Transient control of the intensity of water-to-water interaction creates (a facet of) the action potential

Table 6 from Villegas *et al* demonstrates how during the height of an action potential in a squid axon, the nerve fiber surface undergoes a reversible transient change so that permeability to erythritol, mannitol and sucrose all undergo a sharp increase — *pari passu* with the influx of Na^+ — as diagrammatically illustrated in Figure 59 in consequence of the detachment of the cardinal adsorbent, Ca^{++} . The difference that brings about this depolarization and disorientation of cell surface water and the depolarization and disorientation of the water in the dialysis sacs in our third ultra-simple model is that in one, the key cardinal adsorbent is a divalent cation (Ca^{++}) while in the other it is a monovalent cation (H^+).

I thank Dr. Raymond Damadian and his Fonar Corporation for their continued support, Dr. Ludwig Edelmann for his gifts of the EM picture of two red blood cells reproduced here as Figure 1 and for a copy of the original German version of Theodor Schwann's "*Übereinstimmung....*" and Margaret Ochsenfeld for her painstaking and skilled work on improving this article.

Endnote 1.

Many years ago, I learnt form a source that I can no longer remember that the membrane theory was introduced by Wilhelm Pfeffer (1845–1920.) I did not question the validity of this belief until many years later, when I finally laid my hand on a copy of the English translation of Pfeffer's book, "Osmotische Untersuchungen." (Pfeffer 1877, English transl. 1985.) A careful reading of this book led me to the realization that Pfeffer did not mention once the term, Membrane Theory in the first edition of the book or (naturally) in the unaltered second edition as well. Many more years were to pass before I dug deeper into the history, only to find out that the Membrane Theory did not have an original author. It was a combination of (largely mistaken) ideas that Theodor Schwann introduced in the monograph in which he presented his Cell Theory (for details, see Ling 2007.) Unfortuantely, in the years past, I have been unknowingly guilty of passing on the wrong information as true on more than one occasion including my books (Ling 1992, Ling 2001.) For this error, I give my apology with the hope that my detailed account of the full history of the membrane (pump) theory would help to set things right in time to come.

Endnote 2.

$$\psi = \text{constant} + \{RT/F\} \ln \{\Omega / [K^+]_{\text{ex}}\} + \{RT/F\} \{(u-v)/(u+v)\} \ln \{[Na^+]_{\text{in}} / [Na^+]_{\text{ex}}\}. \quad (35)$$

Now, there are three terms on the right. Let us begin with the second term on the right. This is the term that describes the resting potential component of the action potential (Equation 26.) The auto-cooperative transition of this component of the action potential also resembles the ouabain-induced all-or-none transition of the whole cell from the K⁺ state to the Na⁺ state (See Figure 34 on p. 174.)

Next, we turn to the last term of the right-hand side of Equation 35. Here, u and v represent the mobilities of the cation and anion respectively.

The prevailing negatively-charged sites at the cell surface strongly inhibits anion entry. As a result, v → 0. And, (u-v)/(u+v) → 1. As a result, Equation 35 simplifies to:

$$\psi = \text{constant} + \{RT/F\} \ln \{\Omega / [K^+]_{\text{ex}}\} + \{RT/F\} \ln \{[Na^+]_{\text{in}} / [Na^+]_{\text{ex}}\}. \quad (36)$$

Note that the second term now assumes the same shape as Hodgkin, Huxley and Katz's equation describing what they call the (standing) sodium potential. In the AI model, there is not a standing sodium potential; a sodium potential arises only during the action potential. Since in the AI model, [Na⁺]_{in} represents the equilibrium (free) Na⁺ concentration

in the cell surface water, it is equal to $q_{Na} [Na^+]_{ex}$. q_{Na} is the true equilibrium distribution coefficient of Na^+ in the cell surface water. Substituting and canceling, one obtains

$$\psi = \text{constant} + \{RT/F\} \ln \{\Omega / [K^+]_{ex}\} + \{RT/F\} \ln q_{Na}. \quad (37)$$

Since q_{Na} is a fractional number, the second term is a negative number, accounting for the momentary reversal of polarity and its cause, the "overshoot."

$$\psi = \text{constant} + \{RT/F\} [\ln \{\Omega / [K^+]_{ex}\} + \ln q_{Na}]. \quad (31)$$

References

- Abetsedarskaya, L.A., Miftakhutdinova, F.G. and Fedotov, V.D. (1968) *Biofizika* 13: 630.
- Adair, G.S. (1925) *J. Biol. Chem.* 63: 517.
- Adrian, E.D. and Gelfan, S. (1933) *J. Physiol.* (London) 78: 271.
- Akaike, N. (1975) *Jap. J. Physiol.* 245: 499.
- Ambrose, E.J. and Elliott, A. (1951) *Proc. Roy. Soc. A* 20: 47.
- Andreoli, T.C., Tieffenberg, M. and Tosteson, D.C. (1967) *J. Gen. Physiol.* 50: 2527.
- Atkinson, D.E., Hathaway, J.A. and Smith, E.C. (1965) *J. Biol. Chem.* 40: 2682.
- Baker, J.R. (1949) The Cell Theory: A Restatement, History, and Critique. Part II, *Quart. J. Microsc. Sci.* 90: 87.
- Bamford, C.H., Elliott, A. and Hanby, W.F. (1956) *Synthetic Polypeptides: Preparation, Structure and Properties*, Academic Press, New York.
- Barcroft, J. and Robert, F.L. (1939) *J. Biol. Chem.* 129: 315.
- Benesch, R. and Benesch, R.L. (1967) *Biochem. Biophys. Res. Commun.* 26: 112.
- Benesch, R. and Benesch, R.L. (1969) *Nature* 221: 618.
- Bernstein, J. (1912) *Elektrobiologie*, F. Vieweg und Sohn, Braunschweig.
- Best, C.H. and Taylor, N.B. (1945) *The Physiological Basis of Medical Practice*, 4th ed., William & Wilkins, Baltimore, p. 7, Col. 2, line 19.
- Bohr, C., Hasselbach, K. and Krogh, A. (1904) *Skand. Arch. Physiol.* 16: 402.
- Branch, G.E.K. and Calvin, M. (1941) *The Theory of Organic Chemistry, an Advanced Course*, Prentice-Hall, Englewood Cliffs, New Jersey.
- Boltzmann, L. <http://www.history.mes.St.andrews.ac.uk/Biographies/Boltzmann.html>
- Bungenberg de Jong, H.G. (1949) *Colloid Science*, (ed. H.R. Kruyt.) Vol. II, Chapter XI pp. 433-480. Elsevier Publ. Co., Amsterdam, New York.
- Caillé, J.P., Hinke, J.A.M. (1974) *Canad. J. Physiol. Pharmacol.* 52: 814.
- Cannon, C.O. (1955) *Mikrochim Acta* 2-3: 555.
- Chandler, W.K. and Meves, H. (1965) *J. Physiol.* 180: 788.
- Chanutin, A. and Curnish, R.R. (1967) *Arch. Biochem. Biophys.* 121: 96.
- Chiang, M. and Tai, T. (1963) *Scientia sinica* 12: 785.
- Chou, P.Y. and Fasman, G.D. (1978) *Adv. Enzymol.* 47:45.
- Cohn, F. (1847) *Nova Acta Akademiae Cesareae Leopoldino-Carolinae* [of Halle] 22: 605. For partial English transl., see Huxley T.H. (1872) *The Contemporary Review* 19: 34.
- Cole, K.S. (1949) *Arch. Sci. Physiol.* 3: 253.
- Conant, J.B. and McGrew, R.V. (1930) *J. Biol. Chem.* 85: 421.
- Cope, F. (1967) *Bull. Math. Biophys.* 29: 583.
- Crank, J. (1956) *The Mathematics of Diffusion*, Oxford Univ. Press. Oxford, England, p. 43, Equation (4.7.)
- Crick, F. (1981) *Life Itself: Its Origin and Nature*, Simon and Schuster, New York.

- Dayhoff, M.O. (1972) *Atlas of Protein Sequence and Structure*, National Biomedical Research Fdn., Washington, D.C.
- Dewar, M.J.S. (1949) *The Electronic Theory of Organic Chemistry*, Oxford Univ. Press, Oxford.
- Drabkin, D.L. (1949) *Arch. Biochem. Biophys.* 21: 224.
- Dubois, Reymond, E. (1849) *Untersuchungen über Thierische Elektricität*, Reimer.
- Dujardin, F. (1835) *Annales des science naturelles: partie zoologique*, 2nd Sér., 4: 364.
- Durant, W. (1926 to at least 1961) *The Story of Philosophy*, Pocket Books, a Division of Simon & Schuster, New York.
- Dutrochet, H. (1837) *Mémoire pour servir a l'histoire anatomiques et physiologiques des végétaux et des animaux*, BailliPre, Paris.
- Edelmann, L. (1973) *Ann. NY Acad. Sci.* 204: 534.
- Edelmann, L. (1986) Two opposing theories of the cell: experimental testing by cryomethods and electron microscopy. *Science of Biological Specimen Preparation*, pp. 33-42, SEM Inc. AMP O'Hare (Chicago), IL, 60666-0507, USA.
- Edelmann, L. and Baldauf, J.H. (1971) In: *Proc. First Europ. Biophys. Confer., Baden*, (Brodan, E., Locker, A. and Springer-Lederer, eds.) 3: 243.
- Edsall, J.T. and Wyman, J. (1958) *Biophysical Chemistry*, Vol. 1, p.534 (Table VIII). Encyclopedia Britanica <<http://www.britannica.com/eb/article-37477/cell>>
- Enoki, Y. and Tyuma, I. (1964) *Jap. J. Physiol.* 14: 280.
- Elliott, A. (1953) *Proc. Roy. Soc. A* 221: 104.
- Epstein, E. and Hagen, C.E. (1952) *Plant Physiol.* 27: 457.
- Finch, E.D., Harmon, J. F. and Muller, B.H. (1971) *Arch. Biochem. Biophys.* 147: 299.
- Fischer, E. (1906) *Untersuungen über Amino-Säuren, Polypeptide und Proteine*, Springer, Berlin.
- Fischer, E. (1908) *Ber.* 39: 530.
- Fischer, M.H. (1909) *Trans. College Physicians Philadelphia* 31:457.
- Fischer, M. H. and Suer, W.J. (1935) *Arch. Pathol.* 20: 683.
- Fowler, R.H. and Guggenheim, E.A. (1939) *Statistical Thermodynamics*, Cambridge Univ. Press, Cambridge.
- Gárdos, G. (1954) *Acta Physiologic Academie Scientiarum Hungaricae* 6: 191.
- Garnier, J., Orgathorpe, D.J. and Robson, B. (1978) *J. Mol. Biol.* 120: 97.
- Gerlach, B. (1931) *Ann. Physik* 10: 437.
- Gibbs, W. (1901) *Elementary Principles in Statistical Mechanics: the Rational Foundation of Thermodynamics*, Dover, New York.
- Giguére, P.A. and Harvey, K.B. (1956) *Canad. J. Chemistry* 34: 798.
- Glasstone, S. (1946) *Textbook of Physiological Chemistry*, D. van Nostrand, New York, p. 261, Equation 45.
- Gordon, H.T. and Welsh, J.H. (1948) *J. Cell. Comp. Physiol.* 31: 395.
- Gortner, R.A. (1938) *Outline of Biochemistry*, 2nd ed., John Wiley and Sons, New York.
- Gulati, J. (1973) *Ann. NY Acad. Sci.* 204: 337.
- Gulati, J., Ochsenfeld, M.M. and Ling, G.N. (1971) *Biophys. J.* 11: 973.
- Gurney, R.W. (1949) *Introduction to Statistical Mechanics*, McGraw-Hill Book Co., New York.
- Hall, T.S. (1951) *A Source Book in Animal Biology*, McGraw-Hill, New York.
- Hall, T.S. (1969) *Ideas of Life and Matter; Studies in the History of General Physiology 600 B.C. to 1900 A.D.*, Vol. 2, The Univ. of Chicago Press, Chicago.
- Hazlewood, C.F., Singer, D.B., and Beall, P.T. (1979) *Physiol. Chem. & Physics* 11: 181.
- Harris, H. (1999) *The Birth of the Cell*, Yale Univ. Press, New Haven, London.
- Hartline, H.K. (1934) *J. Cell. Comp. Physiol.* 5: 229.
- Hermans, P.H. (1954) *Introduction to Theoretical Organic Chemistry* (edited and revised by R.E. Reeves), Elsevier, Amsterdam, New York.
- Hill, A.V. (1910) *J. Physiol. (London)* 40: iv.
- Hill, A.V. (1930) *Proc. Roy. Soc. London, Ser. B.* 106: 477.
- Hill, A.V. and Kupalov, P.S. (1930) *Proc. Roy. Soc. London, Ser. B.* 106: 445.

- Hille, B. (1975) In *Membranes: A Series of Advances*, 3: 255.
- Hills, G.J. (1961) In: *Reference Electrodes*. (D.J.G. Ives and G.J. Janz, eds.), Academic Press, New York, pp. 411–432.
- Hinke, J.A. M. (1970) *J. Gen. Physiol.* 56: 521.
- Hodgkin, A.L. (1958) *Proc. Roy. Soc. London, Ser.B.* 148:1.
- Hodgkin, A.L. (1971) *The Conduction of the Nervous Impulse*, Liverpool Univ. Press, Liverpool.
- Hodgkin, A.L. and Katz, B. (1949) *J. Physiol. (London)* 108: 37.
- Hodgkin, A.L. and Huxley, A.F.(1952 a,b,c) *J. Physiol. (London)* 116: 449, 473, 497.
- Hodgkin, A.L. and Huxley, A.F.(1952) *J. Physiol. (London)* 117: 500.
- Hodgkin, A.L., Huxley, A.F.and Katz, B. (1952) *J. Physiol. (London)* 116: 424.
- Hoppe-Seyler, F. (1867) *Medizinisch-Chemische Untersuchungen*, Vol. 2, p. 185.
- Horgan, J. (1996) *The End of Science: Facing the Limits of Knowledge in the Twilight of the Scientific Age*, Addison-Wesley Publ. Co., Reading, Mass.
- Hori, T. (1956) *Low Temperature Science* A15: 34 (Teion Kagaku, Butsuri Hen) English translation: No 62, US Army Snow, Ice and Permafrost Res. Establishment, Corps of Engineers, Wilmette, IL, USA.
- Horovitz, K. (1923) *Z. Physik* 15: 369.
- Hunt, J.A. and Ingram, V.M. (1958) *Biochim. et Biophys. Acta* 28: 546.
- Hunt, J.A. and Ingram, V.M. (1959) *Nature* 184: 640.
- Huxley, T. (1853) *Brit. and Foreign Med. Chron. Rev.* 12: 285.
- Huxley, T.H. (1869) *Fortnightly Review* 5: 129.
- Inoue, I., Ishima, Y. , Horie, H., and Takenaka, T. (1971) *Proc. Japan Acad.* 47: 549.
- Inoue, I., Ishida, N. and Kobatake, Y. (1973) *Bioch. Biophys. Acta* 330: 27.
- Jain, M.K. (1972) *The Bimolecular Lipid Membrane*, van Nostrand-Rheinhold Co., New York.
- Jones, A.W. (1973) *Ann. NY Acad. Sci.* 204: 379.
- Kamiya, N. and Kuroda, K. (1956) *Bot. Mag.(Tokyo)* 69: 544.
- Kanada, Y. (2002) Information was given in the now defunct http://seattlepi.nmsource.com/98912_pi07.shtml Advise search "Yasamasa Kanade" on Google for latest news.
- Karreman, G. (1980) *Cooperative Phenomenon in Biology*, Pergamon Press, New York.
- Katsuki, Y. (ed.) (1960) *Electrical Activities of Single Cells*, Igaku Shoin Ltd., Tokyo, Japan.
- Koshland, D.E., Nemethy, G. and Filmer, D. (1966) *Biochemistry* 5: 365.
- Katz, J.R. (1919) *Kolloidchem. Beih.* 9: 1.
- Lewis, G.N. (1923) *Valence and the Structure of Atoms and Molecules*, Chemical Catalog. Co., New York.
- Lewis, M.S. and Saroff, H.A. (1957) *J. Amer. Chem. Soc.* 79: 2112.
- Ling, G.N. (1952) The role of phosphate in the maintenance of the resting potential and selective ionic accumulation in frog muscle cells. In *Phosphorus Metabolism* (W.D. McElroy and B. Glass, eds.), Vol. II , p. 748, Johns Hopkins University Press, Baltimore, Maryland.
- Ling, G.N. (1953) Ionic permeability according to the fixed-charge hypothesis. *Proc. 19th Internat. Physiol. Congress*, Montreal, Canada, p. 566.
- Ling, G.N. (1955) New hypothesis for the mechanism of cellular resting potential. *Fed. Proc.* 14: 93.
- Ling, G.N. (1959) On the mechanisms of cell potential. *Fed. Proc.* 18: 371.
- Ling, G.N. (1960) The interpretation of selective ionic permeability and cellular potentials in terms of the fixed charge-induction hypothesis. *J. Gen. Physiol.* 43: 149.
- Ling, G.N. (1962) *A Physical Theory of the Living State: the Association-Induction Hypothesis*, Blaisdell Publishing Co., Waltham, MA.
- Ling, G.N. (1964) Association-induction hypothesis. *Texas Report on Biol. & Med.* 22: 244.
- Ling, G.N. (1964a) The role of inductive effect in cooperative phenomena of proteins. *Biopolymers Symposia* 1: 91.
- Ling, G.N. (1965) The physical state of water in living cell and model systems. *Ann. NY Acad. Sci.* 125:401.
- Ling, G.N. (1965a) Physiology and anatomy of the cell membrane: the physical state of water in the living cell. *Fed. Proc. (Symposium)* 24: S103.

- Ling, G.N. (1965b) The membrane theory and other views for solute permeability, distribution and transport in living cells. *Persp. Biol. Med.* 9: 87.
- Ling, G.N. (1966) All-or-nothing adsorption by living cells and model protein-water systems. *Fed. Proc. (Symposium)* 25: 958.
- Ling, G.N. (1967) In *Glass Electrode for Hydrogen and Other Cations* (G. Eisenman, ed.), Marcel-Dekker, Inc., New York, pp. 284-292.
- Ling, G.N. (1969) A new model of the living cell: a summary of the theory and recent experimental evidence in its support. *Intern. Rev. Cytol.* 26: 1.
- Ling, G.N. (1970) Diphosphoglycerate and inosine hexaphosphate control of oxygen binding by hemoglobin: a theoretical interpretation of experimental data. *Proc. Natl. Acad. Sci.* 67: 296.
- Ling, G.N. (1972) Hydration of Macromolecules, in *Water and Aqueous Solutions: Structure Thermodynamics and Transport Properties* (A.R. Horne, ed), Wiley -Interscience, New York.
- Ling, G.N. (1973) What component of the living cell is responsible for its semipermeable properties? Polarized water or lipids? *Biophys. J.* 13: 807.
- Ling, G.N. (1977) The physical state of water and ions in living cells and a new theory of the energization of biological work performance by ATP. *Mol. Cell Biochem* 15: 159.
- Ling, G.N. (1978) Experimental confirmation of a key prediction of the polarized multilayer theory of cell water from model studies. *Sixth Intern. Biophys. Congress (Tokyo) Japan*. September 3-9, p. 389.
- Ling, G.N. (1979) The equations for cellular resting potentials according to the surface adsorption theory, a corollary of the association-induction hypothesis. *Physiol. Chem. Phys.* 11: 59. Also available via: http://www.physiologicalchemistryandphysics.com/pdf/PCP11-59_ling.pdf
- Ling, G.N. (1980-1981) Water and the living cell as seen from the viewpoint of a new paradigm. *Intern. Cell Biology* 1980-1981 (edited by H.G.Schweiger), p. 908.
- Ling, G.N. (1980a) The theory of allosteric control of cooperative adsorption and conformation changes: a molecular model for physiological activities according to the association-induction hypothesis. In *Cooperative Phenomena in Biology*, (G. Karreman, ed.) Pergamon Press, New York, pp. 39-69.
- Ling, G.N. (1981) Electrische potentielle lebender zellen. In: *Die Zelle: Struktur und Funktion*, 3rd ed. (Metzner, H., ed.) Wissenenschaftlich Verlagsgesellschaft mbh, Stuttgart, Germany, p. 356.
- Ling, G.N. (1981a) Oxidative phosphorylation and mitochondrial physiology: a critical review of the chemiosmotic theory, and reinterpretation on the basis of the association-induction hypothesis. *Physiol. Chem. Phys.* 13: 29. Also available via: http://www.physiologicalchemistryandphysics.com/pdf/PCP13-29_ling.pdf. Or, go to <www.gilbertling.com>, choose volume and article from drop-down list and click.
- Ling, G.N. (1982) The cellular resting and action potentials: interpretation based on the association-induction hypothesis. *Physiol. Chem. Physics* 14: 47. Also available via: <http://www.physiologicalchemistryandphysics.com/pdf/PCP14-47_ling.pdf>. Or, go to <www.gilbertling.com>, choose volume and article from drop-down list and click.
- Ling, G.N. (1983) The molecular mechanisms of cellular potentials. In: *Structure and Function in Excitable Cells* (Chang, D.C., Tasaki, I., Adelman, Jr., W.J. and Leuchtag, H.R., eds.) Plenum Publishing Corp., New York, p. 365.
- Ling, G.N. (1984) *In Search of the Physical Basis of Life*, Plenum Publishing Co., New York.
- Ling, G.N. (1985) *Water and Ions in Biological Systems* (eds: A Pullman, V. Vasilescu and L. Packer) Plenum Press, New York, p. 91.
- Ling, G.N. (1986) The role of inductive effect in the determination of protein structure. *Physiol. Chem. Phys. & Med. NMR* 18: 3. Also available via: <http://www.physiologicalchemistryandphysics.com/pdf/PCP18-3_ling.pdf>. Or, go to <www.gilbertling.com>, choose volume and article from drop-down list and click.
- Ling, G.N. (1986a) Cooperative interaction among surface β - and γ -carboxyl groups mediating the permeation of ions into frog muscle cells. *Physiol. Chem. Phys. & Med. NMR* 18: 125. Also available via: <http://www.physiologicalchemistryandphysics.com/pdf/PCP18-125_ling.pdf>

- 125_ling.pdf>. Or, go to <www.gilbertling.com>, choose volume and article from drop-down list and click.
- Ling, G.N. (1987) Studies on the physical state of water in living cells and model systems. VII. Exclusion of sugars and sugar alcohols from the water in sulfonate exchange resin: the “size rule”, *Physiol. Chem. Phys. & Med. NMR* 19: 193. Also available via: <http://www.physiologicalchemistryandphysics.com/pdf/PCP19-193_ling.pdf>. Or, go to <www.gilbertling.com>, choose volume and article from drop-down list and click.
- Ling, G.N. (1992) *A Revolution in the Physiology of the Living Cell*, Krieger Publishing Co., Malabar, FL
- Ling, G.N. (1993) A quantitative theory of solute distribution in cell water according to molecular size. *Physiol. Chem. Phys. & Med. NMR* 25:145. Also available via: <http://www.physiologicalchemistryandphysics.com/pdf/PCP25-145_ling.pdf>
- Ling, G.N. (1993a) Predictions of polarized multilayer theory of solute distribution confirmed from a study of the equilibrium distribution in frog muscle of twenty-one nonelectrolytes including five cryoprotectants. *Physiol. Chem. Phys. & Med. NMR* 25:177. Also available via: <http://www.physiologicalchemistryandphysics.com/pdf/PCP25-177_ling.pdf>, Or, go to <www.gilbertling.com>, choose volume and article from drop-down list and click.
- Ling, G.N. (1994) The new cell physiology. *Physiol. Chem. Phys. & Med. NMR* 26: 121. Also available via: http://www.physiologicalchemistryandphysics.com/pdf/PCP26-121_ling.pdf, Or, go to <www.gilbertling.com>, choose volume and article from drop-down list and click.
- Ling, G.N. (1997) <http://www.gilbertling.org>
- Ling, G.N. (1997a) Debunking the alleged resurrection of the sodium pump hypothesis. *Physiol. Chem. Phys. & Med. NMR* 29: 123. Also available via: <http://www.physiologicalchemistryandphysics.com/pdf/PCP29-2_ling.pdf>. Or, go to <www.gilbertling.com>, choose volume and article from drop-down list and click.
- Ling, G.N. (1998) <http://www.gilbertling.org>
- Ling, G.N. (2001) *Life at the Cell and Below-Cell Level: The Hidden History of a Fundamental Revolution in Biology*, Pacific Press, New York.
- Ling, G.N. (2003) A new theoretical foundation for the polarized-oriented multilayer theory of cell water and for inanimate systems demonstrating long-range dynamic structuring of water molecules. *Physiol. Chem. Phys. & Med. NMR* 35:91. Also available via: <http://www.physiologicalchemistryandphysics.com/pdf/PCP35-91_ling.pdf>. Or, go to <www.gilbertling.com>, choose volume and article from drop-down list and click.
- Ling, G.N. (2004) What determines the normal water content of a living cell? *Physiol. Chem. Phys. & Med. NMR* 36:1. Also available via: <http://www.physiologicalchemistryandphysics.com/pdf/PCP36-1_ling.pdf>. Or, go to <www.gilbertling.com>, choose volume and article from drop-down list and click.
- Ling, G.N. (2005) An updated and further developed theory and evidence for the close-contact one-on-one association of nearly all cell K⁺ with β-, and γ-carboxyl groups of intracellular proteins. *Physiol. Chem. Phys. & Med. NMR* 37:1. Also available via: <http://www.physiologicalchemistryandphysics.com/pdf/PCP37-1_ling.pdf>. Or, go to <www.gilbertling.com>, choose volume and article from drop-down list and click.
- Ling, G.N. (2005a) What befalls the proteins and water in a living cell when the cell dies? *Physiol. Chem. Phys. & Med. NMR* 37: 141. Also available via: <http://www.physiologicalchemistryandphysics.com/pdf/PCP37-141_ling.pdf>. Or, go to <www.gilbertling.com>, choose volume and article from drop-down list and click.
- Ling, G.N. (2006) Chapter 1, A Convergence of Experimental and Theoretical Breakthroughs Affirms the PM Theory of Dynamically Structured Cell Water at the Theory's 40th Birthday in: *Water and the Cell* (Pollack, G.H., Cameron, I. L. and Wheatley, D.N., eds.) Springer Verlag, Berlin, New York. Can also be reached by going to www.gilbertling.org and click listed title on first page of website.
- Ling, G.N. (2006a) In response to an open invitation for comments on AAAS Project 2061's Benchmark Books on Science. Part 1. Documentation of serious errors in cell biology.

- Physiol. Chem. Phys. & Med. NMR* 38:55. Also available at: <http://www.physiologicalchemistryandphysics.com/pdf/PCP38-55_ling.pdf>. Or, go to <www.gilbertling.com>, choose volume and article from drop-down list and click.
- Ling, G.N. (2006b) An ultra simple model of protoplasm to test the theory of its long-range coherence and control so far tested (and affirmed) mostly on intact cell(s). *Physiol. Chem. Phys. & Med. NMR* 38:105. Also available at: <www.physiologicalchemistryandphysics.com/pdf/PCP38-105_ling.pdf>. Or, go to <www.gilbertling.com>, choose volume and article from drop-down list and click.
- Ling, G.N. (2007) History of the membrane (pump) theory of the living cell from its beginning in mid-19th century to its disproof 45 years ago — though still taught worldwide today as established truth. *Physiol. Chem. Phys. & Med. NMR* 39:1. Also available at: <www.physiologicalchemistryandphysics.com/pdf/PCP39-1_ling.pdf>. Or, go to <www.gilbertling.com>, choose volume and article from drop-down list and click.
- Ling, G.N. and Bohr, G. (1969) Studies on ionic distribution in living cells. I. Long-term preservation of isolated frog muscles. *Physiol. Chem. Phys.* 1: 591. Also available via: http://www.physiologicalchemistryandphysics.com/pdf/PCP1-591_ling_bohr.pdf. Or, go to <www.gilbertling.com>, choose volume and article from drop-down list and click.
- Ling, G.N. and Bohr, G. (1970) Studies on ionic distribution in living cells. II. Cooperative interaction between intracellular K⁺ and Na⁺ ions. *Biophys. J.* 10: 519.
- Ling, G.N. and Bohr, G. (1971) Studies on ionic distribution in living cells. III. Cooperative control of electrolyte accumulation by ouabain in frog muscle. *Physiol. Chem. Phys.* 3: 431. Also available via: http://www.physiologicalchemistryandphysics.com/pdf/PCP3-431_ling_bohr.pdf. Or, go to <www.gilbertling.com>, choose volume and article from drop-down list and click.
- Ling, G.N. and Fu, Y. (1988) An electronic mechanism in the action of drugs, ATP, transmitters and other cardinal adsorbents. II. Effect of ouabain on the relative affinities for Li⁺, Na⁺, K⁺ and Rb⁺ of surface anionic sites that mediate the entry of Cs⁺ into frog ovarian eggs. *Physiol. Chem. Phys. & Med. NMR* 20: 61. Also available via: http://www.physiologicalchemistryandphysics.com/pdf/PCP20-61_ling_fu.pdf. Or, go to <www.gilbertling.com>, choose volume and article from drop-down list and click.
- Ling, G.N. and Gerard, R.W. (1949) The normal membrane potential of frog sartorius fibers. *J. Cell. Comp. Physiol.* 34: 383.
- Ling, G.N. and Gerard, R.W. (1949a) The influence of stretch on the membrane potential of the striated muscle fiber. *J. Cell. Comp. Physiol.* 34: 397.
- Ling, G.N. and Gerard, R.W. (1949b) The membrane potential and metabolism of muscle fibers. *J. Cell. Comp. Physiol.* 34: 413.
- Ling, G.N. and Hu, W.X. (1987) Studies on the physical state of water in living cells and model systems. VIII. Water vapor sorption on proteins and oxygen-containing polymers at physiological vapor pressure: presenting a new method for the study of vapor pressure at close to and including saturation. *Physiol. Chem. Phys. & Med. NMR* 19: 251. Also available via: <http://www.physiologicalchemistryandphysics.com/pdf/PCP19-251_ling_hu.pdf>. Or, go to <www.gilbertling.com>, choose volume and article from drop-down list and click.
- Ling, G.N. and Kwon, Y. (1983) Cold injury-induced swelling of brain and other tissues: its molecular mechanism. *Physiol. Chem. Phys. & Med. NMR* 15: 239. Also available via: http://www.physiologicalchemistryandphysics.com/pdf/PCP15-239_ling_kwon.pdf. Or, go to <www.gilbertling.com>, choose volume and article from drop-down list and click.
- Ling, G.N. and Negendank, W. (1970) The physical state of water in frog muscles. *Physiol. Chem. Phys.* 2: 15. Also via: http://www.physiologicalchemistryandphysics.com/pdf/PCP2-15_ling_negendank.pdf. Or, go to <www.gilbertling.com>, choose volume and article from drop-down list and click.
- Ling, G.N. and Ochsenfeld, M.M. (1965) Studies on the ionic permeability of muscle cells and their models. *Biophys. J.* 5: 777.

- Ling, G.N. and Ochsenfeld, M.M. (1986) Membrane lipid bilayers vs. polarized water dominated by fixed ions: a comparative study of the effects of three macrocyclic ionophores on the K⁺ permeability of frog skeletal muscle, frog ovarian eggs and human erythrocytes. *Physiol. Chem. Phys. & Med NMR* 18: 109. Also available via <http://www.physiologicalchemistryandphysics.com/pdf/PCP18-109_ling_ochsenfeld.pdf>. Or, go to <www.gilbertling.com>, choose volume and article from drop-down list and click.
- Ling, G.N. and Ochsenfeld, M.M. (1988) Studies on the physical state of water in living cells and model systems: XI. The equilibrium distribution coefficients of pentoses in muscle cell water. *Physiol. Chem. Phys. & Med NMR* 20: 309. Also available via: <http://www.physiologicalchemistryandphysics.com/pdf/PCP20-309_ling_ochsenfeld.pdf>. Or, go to <www.gilbertling.com>, choose volume and article from drop-down list and click.
- Ling, G.N. and Ochsenfeld, M.M. (1989) The physical state of water in living cells and model systems. XII. The influence of the conformation of a protein on the solubility of Na⁺ (sulfate), sucrose, glycine and urea in the water in which the protein is also dissolved. *Physiol. Chem. Phys. & Med NMR* 21: 19. Also available via: <http://www.physiologicalchemistryandphysics.com/pdf/PCP21-19_ling_ochsenfeld.pdf>. Or, go to <www.gilbertling.com>, choose volume and article from drop-down list and click.
- Ling, G.N. and Ochsenfeld, M.M. (1991) The majority of potassium ions in muscle cells is adsorbed on β- and γ-carboxyl groups of myosin: Potassium-ion-adsorbing carboxyl groups on myosin heads engage in cross-bridge formation during contraction. *Physiol. Chem. Phys. & Med NMR* 23: 133. Also available via: <http://www.physiologicalchemistryandphysics.com/pdf/PCP23-133_ling_ochsenfeld.pdf>. Or, go to <www.gilbertling.com>, choose volume and article from drop-down list and click.
- Ling, G.N. and Peterson, K. (1977) A theory of cell swelling in high concentrations of KCl and other chloride salts. *Bull. Math. Biol.* 39: 721.
- Ling, G.N. and Tucker, M. (1983) Only solid red blood cell ghosts transport K⁺ and Na⁺ against concentration gradients: hollow intact ghosts with K⁺ - Na⁺ activated ATPase do not. *Physiol. Chem. Phys. & Med NMR* 15: 311. Also available via: <http://www.physiologicalchemistryandphysics.com/pdf/PCP15-311_ling_tucker.pdf>. Or, go to <www.gilbertling.com>, choose volume and article from drop-down list and click.
- Ling, G.N. and Walton, C. (1975) A simple rapid method for the quantitative separation of the extracellular fluid in frog muscle. *Physiol. Chem. Phys. & Med. NMR* 7: 215. Also available via <http://www.physiologicalchemistryandphysics.com/pdf/PCP7-215_ling_walton.pdf>. Or, go to <www.gilbertling.com>, choose volume and article from drop-down list and click.
- Ling, G.N. and Will, S. (1969) Studies on insulin action. III. Linear distribution of D-glucose, D-ribose and methanol in frog muscle cells at 0°C in the absence of insulin. *Physiol. Chem. Phys.* 1: 263. Also available via: http://www.physiologicalchemistryandphysics.com/pdf/PCP1-263_ling_will.pdf. Or, go to <www.gilbertling.com>, choose volume and article from drop-down list and click.
- Ling, G.N. and Will, S. (1976) Studies on insulin action. V. Structural requirements of primers for subsequent accumulation of D-glucose at 0° C in insulinized frog muscles. *Physiol. Chem. Phys.* 8: 115. Also available via: http://www.physiologicalchemistryandphysics.com/pdf/PCP8-115_ling_will.pdf. Or, go to <www.gilbertling.com>, choose volume and article from drop-down list and click.
- Ling, G.N. and Woodbury, J.W. (1949) Effect of temperature on the membrane potential of frog muscle fibers. *J. Cell. Comp. Physiol.* 34: 407.
- Ling, G.N. and Zhang, Z.L. (1984) A study of selective adsorption of Na⁺ and other alkali metal ions on isolated proteins: a test of the salt-linkage hypothesis. *Physiol. Chem. Phys. & Med. NMR* 16: 221. Also available via http://www.physiologicalchemistryandphysics.com/pdf/PCP16-221_ling_zhang.pdf. Or, go to <www.gilbertling.com>, choose volume and article from drop-down list and click.

- Ling, G.N., Baxter, J.D. and Leitman, M. I. (1984) Effects of adrenaline, calcium and ouabain on the resting potential of frog muscle: Interpretation based on the theory of allosteric control of cooperative interaction among surface anionic sites *Physiol. Chem. Phys. & Med. NMR* 16: 405. Also available via <http://www.physiologicalchemistryandphysics.com/pdf/PCP16-405_ling_baxter_leitman.pdf>. Or, go to <www.gilbertling.com>, choose volume and article from drop-down list and click.
- Ling, G.N., Miller, C. and Ochsenfeld, M.M. (1973) The physical state of solutes and water in living cells according to the association-induction hypothesis. *Ann. N.Y. Acad. Sci.* 204: 6.
- Ling, G.N., Niu, Z. and Ochsenfeld, M. (1993) Prediction of the PM theory of solute distribution confirmed. *Physiol. Chem. Phys. & Med. NMR* 25: 177. Also available via: <http://www.physiologicalchemistryandphysics.com/pdf/PCP25-177_ling_niu_ochsenfeld.pdf>. Or, go to <www.gilbertling.com>, choose volume and article from drop-down list and click.
- Ling, G.N., Ochsenfeld, M.M. and Karreman, G. (1967) Is the cell membrane a universal rate-limiting barrier to the movement of water between the living cell and its surrounding medium? *J. Gen. Physiol.* 50: 1807.
- Ling, G.N., Walton, C. and Ling, M. (1979) Mg^{++} and K^+ distribution in frog muscle and egg: A disproof of the Donnan Theory of membrane equilibrium applied to the living cells. *J. Cell. Comp. Physiol.* 101: 261.
- Ling, G.N., Walton, C. and Bersinger, T. J.. (1980) Reduced solubility of polymer-oriented water for sodium sulfate, amino acids, and other solutes normally maintained at low levels in living cells. *Physiol. Chem. Phys.* 12: 111 <http://www.physiologicalchemistryandphysics.com/pdf/PCP12-111_ling_niu_ochsenfeld.pdf>. Or, go to <www.gilbertling.com>, choose volume and article from drop-down list and click.
- Ling, G.N., Ochsenfeld, M.M., Walton, C. and Bersinger, T.J. (1980a) Mechanism of solute exclusion from cells: the role of protein-water interaction. *Physiol. Chem. Phys.* 12: 3. <http://www.physiologicalchemistryandphysics.com/pdf/PCP12-3_ling_ochsenfeld_walton_bersinger.pdf>. Or go to <www.gilbertling.com>, choose volume and article from drop-down list.
- Ling, G.N., Walton, C.L. and Ochsenfeld, M.M. (1983) Indifference of the resting potential of frog muscle cells to external Mg^{++} in the face of high Mg^{++} permeability. *Physiol. Chem. Phys. & Med. NMR* 15: 379. Also via: <http://www.physiologicalchemistryandphysics.com/pdf/PCP15-379_ling_walton_ochsenfeld.pdf>. Or, go to <www.gilbertling.com>, choose volume and article from drop-down list and click.
- Ling, G.N., Zodda, D. and Sellers, M. (1984) Quantitative relationships between the concentration of proteins and the concentration of K^+ and Na^+ in red cell ghosts. *Physiol. Chem. Phys. & Med. NMR* 16: 381. Also via: <http://www.physiologicalchemistryandphysics.com/pdf/PCP16-381_ling_zodda_sellers.pdf>. Or, go to <www.gilbertling.com>, choose volume and article from drop-down list and click.
- Lipmann, F. (1941) *Adv. Enzymol.* 1: 99.
- Lister, A. (1888) *Ann. Bot.* 2: 1.
- Lyster, R.L.J. (1955) Ph.D. Thesis, Cambridge University, Cambridge, England.
- Locy, W.A. (1908, 1923) *Biology and Its Makers*, Henry Holt & Co., New York.
- Maloff, B.L., Scordillis, S.P., Reynold,C. and Tedeschi, H. (1978) *J. Cell Biol.* 78: 199.
- Manwell, C. (1958) *Science* 127: 593.
- Mencken, H.L. (1925) *A Tribute to H.L. Mencken* http://www.freepd.nest.com/mencken_huxley.html
- Mitchell, H.H., Hamilton, T.S., Steggerda, F.R. and Beans, H.W. (1945) *J. Biol. Chem.* 158: 625.
- Mizushima, S., Shimanouchi, T., Nagakura, S., Kuratani, K., Tsuboi, M., Baba, H. and Fujioka, O. (1950) *J. Amer. Chem. Soc.*, 72: 3490.
- Mizushima, S., Tsuboi, M., Shimanouchi, T. and Tsuboi, Y. (1955) *Spectrochimica Acta* 7: 160.
- Miyamoto, V. K. (1966) The electrical properties of lipid bilayer membranes. (Ph.D.thesis), Johns Hopkins University, Baltimore. MD.
- Miyamoto, V.K., and Thompson, T.E. (1973) *J. Coll. Interf. Sci.* 25: 16.

- Mohl, H. von (1846) *Bot. Z.* 4: 73, 84.
- Monod, J., Wyman, J. and Changeux, J. (1965) *Mol. Biol.* 12:88.
- Moore, B., Roaf, H.E. and Webster, A. (1912) *Biochem. J.* 6: 110.
- Müller, P. (1975) *Ann. NY Acad. Sci.* 264: 97.
- Nakao, M., Nakao, T. and Yamazoe, S. (1960) *Nature* 187: 915.
- Nakao, M., Nakao, T., Yamazoe, S. and Yoshikawa, H. (1961) *J. Biochem.* 49: 487.
- Negendank, W. (1982) *Biochem. Biophys. Acta* 694: 123
- Negendank, W. and Shaller, C. (1979) *J. Cell. Physiol.* 98: 95.
- Negendank, W. and Shaller, C. (1982) *Biochem. Biophys. Acta* 688: 316.
- Neihof, R.A. (1954) *J. Phys. Chem.* 58: 916.
- Oken, L. (1805) *Die Zeugung*, Bamberg; Wirzburg; J. A. Goebhardt.
- Perutz, M.F. (1969) *Proc. R. Soc. London Series B* 173: 113.
- Pfeffer, M.F. (1877, 1st ed.; 1921, 2nd ed.) *Osmotische Untersuchungen: Studien zur Zell-Mechanik*, Engelmann, Leipzig.
- Pfeffer, M.F. (1985) *Osmotic Investigations; Studies on Cell Mechanics* (English Transl. by G. R. Kepner and Ed. J. Stadelmann), van Nostrand-Rheinhold., New York.
- Poethig, R.S. (2001) *Genome Research* 11: 313.
- Podolsky, R.J. and Morales, M.F. (1956) *J. Biol. Chem.* 218: 946.
- Pollack, G.H., Cameron, I. L. and Wheatley, D.N. (2006) *Water and the Cell*, Springer, Dordrecht, The Netherlands.
- Ponder, E. (1948, 1971) *Hemolysis and Related Phenomena*, Grune and Stratton, New York.
- Purkinje, J. (1834) see Harris 1999, p. 86.
- Purkinje, J. (1840) *Über Arb. Veränd. schles. Ges. vat. Kult.* 16: 81.
- Rapoport, S and Guest, G.M. (1941) *J. Biol. Chem.* 138:269.
- Reisin, I.L. and Gulati, J. (1973) *Ann. NY Acad. Sci.* 204: 358.
- Reisin, I. L. and Ling, G.N. (1973) *Physiol. Chem. Phys.* 5: 183. Also available via: <http://www.physiologicalchemistryandphysics.com/pdf/PCP5-183_reisin_ling.pdf>
- Remak, R. (1852) *Müllers Arch. f. Anatom. Physiol. u. wissen. Med. (Berlin)* p. 49.
- Rothschuh, K.E. (1973) *History of Physiology*. R.E. Krieger Publi. Co., Huntington, NY; Malabar, FL.
- Rushbrooke, G.S. (1949) *Introduction to Statistical Mechanics*, Oxford University Press (Clarenden), London.
- Rossi Fanelli, A., Antonini, E. and Caputo, A. (1964) *Adv. Protein Chem.* 19: 73. (Fig.17, p. 167).
- Schleiden, M. J. (1838) Beiträge zur Phytogenesis. *Müller Arch Anat. Physiol. wiss. Med* (no volume number) p. 137. Transl. In Sydenham Soc. (London)(1847).
- Schrödinger, E. (1944) *What is Life? The Physical Aspect of the Living Cell*, Cambridge University Press, Cambridge.
- Schultz, R.D. and Asunmaa, S.K. (1969) *Rec. Prog. Surf. Sci.* 3: 291.
- Schultze, M. (1861) *Arch. Anat. Physiol. wiss. Med.* 1861: 1. English transl. of part of this article found in Hall, 1951, pp. 449-455.
- Schwann, T. (1839) *Mikroskopische Untersuchungen über die Übereinstimmung in der Struktur und dem Wachstum der Thiere und Pflanzens*, Engelmann, Leipzig.
- Smith, H. (1847) *Microscopical Researches into the Accordance in the Structure and Growth of Animals and Plants*, printed for the Siedenheim Society. Reprinted by Kraus Reprint Co., New York in 1969.
- Sollner, K. (1949) *J. Phys. Colloid Chem.* 53: 1211.
- Sollner, K., Abrams, I. and Carr, C.W. (1941) *J. Gen. Physiol.* 24: 467.
- Speakman, J.B. and Hirst, M.C. (1931) *Nature* 127: 665.
- Spector, W.S., ed. (1956) *Handbook of Biological Data*, Saunders, Philadelphia.
- Stecher, P.G. (1968) *Merck Index*, Merck & Co, Inc.
- Stillman, T.M., Gilbert, D.L. and Robbins, M. (1970) *Biochim. Biophys. Acta* 203: 338.
- Taft, R.W. (1953) *J. Amer. Chem. Soc.* 75: 4231.
- Tanaka, S. and Scheraga, H.A. (1976) *Macromol.* 9: 168.

- Thovert, J. (1914) *Ann. chim. phys.* 26: 366.
- Troshin, A.S. (1951) The distribution of substances between cell and medium. Comm. 1, The distribution of galactose and sucrose in complex coacervate systems (model experiment) *Byull. eksp. biol. i med.* 31: 180.
- Troshin, A.S. (1966) *Problems of Cell Permeability* (Revised Ed.), Pergamon Press. London, New York.
- Valentin, G (1836) *Nova Acta Phys-Med. Acad. Caesar. Leopold-Carolinae, Nat. Curios* 18: 51.
- Villegas, R., Blei, M. and Villegas, G.M. (1965) *J. Gen. Physiol.* 48: 35.
- Walter, J.A. and Hope, A.B. (1971) *Aust. J. Biol. Sci.* 24: 497.
- Weidemann, S. (1971) "The Microelectrode and the Heart" in *Research in Physiology* in memory of Chandler M. Brooks, (F.F. Kao, K. Koizumi and M. Vassale. eds.) Auto Gaggi, Bologna.
- Weissbluth, M. (1974) *Hemoglobin: Cooperativity and Electronic Properties*, Springer-Verlag, New York.
- Wood, R.E., Wirth, F.P., and Morgan, H.E. (1968) *Biochem. Biophys. Acta* 163: 171.
- Yang, C.N. (1995) Remarks about some developments in statistical mechanics.
<http://www.hep.wisc.edu/~1durand/715html/courseinfo/yangstatmechhistory.html>
- Zheng, J. and Pollack, G.H. (2003) *Phys. Rev. E* 68: 031408.